On the Quantification of Safety Margins

by

Lorenzo P. Pagani
Diplome d'Ingenieur de Grande Ecole, Ecole Centrale de Paris (1998)
Laurea in Ingegneria Nucleare, Politecnico di Milano, Italy (1998)

Submitted to the Department of Nuclear Engineering
in Partial Fulfillment of the Requirements for the Degree of

DOCTOR of PHILOSOPHY
at the
MASSACHUSETTS INSTITUTE OF TECHNOLOGY

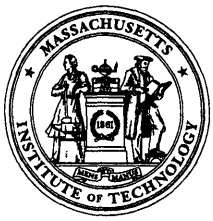

September 2004

Author.....
Lorenzo P. Pagani, MIT
Department of Nuclear Engineering
September 2004

Certified by.....
George E. Apostolakis, MIT
Professor of Nuclear Engineering
Thesis Supervisor

Certified by.....
Neil E. Todreas, MIT
KEPCO Professor of Nuclear Engineering
Thesis Reader

Accepted by.....
Jeffrey Coderre, MIT
Professor of Nuclear Engineering
Chairman, Department Committee on Graduate Students

On the Quantification of Safety Margins

by

Lorenzo P. Pagani

Submitted to the Department of Nuclear Engineering on August 19, 2004, in partial fulfillment of the requirements for the degree of Doctor of Philosophy at the Massachusetts Institute of Technology

ABSTRACT

The nuclear industry has relied on the concept of Defense in Depth (DID) and traditional safety margins to deal with the uncertainties associated with the design and operation of nuclear facilities. These concepts were formulated in the early days of development of nuclear power when these uncertainties could not be quantified. The subsequent development of Probabilistic Risk Assessment (PRA) has provided the analytical tools that allow the quantification of uncertainties associated with accident initiation and progression. But, while the impact of redundancy has been explicitly modeled and quantified, the role of safety margins is still not explicitly taken into account. The present work identifies the impact of safety margins in the PRA and proposes a methodology to quantify them. Practical examples are developed and discussed in two case studies. In the first study, we analyze the passive cooling of a gas-cooled fast reactor and we use an importance sampling Monte Carlo technique to propagate the epistemic uncertainties and to calculate the overall probability of failure. A comparison with an alternative active design is considered also. The results show that the active system can have, for this particular application, better reliability than the passive one. An approach to derive the uncertainty distribution on the capacity is presented in the second case study, where computer simulations are performed to propagate uncertainties and to derive a probabilistic failure limit for high burnup fuel in a PWR rod ejection accident.

Supervisor: Professor George E. Apostolakis

ACKNOWLEDGMENTS

I thank my advisor, Professor George Apostolakis for his pedagogical, financial, and personal support during my stay at MIT. Thanks to him I was able to approach current issues in risk analysis and decision theory in a pragmatic way. Special thanks go to Professor Enrico Zio of Politecnico di Milano; if it was not for him, I would not have pursued a Ph.D. program in the first place.

I also thank Professor Neil Todreas, Professor Michael Driscoll, and Dr. Pavel Hejzlar of the Massachusetts Institute of Technology for their useful comments. I also appreciate the support and comments I have received from Hossein Hamzehee, Prasad Kadambi, Ralph Meyer, Harold Scott, and John Voglewede of the Office of Nuclear Regulatory Research of the U.S. Nuclear Regulatory Commission (USNRC). Robert Youngblood of ISL, Inc. provided useful insights also.

A special thanks to my family, Giovanna and Marcello, who have helped me go through this commitment and have provided all the necessary (and more) external support.

This work is part of a project on the quantification of safety margins that is supported by the USNRC under a co-operative agreement with the MIT Department of Nuclear Engineering. The views expressed are the author's and do not necessarily reflect the views of the USNRC.

TABLE OF CONTENTS

EXECUTIVE SUMMARY

Introduction

The nuclear industry has relied on the concept of Defense in Depth (DID) and traditional safety margins to deal with uncertainties. This approach suggests making extensive use of redundancy and large margins. The subsequent development of Probabilistic Risk Assessment (PRA) has improved the safety approach by quantifying the risk, in terms of Core Damage Frequency (CDF) and Large Early Release Frequency (LERF), and by determining its main contributors. But, while the impact of redundancy has been explicitly modeled and quantified, safety margins are not taken into account explicitly. This makes it difficult to have a more accurate estimate of risk and to evaluate quantitatively the impact of modifications on plant risk. As an example, let us consider the expected increase in the calculated peak cladding temperature in a LOCA simulation due to a power uprate. This leads to a decrease in safety margins. As long as the calculated temperature value is below the regulatory limit, the change is acceptable; however, current PRA models are not able to predict the increase in the probability of failure due to that increase. To further improve the value of PRA, considering its significance in decision-making, it is important to be able to quantify the safety margins and to evaluate their impact on the final results.

Inclusion of Safety Margins into PRA

The approach that we adopt can be summarized as the following:

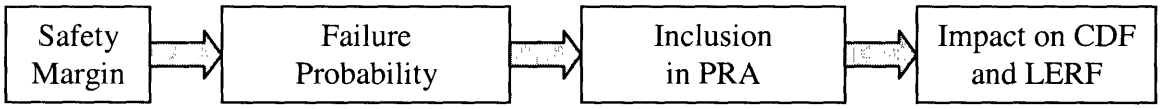

Figure 1 Quantification of safety margin into PRA.

The safety margin must be quantified in terms of the failure probability that is included in the PRA model to calculate the impact on CDF and LERF.

To go from safety margins to failure probabilities, we rely on a reliability physics representation of load and capacity values (Figure 2).

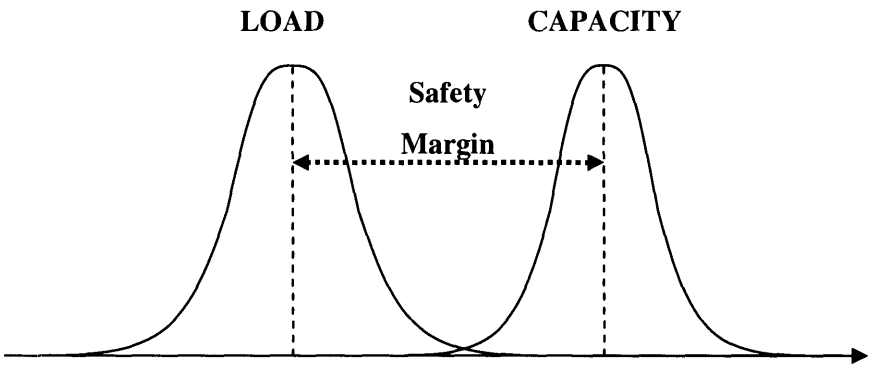

Figure 2 Uncertainty on load and capacity

The two distributions show the uncertainties regarding the numerical values of the load and capacity. **Safety margin is the difference between a characteristic value of the capacity and a characteristic value of the load**. The characteristic values shown in Figure 2 are the median (and mean) values of the symmetric distributions. This is not necessarily the case in all situations. For example, the characteristic value of the load can be an upper percentile of its distribution (a conservatively calculated value) and that of the capacity can be a low percentile of its distribution (a conservatively set failure limit). The distributions themselves do not have to be symmetric.

Safety margins are intended to minimize the probability of failure of the system, i.e., the probability that the load exceeds the capacity. We call a system failure that results from the load exceeding the capacity a **functional failure**.

Once the probability of functional failures is calculated, this quantity has to be implemented into the PRA. The PRA is organized in Event Trees (ET) that represent the possible sequences of events that could lead to accident. An example of an ET is plotted in Figure 3.

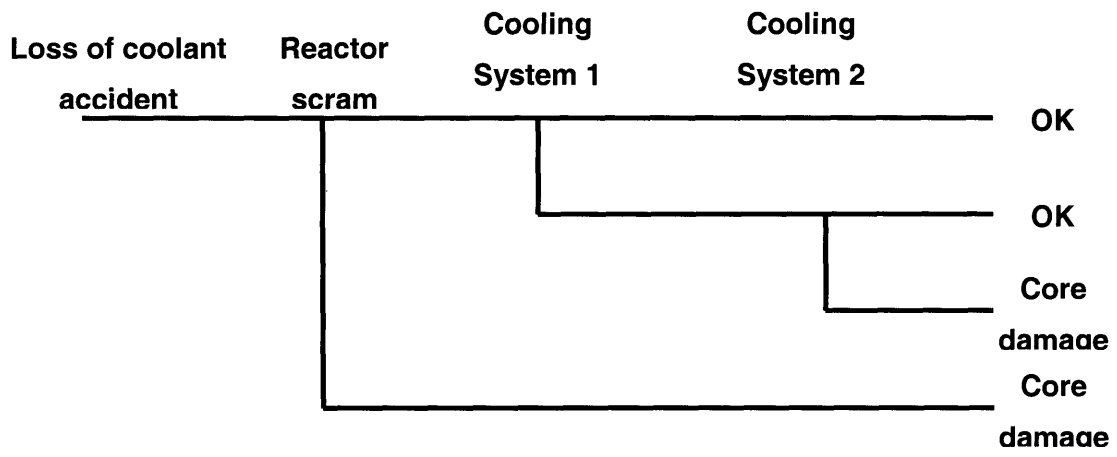

Figure 3 Simplified event tree for a loss of coolant accident

The ET has to be read from left to right, following the chronology of the accident sequence. An ET begins with an Initiating Event (IE). An ET represents all relevant scenarios that can happen following the IE, the potential failures of safety systems being taken into account through the branching nodes. At the end of each sequence, the resulting outcome is reported. The outcome of a sequence is defined to be acceptable if the simulation determines that **acceptance criteria** are met. Acceptance criteria are the limits established for specific parameters to ensure that critical safety functions, such as the cooling of the core and reactivity control are met. An example of acceptance criteria for a LOCA sequence is the requirement to maintain the cladding temperature below 2,200°F and to limit the oxidation of the cladding to 17% of its thickness.

Safety margins have a direct connection with acceptance criteria. If safety margins are positive, this means that the acceptance criteria are met. However, there is always the

possibility of functional failures, even in the presence of positive ("deterministic") safety margins, especially if the uncertainties on the load or capacity are large. The deterministic approach used in current PRAs is equivalent to assuming a zero probability of functional failure whenever the margins are positive and a probability of functional failure equal to unity whenever the margins are negative.

To include functional failures into the PRA, it is necessary to take into account the possibility of a failure even when the acceptance criteria are met and the possibility of success even when the acceptance criteria are violated. The magnitude of the correction depends both on the value of the functional failure probabilities and on the sequence probabilities of occurrence. Numerical examples show that the correction is negligible (on the order of a small percentage of the calculated CDF value) for active systems such as the ECCS, while it can be important for passive systems (a correction by a factor of 1,000).

Two cases involving safety margins are investigated in this work. The first deals with the reliability of a passive system and focuses on the uncertainties in the "load" imposed on the system. The second case deals with the failure limit of the cladding for high-burnup fuels. Its focus is on the "capacity" of the cladding.

Case Study 1 - Passive Cooling

This case study investigates the quantification of functional failure probabilities of a passive cooling system for a Gas-cooled Fast Reactor (GFR). The reactor used in the case study is a 600MW helium-cooled GFR that has been the subject of extensive study at the Massachusetts Institute of Technology for several years. In case of a LOCA, long-term heat removal is assured by forced (by an active system) or natural (by a passive system) circulation in each loop. To simulate the steady-state behavior of the system, a thermal-hydraulic code developed at MIT has been used.

Following the approach shown in Figure 1, aleatory and epistemic uncertainties on the relevant parameters and models have been quantified and functional failure probabilities calculated using a Monte Carlo algorithm.

Uncertainties regarding parameter values have been identified on the power, pressure, and the cooler wall temperature. In addition, (model) uncertainties on the correlations for the Nusselt number and the friction factor have been modeled using a correction factor (ε). That is, the results of the correlations are subject to errors and we write:

$$y = f(x)\varepsilon \tag{1}$$

where: y is the real value of the quantity to be predicted, $f(x)$ is the result of the correlation, and ε is the prediction error.

The calculated functional failure probabilities are reported in Table 1 in which several designs have been considered with varying numbers of loops. The uncertainties result in larger failure probabilities for the passive systems compared to the active ones. The reason why the active designs have such low functional failure probabilities is that the uncertainties in the pressure and the heat transfer correlations are smaller.

Probability of failure	2 Loops	3 Loops	4 Loops	5 Loops
Passive design	4.76E-2	4.05E-4	7.19E-6	9.58E-7
Active design	< 1E-11	< 1E-11	< 1E-11	< 1E-11

Table 1 Probabilities of functional failure of active and passive systems.

The probability values have been included into the PRA event tree that considers also the probability of failure of the active components. The results are reported in Table 2. Without the inclusion of functional failures, the passive system would always be more reliable than the active one (because it is assumed to have a zero failure probability); however, this is not the case when the impact of functional failures is included in the analysis. A comparison of the failure probabilities shows that the active system is actually more reliable than the passive one for the 2- and 3-loop designs.

	2 Loops	3 Loops	4 Loops
Passive design	4.76E-2	4.05E-4	7.19E-6
Active design	5.70E-3	1.58E-4	7.85E-5

Table 2 Conditional probability of system failure for the passive and active systems. Both functional failures and failures due to active component such as pumps are included.

Without the explicit inclusion of functional failures (safety margin quantification) into the PRA, it would have been impossible to correctly estimate the frequencies of the relevant accident sequences. This is due to the combination of large uncertainties and high hardware reliability typical of passive safety systems that emphasizes the importance of functional failures and makes it necessary to include them in the PRA explicitly. Failure to do this would lead to optimistic results.

Case Study 2 – High Burnup Failure Limit

The second case study is an example of quantification of the uncertainty on the capacity (Figure 2). We investigate the failure limit of the cladding in a rod ejection accident in a

PWR at different burnup levels. The subject of the case study is interesting from two points of view:

- Within the scope of the work presented in this report, it shows a practical example of quantification of epistemic uncertainty on the capacity necessary to evaluate the probability of functional failure.
- It is also interesting because of the importance of the issue in current research programs worldwide.

We focus our attention on a rod ejection accident in a PWR. Issues arise because safety limits that were initially defined on the basis of databases containing only data coming from low burnup fuels are not applicable to higher levels. Experimental programs in France, Japan, and Russia have shown new phenomena occurring at burnup levels larger than 40 GWd/MTU, which decrease the fuel failure limit. It is, then, necessary to redefine the failure limits making use of the new experience. The rod ejection accident is based on the assumption that a control rod assembly is expelled by the internal core pressure because of a mechanical failure of the housing of the drive mechanism. The ejection induces a reactivity increase that causes a local power peak. Failures of the cladding can result, and fuel particles can be expelled into the coolant. Understanding the failure modes and the high-burnup fuel behavior in accident conditions is important in order to determine its capacity to withstand the accident.

Experimental results show that the failure of the cladding can be caused by a number of mechanisms ranging from departure from nucleate boiling to mechanical stresses due to pellet-clad mechanical interaction or molten fuel. Cladding failures are more likely whenever oxidation, and eventually spallation[1], is present because of the reduction in cladding ductility due to consequent hydride formation.

---

[1] For very thick oxide layers, blisters can detach from the outer cladding surface and disperse in the coolant. This phenomenon is called spallation.

To derive the distribution of the failure limit for a rod ejection accident in a PWR, we quantify the uncertainties in relevant parameters and propagate them using the Fraptran and Frapcon computer codes. A large number of simulated experiments has been performed to propagate the uncertainties and to obtain sufficient data to derive the probabilistic failure limit. The simulations are performed following the process represented in the diagram of Figure 4.

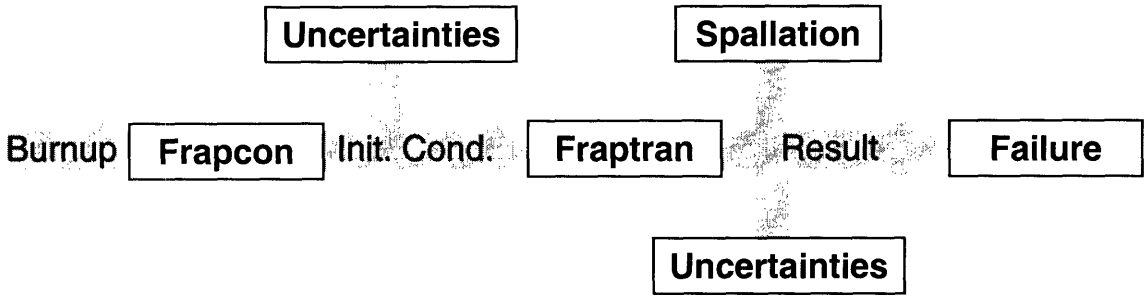

Figure 4 Virtual simulation process

Frapcon (version 3.2) is used to obtain the initial conditions of the rod at a given burnup level. The initial estimates of oxide layer thickness and hydrogen content obtained from Frapcon are corrected to take into account their uncertainty. Fraptran (version 1.2) is then used to perform the accident simulation and to obtain the time evolution of temperature and strain energy density in the rod. Once the Fraptran code simulation is performed, a simple model has been developed and is used to determine the spallation state of the cladding and to determine whether the rod has failed or not.

In Figure 5, the data from the virtual experiments are plotted. Failures are plotted in solid symbols. The plots differentiate between non-spallated samples (circles) and spallated samples (triangles). In the case of no failures, the enthalpy value refers to the maximum enthalpy reached during the transient, while, in the case of failures, the enthalpy value refers to the enthalpy level where the failure began occurring.

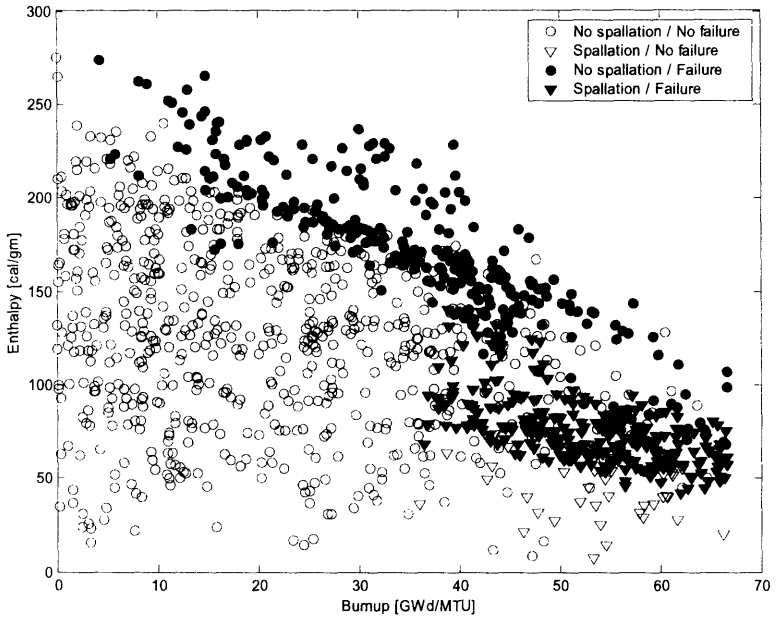

Figure 5 Results of the virtual experiments.

Because of the uncertainties, the data are very scattered, showing non-failure points interspersed with failure points all over the burnup range. To interpret the above data, instead of defining a conservative limit, we determine a probabilistic limit as a function of enthalpy at a given level of burnup. We will find a function that gives the probability of failure as a function of enthalpy and burnup, i.e.,

$$\Phi(h/\mu,\sigma) = \int_0^h \frac{1}{x\sqrt{2\pi}\sigma} \exp[-\frac{(\log x - \mu)^2}{2\sigma^2}]dx$$

$$\mu = \mu_0 + \mu_1 B \qquad (2)$$

$$\sigma = \sigma_0 + \sigma_1 B$$

where h is the enthalpy level and B is the burnup level and μ_0, μ_1, σ_0, and σ_1 are constant parameters. The function Φ depends on these four parameters that must be determined

from the data points. The point values of these parameters are determined by fitting the function to the data points through the Maximum Likelihood Estimate (MLE) method. Because of the regime shift due to spallation, two different fits are determined: one set for spallated samples and one set for non-spallated samples. The results from the fits are then merged together to obtain the failure probability as a function of burnup and enthalpy. The results of the analysis are shown graphically in Figure 6. In the figure, limits corresponding to different failure probabilities are shown.

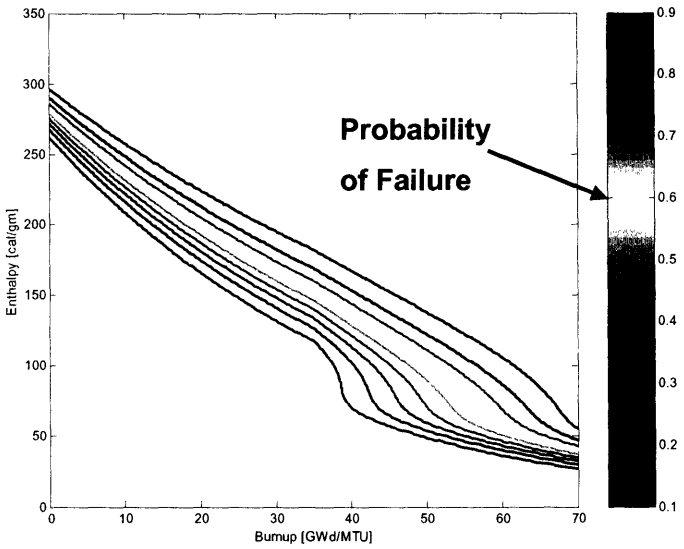

Figure 6 Failure limit

It is possible to obtain the probability distribution on the failure limit f(h,B), i.e. the epistemic distribution on capacity, by taking the partial derivative of $\Phi(h,B)$ with respect to h. The results are plotted in Figure 7 for different burnup levels and are summarized in Table 3.

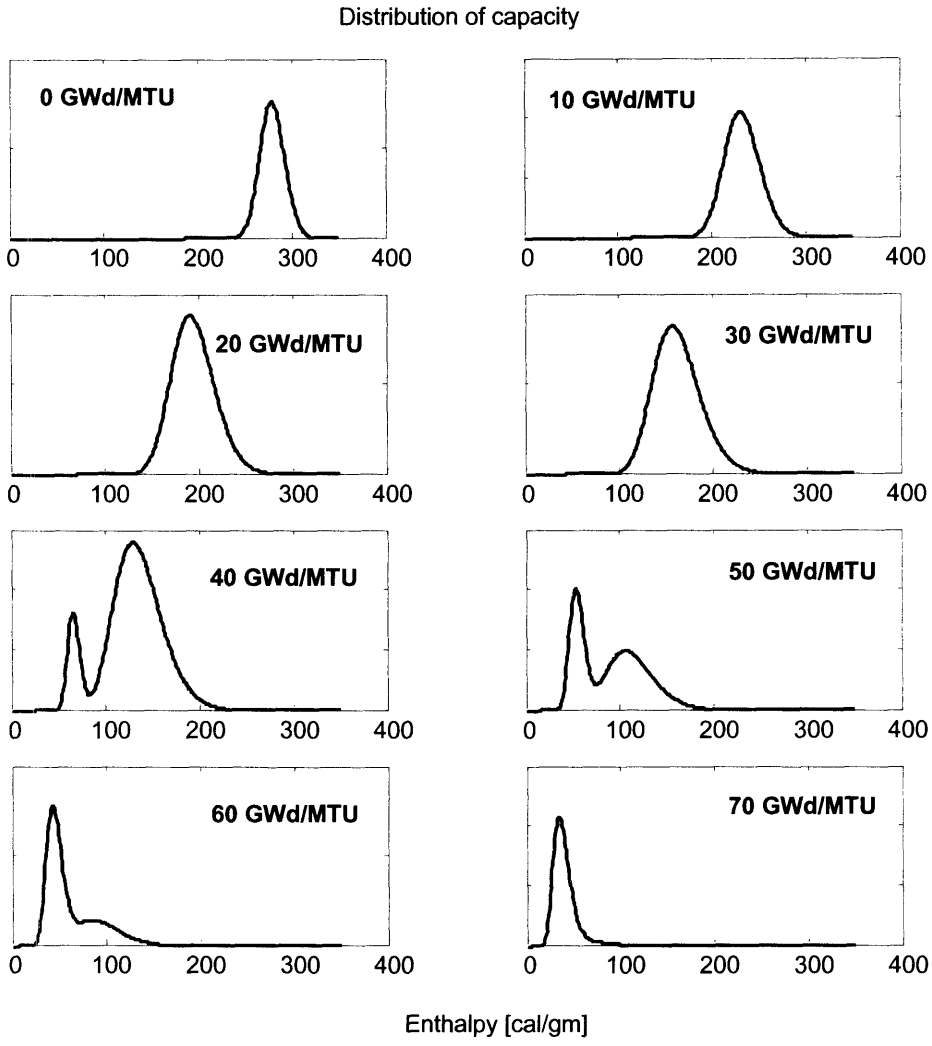

Figure 7 Epistemic distribution of the capacity

Burnup [GWd/MTU]	5th percentile [cal/gm]	50th percentile [cal/gm]	95th percentile [cal/gm]
0	258	279	302
10	203	232	266
20	159	193	234
30	125	161	206
40	64	129	180
50	46	90	151
60	34	51	121
70	25	38	68

Table 3 Characteristic values of the probability distributions of the failure limit

Figure 7 and Table 3 show that the failure limit decreases as the burnup level increases. The effect of spallation is also shown. For low burnup (0-30 GWd/MTU), the failure distribution is unimodal (lognormal), because spallation is not possible. With the increase in burnup, spallation becomes important and the failure distribution is composed by two lognormal distributions, one for the spallated samples and the other for the non-spallated samples. For this reason, the distribution is bimodal between 40 and 60 GWd/MTU. For higher burnup (70 GWd/MTU), the spallation probability increases and the distribution for spallated samples dominates and the distribution is unimodal again.

The above probabilistic analysis describes a process for the derivation of the distribution of the failure limit from existing data. The calculated distribution represents the epistemic uncertainty on the capacity and can be used to calculate the functional failure probability.

Conclusions

The results of the research show the necessity to better model uncertainties and to include them in the PRA especially for those types of failure scenarios in which large uncertainty is present. Most of the accident sequences in PRAs for LWRs model active systems whose behavior is well understood; therefore, the quantification of safety margins will not impact the PRA results. On the other hand, for some accident sequences characterized by large uncertainty (RIA with high burnup fuel, or new designs relying on passive systems), the impact of safety margin should be included in the PRA.

The inclusion of safety margins in PRA, using a load-capacity approach, such as the one introduced in this work, will allow better risk-informed decision making and could eventually reduce the need for excessive conservatism, thus avoiding unnecessary regulatory burden.

INTRODUCTION

Since its early days, the nuclear industry has relied on the concept of Defense in Depth (DID) and safety margins to deal with the uncertainties associated with the design and operation of nuclear facilities. This approach suggests making extensive use of redundancy and large margins to guarantee that the probability of undesired events is sufficiently low. Both these solutions were able to decrease the overall risk by introducing conservatism into the system. This risk, however, remained unquantified, since the accident probabilities were unknown.

The subsequent development of Probabilistic Risk Assessment (PRA) has improved the safety approach by quantifying this risk, in terms of Core Damage Frequency (CDF) and Large Early Release Frequency (LERF), and by determining the dominant accident sequences. Through the use of PRA, it has been possible to identify accident sequences and important safety components. But, while the impact of redundancy has been explicitly modeled and quantified, the impact of safety margins is still not explicitly taken into account. This makes it difficult to have a more accurate estimate of risk and to evaluate quantitatively the impact of modifications on plant risk. The quantitative impact of margin changes (individually or in combination) on the PRA, that is, their impact on the CDF and LERF, is not known. As an example, let us consider the expected increase in the calculated peak cladding temperature in a LOCA simulation due to a power uprate. This corresponds to a decrease in safety margin. As long as the calculated temperature value is below the regulatory limit, the change is acceptable; however, current PRA models are not able to predict the increase in the probability of failure due to that increase.

To further improve the value of PRA, considering its significance in decision-making, it is important to be able to quantify the safety margins and to evaluate their impact on the final results.

The objective of this research is to identify the impact of safety margins on PRA and to provide a methodology for their quantification. The report is organized as follows:

- In Part I, a discussion about uncertainties and the definition of safety margins used throughout the thesis is provided with examples.
- In Part II, the concept of functional failure, which links safety margins to the probability of failure, is introduced. A formal methodology to calculate functional failures is also presented and discussed.
- In Part III, the impact of safety margins on PRA is investigated and some simple numerical examples are presented which evaluate the magnitude of this impact.
- Part IV and Part V present two case studies. The first case study provides a complete example of quantification of safety margins, and their inclusion in PRA for a passive cooling system in a gas-cooled fast reactor. The second case study is focused on the quantification of uncertainties for high burnup fuel in a rod ejection accident and provides an example of how to determine the distribution of the failure limit necessary to quantify safety margins.
- Details regarding the methodologies and algorithms, including source code for computer simulations are collected in the appendices.

PART I: SAFETY MARGINS

1.1 Uncertainty

Uncertainty is present in almost every aspect of engineering science. Although it is common to use deterministic models in engineering, there are many phenomena that cannot be adequately described using deterministic models. Such phenomena are characterized by a random or stochastic behavior (like the outcome of a coin toss or the time of failure of a component) and have an inherent uncertain or random behavior. This type of uncertainty is called **aleatory uncertainty** [Apostolakis 1990, 1995; USNRC 1998; and Winkler 1996].

Regardless of the type of model used (aleatory or deterministic), an additional level of uncertainty, associated with the confidence of the analyst regarding the "goodness" of the model and the value of the relevant parameters exists. This uncertainty is called **epistemic uncertainty** and can be subdivided into two categories: **parameter uncertainty** and **model uncertainty**.

Parameter uncertainty refers to the uncertainty in the numerical values of model inputs. Models used to describe physical systems rely on the knowledge of the value of relevant parameters. For example, a model for the calculation of the heat transfer in a solid implies knowledge, among others, of the material conductivity. These values have to be used as inputs in the model and are usually known only to a certain level of precision, i.e., uncertainty is associated with them.

In addition to the above type of uncertainty, there is also uncertainty in the model itself (i.e. in the final output). This arises because mathematical models are simplified representations of real systems and, therefore, their results may be affected by error or bias (model uncertainty). Model uncertainty also includes the fact that the model could be too simplified and therefore would neglect some important phenomena affecting the

final result. This type of uncertainty is sometimes identified independently from model uncertainty [USNRC 1998] and is known as **completeness uncertainty**.

The epistemic uncertainty described above is meant to describe the incomplete knowledge of the analyst regarding the real behavior of systems.

The objective of the present research is the quantification of safety margins, i.e., the assessment of the reliability of engineering systems or components. For this purpose, the relevant effects of uncertainties are the ones on the system load and capacity values (Figure 8).

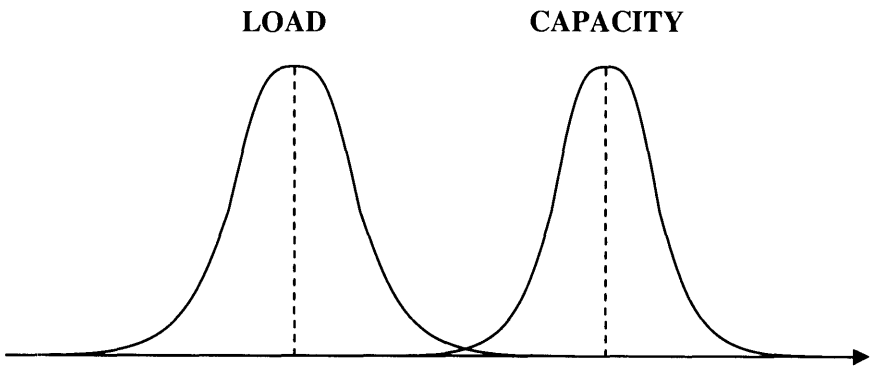

Figure 8 Uncertainty on load and capacity

The figure represents the distribution of the actual load and capacity values. This load-capacity approach has been used in the past to incorporate aging effects into PRA [Smith et al. 2001, Apostolakis 1999], and to evaluate the reliability of concrete structures in nuclear power plants [Ellingwood et al. 1993].

The uncertainty on the load and capacity values can arise from their aleatory nature (they are random results of an aleatory model, such as the maximum load experienced during a transient) or from epistemic uncertainty[2].

A larger uncertainty is represented with a broader distribution (Figure 9).

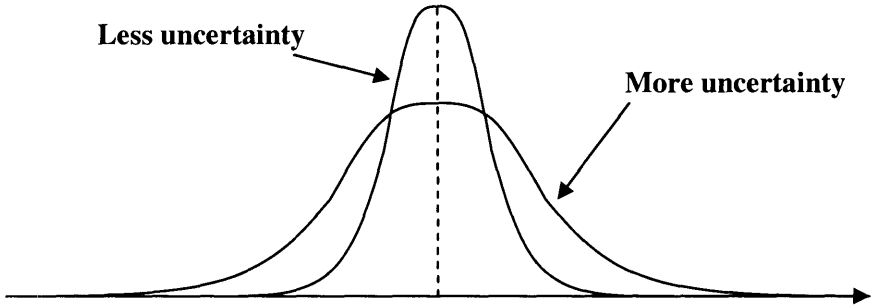

Figure 9 Quantification of uncertainty

Whenever the load exceeds the capacity the component will not be able to perform its function and will fail.

Some authors erroneously graphically represent the probability of failure as the common area below the two distributions in Figure 8. While this representation is certainly helpful and seems intuitive, it is not correct. The probability of failure is given by the probability that the load will exceed the capacity i.e., by the convolution formula

[2] The distinction between aleatory and epistemic uncertainty is sometimes subtle and not straightforward.

$$P(L > C) = \int_{-\infty}^{\infty} [\int_{x}^{\infty} f_L(y)dy] f_C(x)dx \qquad (1.1)$$

where f_C and f_L represent the distributions of the capacity and the load respectively. In this formulation, the two distributions are supposed to be independent.

The objective of the engineer is to avoid altogether the possibility of failure, or to decrease its probability to an acceptable level. This can be done by increasing the distance between the load and capacity characteristic values[3] or by decreasing the uncertainty (Figure 10 and Figure 11).

[3] By characteristic value we mean a single point value used to represent the load or capacity. Depending on the problem, different characteristic values can be used, such as median, mean or specific percentile values. In the figures, the characteristic values are represented as dashed vertical lines.

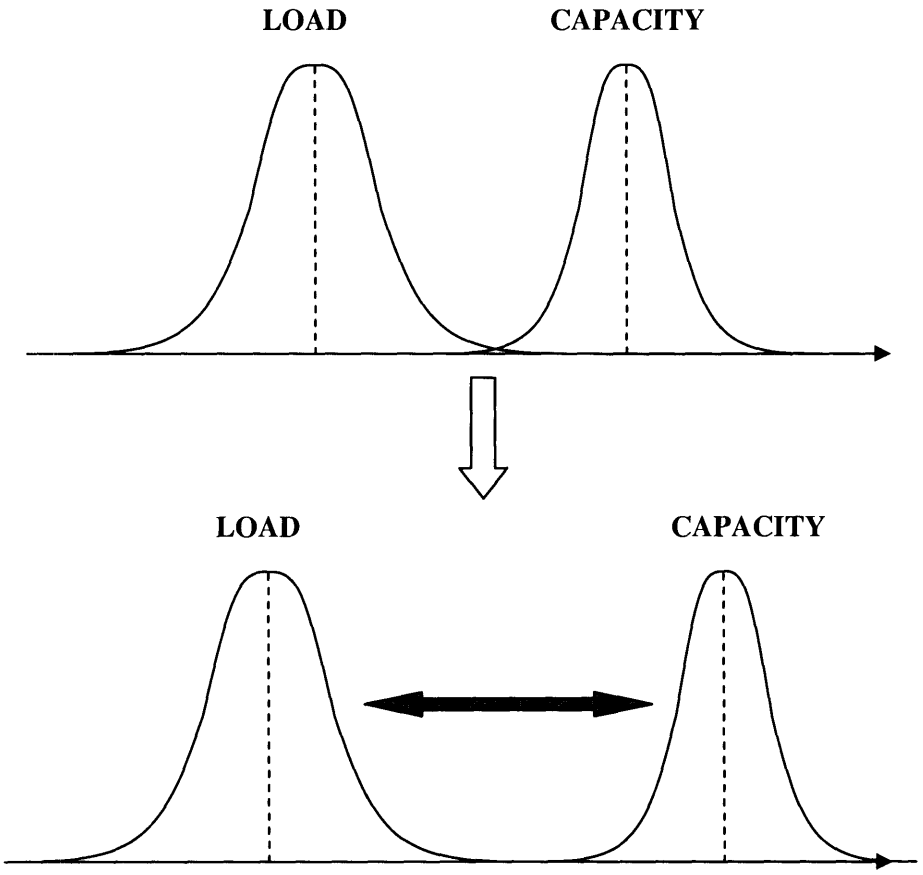

Figure 10 Reduction of failure probability due to an increase in the distance between load and capacity

The former approach (increasing the distance between load and capacity) is more direct and commonly used. It can be achieved by building significant conservatism into the system through the use of larger safety margins.

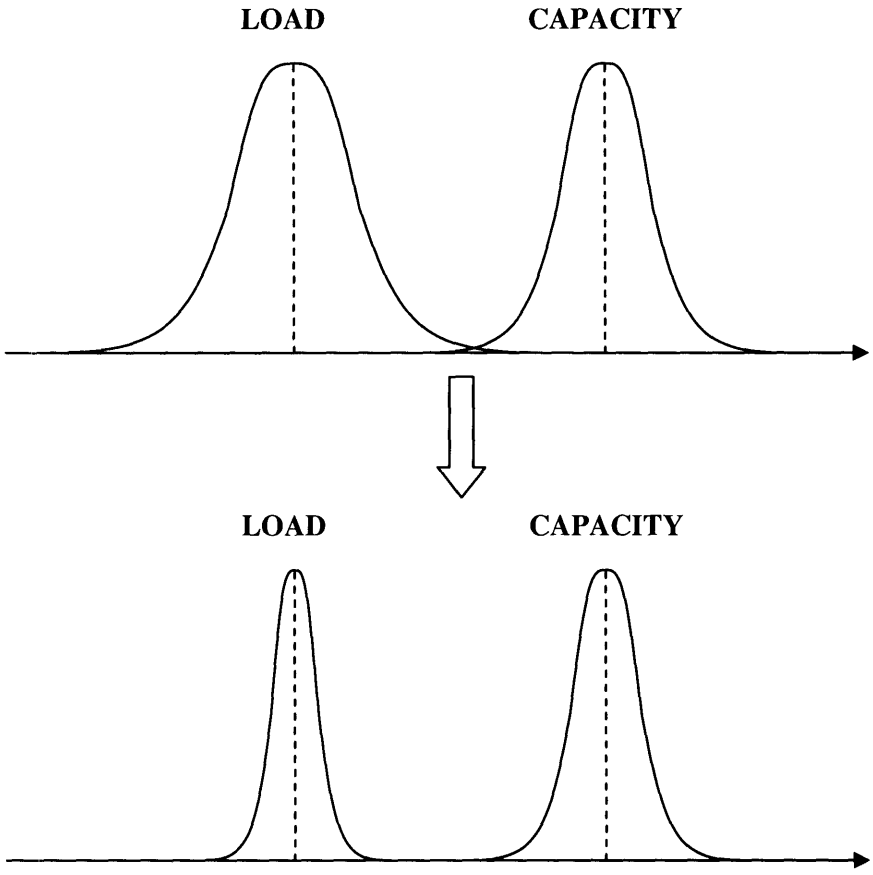

Figure 11 Reduction of failure probability due to a decrease in uncertainty

The second approach (reducing uncertainties) is more difficult to achieve and corresponds to an increase in the state of knowledge of the system (or more generically, to a decrease in uncertainty due to epistemic or aleatory sources). For instance, more detailed and precise models (less prediction error) permit the design of less expensive systems reducing unnecessary conservatism. Another example of reduction in the uncertainty is given by the application of quality control. Strict quality control will reduce the uncertainty on the capacity by filtering "bad" components, therefore reducing the probability of a low capacity value.

1.2 Reliability Approaches and Definition of Safety Margin

Before going into more specific detail of the research it is useful to introduce a definition of safety margin and give a brief overview of the existing reliability approaches. From the classification of reliability methods reported in Madsen et al. [1986], there are four types of reliability approaches. Lower level methods contain less information than higher level methods and are special cases of the latter

1. Safety margins are identified as a Level 1 reliability approach. Within this approach, the load and capacity are described by point estimates (the characteristic values) and the safety of the system is evaluated through a safety margin or coefficient describing the relationship between these two point estimates. This type of approach is the one most commonly implemented in the regulations. Some confusion can arise because different definitions of safety margin can be found in the literature. To have a flavor of the various terms, we provide in Table 4 a list of terms and their interpretation from Ardillon et al. [2000]. This approach has the advantage of being simple, but its validity has to be justified from experience or as a result from higher-level reliability approaches.

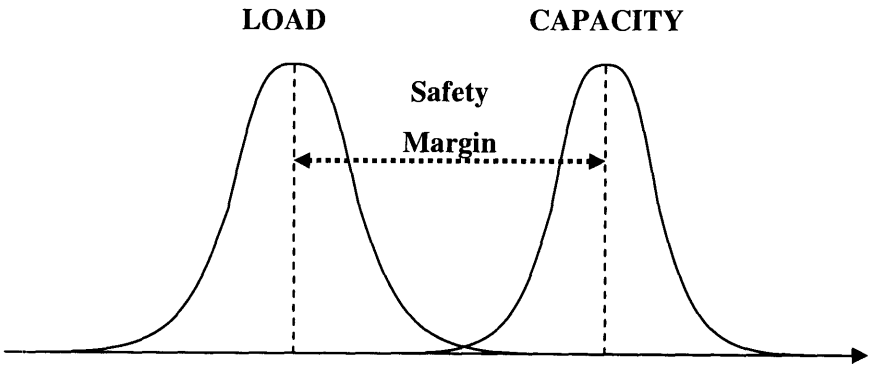

Figure 12 Definition of safety margin

The two distributions plotted in Figure 12 show the uncertainties regarding the numerical values of the load and capacity. **Safety margin is the difference between a characteristic value of the capacity and a characteristic value of the load.** The characteristic values shown in Figure 12 are the median (and mean) values of the symmetric distributions. This is not necessarily the case in all situations. For example, the characteristic value of the load can be an upper percentile of its distribution (a conservatively calculated value) and that of the capacity can be a low percentile of its distribution (a conservatively set failure limit), as shown in Figure 13. The distributions themselves do not have to be symmetric.

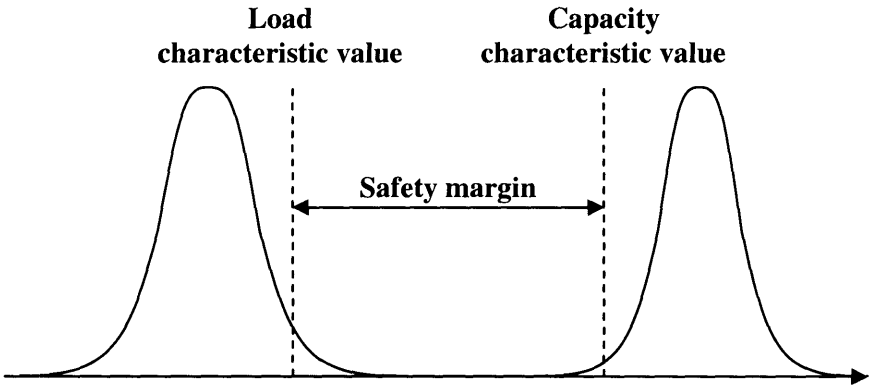

Figure 13 Definition of safety margin (conservative example)

Term	Definition
Characteristic value	Same as reference value, but includes a probabilistic meaning (definition as a distribution fractile for example)
Explicit margin	Same as safety coefficient
Implicit margin	Same as reference value
Margin	Same as safety margin
Overall safety factor	Ratio between a parameter characterizing the material strength and a parameter characterizing the effect of actions (loading)
Reference value	Value of an analysis parameter that is used in the margin equation before application of safety coefficient. It is generally a pessimistic value representing the parameter in the analysis.
Reserve factor	Difference between the threshold value of the criterion and the value derived from the calculation carried out with the problem data including their safety coefficients
Safety coefficient	❶(Sense 1) same as Overall safety factor ❷(Sense 2) = partial safety coefficient = minimum coefficient to be applied to the characteristic values
Safety factor	Same as safety coefficient
Safety margin	❶(Sense 1) same as overall safety factor ❷(Sense 2) Equation arising from the physical model, with the same form as ❶ but that can be applied to whatever variable value. In this sense, the margin can be a random variable ❸(Sense 3) same as partial safety coefficient ❹(Sense 4) same as reserve factor

Table 4 Definitions of safety terms from Ardillon et al. [2000]

2. A level 2 reliability approach assumes normal distributions to describe the load and capacity uncertainty. Within this approach values such as the mean, variance and covariance are sufficient to describe the system uncertainty. The notion of reliability index is introduced to measure the safety of the system. Compared to the level 1 approach, a level 2 approach, through the variance, provides a first quantification of uncertainty. However, for applications where normal distributions are not a good approximation (for example in case the tail effect is important) the approach can provide erroneous results.

3. To overcome the constraint of normal uncertainty distributions, in a level 3 approach the uncertainties are described by generalized probability distributions and the safety of the system is evaluated calculating the probability of failure implied by these distributions through eq. (1.1). The actual calculation is performed using simulating methods, such as Monte Carlo. The advantages of such approach are however balanced by the increased computational needs and the necessity to quantify the uncertainty distributions. This is the approach that we will follow.
4. Finally, the level 4 approach is a comprehensive approach that includes not only safety information, but also the economic aspects of the design. The approach suggests using an optimization process based on the maximization of a utility function. Some examples applied to the nuclear field, taking into account risk, economics, and stakeholder interest objectives in the utility function can be found in Pagani et al. [2004c] and Apostolakis et al. [2004].

1.3 An Example of Safety Margin in Nuclear Engineering

It is useful to show with an example drawn from the nuclear field the concepts of safety margin, characteristic values and how they are used in practice to determine the acceptability of a design.

We will focus on the Design Basis Accident (DBA) for a Loss of Coolant Accident (LOCA) in a light water nuclear reactor.

One of the requirements for this type of accident is that the peak cladding temperature (PCT) during the transient should be below 2,200°F [10 CFR Part 50.46].
Although the real value of capacity is given by the cladding temperature at which the cladding will actually fail and is not known, the chosen characteristic value is fixed by the regulations at 2,200°F. This value has been conservatively set so that the probability

of failure, if this limit is actually reached, will still be low, i.e., the characteristic value for the capacity corresponds to a low percentile of its epistemic distribution (Figure 14).

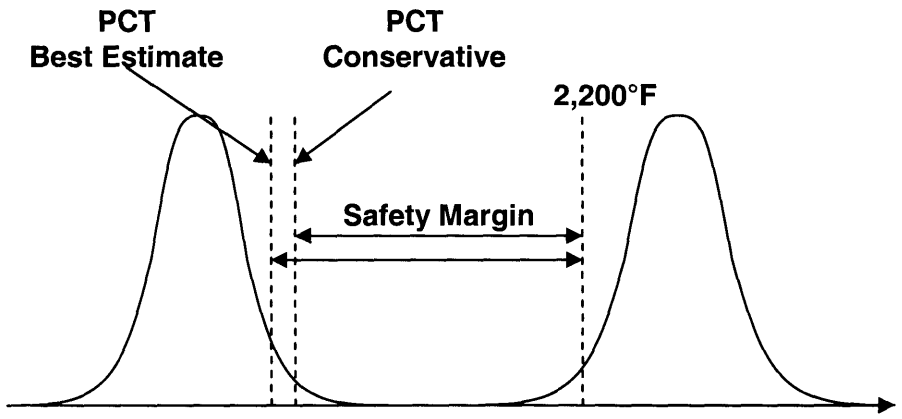

Figure 14 Example of uncertainty for the peak cladding temperature in a LOCA transient

To determine the load, two possible approaches can be used:

- A conservative approach
- A best-estimate approach

In the conservative approach, the models and parameter values to be used in the calculation of the PCT are specified in the regulations [10 CFR Part 50 Appendix K]. Conservative models and parameters are used so that the characteristic value of PCT is shifted toward a high percentile of the uncertainty distribution (Figure 14). A clear advantage of this approach is that it is not necessary to determine the shape of the uncertainty distribution, and the design is considered acceptable if the safety margin has a positive value.

On the other hand, in the best estimate approach [Boyack et al. 1989] the uncertainty on the calculated value of the PCT must be quantified, i.e. the uncerainty distribution has to be determined, and the 95th percentile be used as characteristic value to be compared with the 2,200°F limit.

Both approaches assure a sufficiently low value of the probability of failure by setting a high percentile for the calculated PCT and a low percentile for the limit, though they do it in a different way.

The conservative approach is actually a deterministic way to handle uncertainty. By appropriately defining conservative procedures to perform the calculations, the characteristic value of the load will correspond to a high percentile of the distribution, without actually specifying it, and the resulting failure probability will be very low. However, the concept of sufficient conservatism or sufficient margin is not quantified in this approach. The validity of the approach is justified from experience. The conservative assumptions resulted in satisfactory results in the past; therefore they are justified in current practice[4]. To maintain sufficient safety margins, this practice could easily lead to over-designing the Emergency Core Cooling System (ECCS) thus imposing unnecessary burden.

The best estimate approach makes a step further and quantifies the uncertainty distribution to determine the 95th percentile to be used as the calculated PCT. The advantage of this approach is a better understanding of the system uncertainties and a more optimal dimensioning of the ECCS[5]. This advantage is gained at the expense of a

---

[4] This aspect is developed well in an interesting discussion on the history of the safety margin and the historical concept of acceptable probability of failure in the aeronautical field in Long et al. [1999].

[5] It should be noted that, even if the quantification of the epistemic uncertainty were ideally performed, it should still be necessary to address the issue of incompleteness. This is done by

more complex approach to assess the uncertainty on individual parameters and models used and finally to propagate it to determine the uncertainty on the final PCT value.

While the best estimate approach constitutes an improvement compared to the conservative approach, it should be noted that it still relies on past experience to justify the choice of the 95th percentile as the appropriate characteristic level. This choice implies that a probability of exceeding the capacity characteristic value of 2,200°F lower than 5% is considered sufficiently low[6]. A further step would consist of calculating explicitly the probability of failure and implementing it in a probabilistic model of the whole system (such as a PRA). The concept of "sufficiently low" probability of failure would then be justified in light of its impact on the overall failure probability of the system (the Core Damage Frequency result in a PRA). The CDF value can then be interpreted as a final measure of the safety of the system.

---

adding conservatism in the best estimate approach by keeping the margin at a comfortable positive level and not allowing it to be zero (theoretically possible in the ideal case).

[6] This means that the actual probability of failure will be much lower than 5%, because the epistemic uncertainty on the limit should be taken into account also (remember that the characteristic value on the capacity is supposed to correspond to a low percentile of the capacity epistemic distribution).

PART II: A METHODOLOGY FOR THE QUANTIFICATION OF SAFETY MARGINS

2.1 Functional Failures

In the previous chapter, it was been shown that safety margins provide a measure of the distance between the characteristic values of load and capacity. However, the interpretations and implications of this measure depend on the nature of the characteristic values (for example whether they are median values as in Figure 8, or conservative values as in Figure 14) and on the amount of uncertainties associated as described by the shape of the uncertainty distribution.

The same value of safety margin can imply a lower probability of failure if conservative measures are used as characteristic values or if smaller uncertainty is associated with the load and capacity values . One of the objectives of reliability analysis is to assess the probability of failure of a system. Therefore, deterministic safety margins provide only part of the necessary information to completely identify the risk of a system[7]. The complete information is given by the actual probability of failure, i.e., the probability that the load will exceed the capacity.

The outcome of a given scenario is usually determined by deterministic thermal hydraulic calculations. The success being defined whenever the load does not exceed the capacity. To take into account the uncertainty in the deterministic calculation, it is possible to apply a reliability physics approach and calculate the associated probability that the load

---

[7] From the classification of reliability methods reported in Madsen et al. [1986] in fact (see paragraph 1.2), safety margins are identified as a Level 1 reliability approach, while the measure of the probability of failure is defined as a Level 3 reliability method, and lower level methods contain less information than higher level methods.

will exceed the capacity[8]. This event corresponds to a failure that will be referred to with the term **functional failure**[9]. The term functional failure has been borrowed from Burgazzi [2003] who uses it in the context of the assessment of passive system reliability. Assuming independence between load and capacity, the numerical value of functional failure probability can be calculated from eq. (1.1), given below as eq. (2.1).

$$P(L > C) = \int_{-\infty}^{\infty} [\int_{x}^{\infty} f_L(y \mid S)dy] f_C(x \mid S)dx \qquad (2.1)$$

where $f_C(c|S)$ and $f_L(l|S)$ are the uncertainty distributions on the capacity and on the load, conditional on the scenario S.

Let us consider the example of section 1.3 and assume a specific scenario, for instance described by the following sequence of events:

- Large break in the primary
- Loss of offsite power
- One ECCS train unavailable

Thermal hydraulic models can be used to simulate the behavior of the system in such situation and calculate the load (PCT). While the traditional approach would require the

---

[8] As will be described in more detail in the next chapter, the occurrence of different scenarios is modeled in the PRA with aleatory models. These models take into account the frequency of initiating events and the probability of failure of safety systems. The accident scenario frequency is the result of an aleatory model, and an epistemic uncertain distribution can be associated with its value.

[9] The load and capacity values are usually the result of deterministic calculations; no uncertainty is explicitly modeled in these calculations. The inclusion of epistemic and aleatory uncertainties makes it possible to calculate the probability of the load having a larger value than the capacity. A similar approach has been adopted to calculate the conditional failure probability of the containment in NUREG-1150.

calculation of a conservative value for the PCT, in the reliability physics approach the distribution on the load is calculated explicitly. Also, instead of using the conservative value of 2,200°F to define the capacity, a model for the strength of the cladding has to be used to calculate explicitly the uncertainty distribution on the capacity. The two distributions are then combined using eq. (2.1) to give the probability of functional failure. This estimate is conditional to the sequence of events described above and contains all information regarding the uncertainty in the models and parameters used.

2.2 Functional Failures and State of Knowledge

Uncertainties about the state of knowledge (epistemic uncertainties) affect scenario occurrences and functional failures differently. The occurrence of a scenario can be described with aleatory models of the world [Apostolakis 1995]. Epistemic uncertainty in the model would affect the value of the probability of occurrence. For scenario occurrences, there are two different tiers of uncertainty: the first tier, involving the aleatory model, and the second tier, involving the epistemic uncertainty in the model and its parameters. Functional failures, on the other hand, include both aleatory and epistemic uncertainties without distinction. If there were no epistemic or aleatory uncertainty, functional failures would be equal to zero[10].

For scenario occurrences, a more precise estimate of the failure probability results from an improved state of knowledge (this is plotted in Figure 15 as a shrinking in the uncertainty range for the probability estimate), while for functional failures, their probability will decrease (this is plotted in Figure 15 as an ever decreasing probability estimate).

---

[10] This assumes that the system has been well designed, i.e., the capacity is larger than the load. Otherwise, the probability of functional failure would be equal to unity.

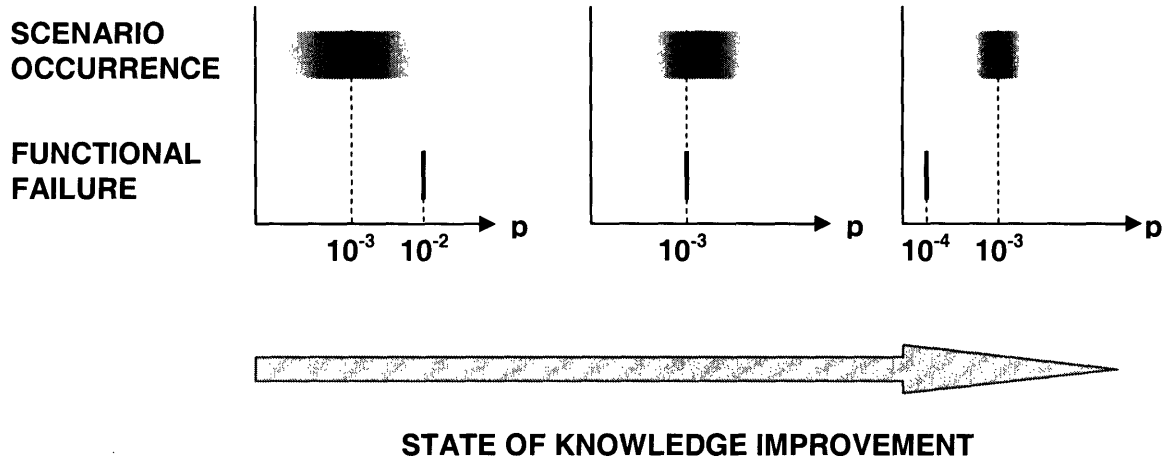

Figure 15 Effect of state of knowledge improvement on scenario occurrences and on functional failures. The shadowed area represents the uncertainty range on the value of scenario occurrence probability. An increase in the state of knowledge will reduce the uncertainty (represented by a shrinking gray area). The solid black line represents the value of functional failure probability. An increase in the state of knowledge will actually decrease the value of the functional failure probability (the deterministic models are less uncertain).

The above discussion shows that, while there is epistemic uncertainty in the value of the scenario occurrence probability, the value of the functional failure probability can in theory be determined with precision. No additional epistemic uncertainty should be associated with its value, because it is the epistemic uncertainty itself, together to the aleatory one, which determines it. A change in the epistemic distribution will translate into a different value for the functional failure probability.

2.3 A Methodology to Calculate Functional Failures

It is important to take into account contributions from both hardware and functional failures to evaluate the total reliability of a system. Although the contribution from other types of failure (such as hardware failures and human errors) is currently included and quantified in PRA, the contribution from functional failures is not. This difference arises from the fact that functional failures for systems that meet deterministic acceptance criteria, i.e., that have positive safety margins, are supposed to be equal to zero. Part III of the thesis will deal with the inclusion of functional failures in PRA models and the determination of a threshold criterion to assess their importance within an event tree.

A first step in including the contribution of functional failures into PRA is given by their quantification. Approaches targeted to the quantification of uncertainties have already been developed for some particular applications like LOCA calculations [Boyack et al. 1989] within the methodology known as Code Scaling, Applicability and Uncertainty evaluation (CSAU), and passive system reliability [Marques et al., 2004]. We will present in this section a methodology to quantify functional failures that develops the logic flow of the above approaches. The methodology is tailored to the calculation of functional failures with the objective to include them into the PRA.

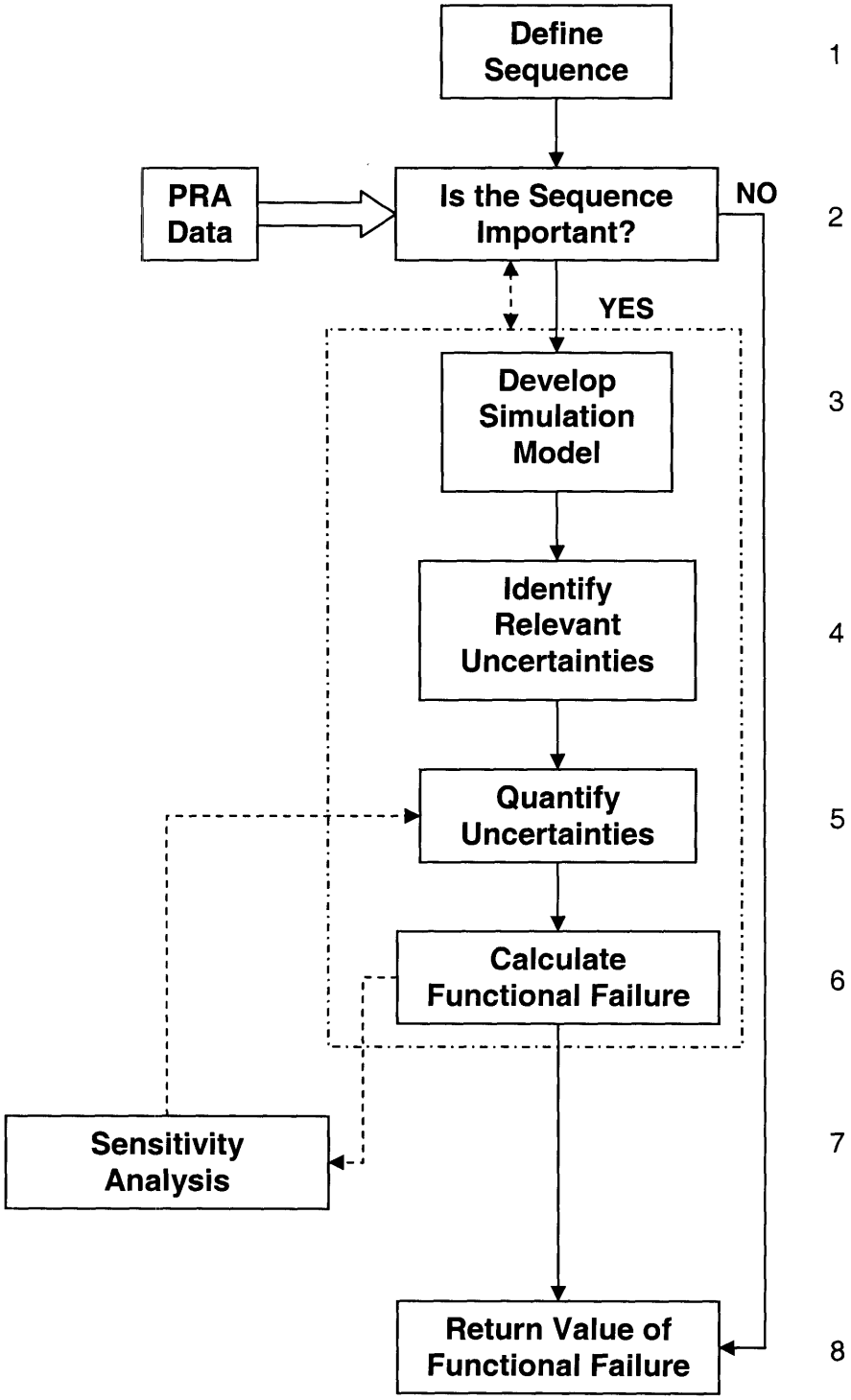

Figure 16 Flow diagram of a methodology to calculate functional failures

A flow diagram of the methodology is plotted in Figure 16. The methodology is composed by the following 8 steps:

1. **Define sequence.**

   In this step, the analyst defines the scenario to be evaluated. The scenario definition should contain all the information necessary to determine the loads and capacities. Since we are interested in quantifying functional failures with the objective to implement them into the PRA, a scenario will usually describe an accident sequence as it appears in an Event Tree.

2. **Determine the importance of the sequence.**

   In this step, a preliminary estimate of the functional failure value is performed. The estimate is used to determine whether the functional failure is negligible compared to other failures included into the PRA model. A decision criterion will be shown in Part III of the thesis.

   To perform this preliminary evaluation, it is necessary to do steps 3 to 6 (dashed area in Figure 16). However, while these steps are very demanding in terms of time and computational power, simplified models and approximate uncertainty evaluations can be used for this step[11]. While this step is not necessary, it is intended as a filter to select only the important sequences whose functional failures impact the result of the PRA and to analyze them in detail. The time spent in filtering the important sequences should pay off for the time that would have been needed if a detailed calculation of functional failures had been performed for all the sequences.

---

[11] A simplified evaluation of functional failure probability can be obtained for instance following the methodology reported in Chelemer et al. [1975]. A brief description of the process is given in Appendix C.

If the sequence is not important then the associated functional failure can be neglected and a value equal to zero is returned.

3. **Develop simulation model.**

   In this step, the model used to simulate the evolution of the loads and capacities during the sequence is developed (or chosen among existing ones). The model should be a best estimate model, so that uncertainties in the parameters can be propagated without the need to correct for conservative bias.

   The level of detail depends on the type of analysis performed. If a preliminary analysis to assess the relative order of magnitude of functional failure is to be performed, then simplified models or conservative models are sufficient for the task; otherwise, state of the art models could be necessary. Unfortunately, extremely detailed models are also extremely demanding in terms of computing time and a tradeoff should be made in view of the necessary calculations to be performed in step 6.

4. **Identify relevant uncertainties.**

   In this step, the relevant uncertainties must be identified. Uncertainties include parameter ranges and model uncertainties. Quantitative methods can be used to perform sensitivity analyses on the parameters to identify the most important uncertainties; however, the opinion of experts is always needed to make sure that all relevant phenomena are taken into account. The CSAU methodology proposes a structured methodology to collect and process expert opinion called Phenomena Identification and Ranking Table (PIRT) that can be used as a guidance for this task [Boyack et al. 1989].

5. **Quantify uncertainties.**

   In this step, the relevant uncertainties previously identified must be quantified. This means that uncertainty distributions for all relevant parameters and for the

model outputs must be determined. Uncertainty distributions have to reflect all the available information, including expert opinions, data from the same system and data from similar systems.

While classical statistical methods can be used to derive uncertainty distributions when large sets of data exist, this is rarely the case for very low probability events such as functional failures. In this case, the amount of observations is small or non-existent and different techniques, such as Bayesian estimation [Siu et al., 1998; Mosleh et al., 1985] and expert opinion elicitation [Mosleh, 1986; Zio et al., 1996; Budnitz et al., 1998] have to be used to derive the uncertainty distribution. The most important part of this step is to make sure that all available information is collected and represented in the uncertainty distributions. Ideally, particular attention should be focused on the determination of the tails of the uncertainty distributions, because for low probability events the tails are the part of the distribution determining the final result. Unfortunately, most of the time this is not possible and assumptions have to be made regarding the shape of the uncertainty distribution for practical purposes.

6. **Calculate functional failure.**

Once a simulation model has been developed and all relevant uncertainties have been quantified it is possible to propagate the uncertainties of the load and capacity values and to calculate the probability that the former will exceed the latter.

Various techniques can be used to perform this task ranging from crude Monte Carlo algorithms to complex variance reducing techniques[12] or approximate methods such as the response surface methodology. The main issue is the fact that a reliable probability estimate requires a large number of simulations (on the

[12] A variance reducing technique based on the coupling of importance sampling and stochastic search of the optimal sampling point has been developed and used for the GFR case study. The development of this technique can be found in Appendix A.

order of 100,000 or more) and this is time demanding for thermal hydraulic codes that can take hours to perform a single simulation.

One of the widely used techniques is the response surface methodology where a small number of model simulations are performed and the output of the model is approximated through a fitting surface. Then, Monte Carlo calculations are performed using the response surface rather than the original model, resulting in a faster but also more approximate calculation.

7. **Sensitivity analysis.**

The shape of the uncertainty distributions determined in step 5 can affect the final results. Therefore, it is useful to perform sensitivity analyses to assess the impact on the functional failure probability of different uncertainty distributions.

Advanced techniques should be used as much as possible to make use of the information already collected in step 6 and avoid repeating the calculations from scratch.

It should be noted, however, that the sensitivity analysis should not be interpreted as an uncertainty assessment of the uncertainty distributions, because, as already discussed in the previous section, any uncertainty should already be included in the uncertainty distribution. The added value of sensitivity analyses can be seen in determining the value of information derived from an increase in the state of knowledge. The analysis should be used to answer the question: "What would happen if this new information were available and the uncertainty distribution were updated?" In this context, sensitivity analysis would allow different competing improvements to be ranked to make a decision to allocate resources.

8. **Return value of functional failure.**

The calculated probability of functional failure is included in the PRA to obtain a more reliable assessment of the risk of the system. The correction due to the

inclusion of functional failures in the PRA can be important. Examples of calculations will be provided in the GFR case study.

The main drawback of the above or similar approaches is that the number of necessary calculations (step 6) is in the order of 100,000 or more and requires a considerable time. To overcome this issue two different ways can be followed:

- Fit the thermal hydraulic model results and use the fitting function to accelerate the calculation procedure, using a method like response surfaces.
- Approximate the thermal hydraulic model used to simulate the system.

The first approach (response surface) is the one used in Boyack et al. [1989]. The main issue is that the response surface represents only an approximation of the original model output and the type of parametric form for the fitting surface largely affects the approximation. The precision of the simulating model is then lost in the surface approximation. Also, the type of approximation induced by the fitting surface is not easily quantifiable. The approach is similar to a black box that approximates the original result but gives no information regarding the type and magnitude of the errors introduced. It would be more desirable, then, to decrease the level of detail of the simulating model (second approach) and to use it directly coupled with an efficient Monte Carlo method. The advantage of this approach is given by the fact that the approximations induced by the simplified model are controlled by the analyst, therefore easier to identify than the ones induced by the response surface. This second type of approach has been chosen in the GFR case study, where a simplified thermal hydraulic model has been coupled with an efficient Monte Carlo technique. The particular Monte Carlo technique is presented in Appendix A.

PART III: INCLUSION OF FUNCTIONAL FAILURES IN PRA

In Part I of the thesis it has been shown that a way to quantify safety margins within a risk related framework is to explicitly calculate the probability of functional failure associated with them. In Part II, a methodology for the calculation of functional failure probabilities has been introduced, together with a discussion regarding practical aspects of its implementation. In this chapter, the effects of functional failures on PRA results are evaluated and a criterion to determine their importance is given. This criterion can be used as a filter in step 2 of the methodology plotted in Figure 16.

3.1 PRA Architecture and Acceptance Criteria

The purpose of a Probabilistic Risk Assessment (PRA) is to identify and quantify different failure modes of an engineering system and to quantify the risk importance of its components. The first study of this kind was directed by Professor Rasmussen in 1975 [Rasmussen 1975]. The PRA is organized in **Event Trees** (ET) that represent the possible sequences of events that could lead to accident. An example of an ET is plotted in Figure 17.

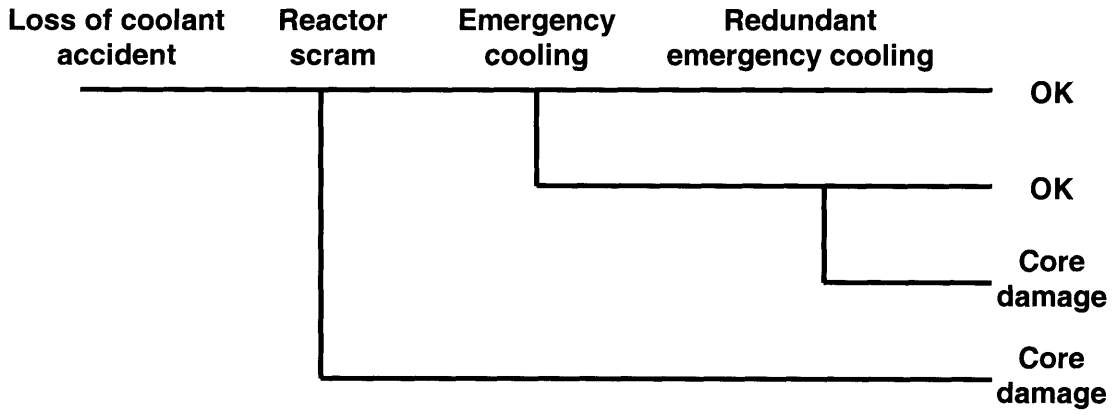

Figure 17 Simplified event tree for a loss of coolant accident

The ET has to be read from left to right, following the chronology of the accident sequence. An ET begins with an **Initiating Event** (IE). These events are those events that are likely to lead to core meltdown, either directly or as a result of the failure of safety systems. Examples are earthquakes, pipe breaks, or spurious boron injections. Each branching node in the ET represents the possible outcomes or states associated with safety systems or operator actions. By definition, the upper branch refers to the correct functioning of the safety system or correct operator action. The lower branches represent a failure in the system or a wrong action by the operator. The probability associated with each branch is calculated through appropriate **Fault Trees** (FT) modeling the reliability behavior of the safety systems or human actions. An ET represents all relevant scenarios that can happen following the IE, the potential failures being taken into account through the branching nodes. At the end of each sequence the resulting outcome is reported.

The above type of representation is not unique, but the architecture of the ET is particularly useful for communication purposes. The visualization of the chronology of the possible accident sequences within an ET is very useful to understand the dynamic of an accident.

The total risk of the plant is defined as the probability of having an undesirable outcome and can be easily calculated adding together the probability of occurrence of each sequence leading to an undesired outcome. It should be noted however that the information regarding the probability of a sequence and regarding the outcome of a sequence are of different nature. The probability of occurrence is by its own nature probabilistic. It derives from stochastic models for the failure of safety systems or from stochastic models for human reliability. On the other hand, the outcome associated with a sequence is the result of a deterministic calculation (usually a thermal hydraulic calculation) and does not contain explicitly any probabilistic information.

The outcome of a sequence is defined to be acceptable if the simulation determines that the **acceptance criteria** are met. Acceptance criteria are the limits established for specific parameters to ensure that critical safety functions, such as the cooling of the core and reactivity control are met[13]. An example of acceptance criteria for a LOCA sequence is to maintain the cladding temperature below 2,200°F and to limit the oxidation of the cladding to 17% of its thickness.

Given the deterministic nature of the above limits, safety margins have a direct connection with acceptance criteria. If safety margins are positive, then the acceptance criteria are met. However, it has been mentioned in the previous chapters that there is always the possibility of functional failures, even in the presence of positive safety margins, especially if the uncertainties on the load or capacity are large. The deterministic approach used in current PRAs is equivalent to assume a zero probability of functional failure whenever the margins are positive and a probability of functional failure equal to one whenever the margins are negative. The first approximation introduces optimism into the PRA, by neglecting the role of functional failures and their potential impact on the plant total risk. The second approximation, on the contrary, introduces conservatism in the calculations by assuming a failure as soon as the margins assume a negative value.

3.2 Inclusion of Functional Failures into the PRA

To include functional failures into the PRA, it is necessary to take into account the possibility of a failure even when the acceptance criteria are met and the possibility of success even when the acceptance criteria are violated. The magnitude of the correction will depend both on the value of the functional failure probabilities and on the sequence

---

[13] A more detailed discussion and a practical example of acceptance criteria and critical functions can be found in the AP1000 Probabilistic Risk Assessment [Westinghouse, 2004].

probabilities of occurrence. It is useful to show with a numerical example the impact of the correction.

3.2.1 Numerical Example (LOCA in a PWR)

For the numerical example it is necessary first to quantify the failure probabilities of the safety systems that define every branching node. Realistic values for these failure probabilities are shown in Figure 18 together with the yearly frequency for the IE.

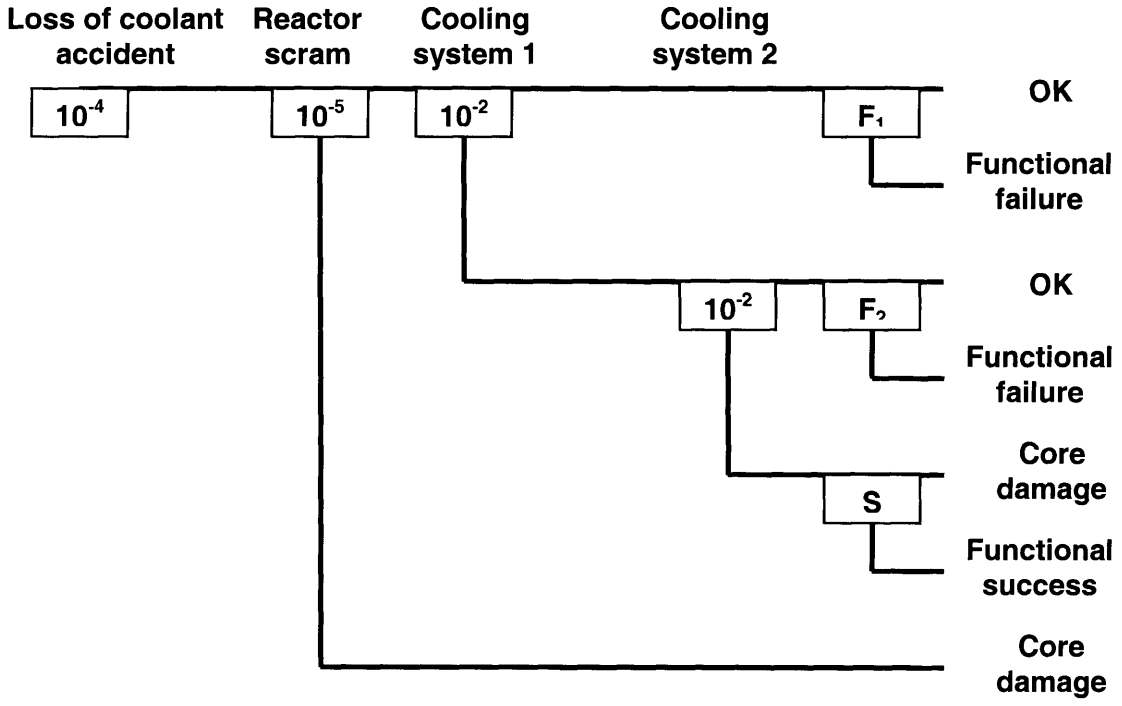

Figure 18 Simplified event tree with probabilities of failure. Branching representing functional failures and success are included.

The risk of the plant, neglecting functional failures can be written as

$$P = 10^{-4}[10^{-5} + (1-10^{-5})10^{-2} \cdot 10^{-2}] \approx 1.1 \cdot 10^{-8} \qquad (3.1)$$

If the impact of functional failures is included then the result of (3.1) has to be modified to[14]

$$P = 10^{-4}\left(10^{-2}\cdot 10^{-2} + 10^{-5} + (1-10^{-5})(1-10^{-2})F_1 + (1-10^{-5})(1-10^{-2})10^{-2}F_2\right) \approx$$
$$\approx 10^{-4}\left(10^{-2}\cdot 10^{-2} + 10^{-5} + F_1 + 10^{-2}F_2\right) \quad (3.2)$$

To obtain reasonable values for F_1 and F_2, the results of Depisch et al. [1998] have been used. From the work of Depisch et al. the probability of functional failure for a LOCA sequence in a PWR assuming one safety system failure results to be in the order of 10^{-4}. This value can be used for F_2, while a smaller value should be used for F_1 (a tenth of F_2 will be used). Substituting these numerical values into (3.2) it is possible to obtain

$$P \approx 10^{-4}\left(10^{-2}\cdot 10^{-2} + 10^{-5} + 10^{-5} + 10^{-2}\cdot 10^{-4}\right) = 1.21\cdot 10^{-8} \quad (3.3)$$

The impact of functional failures has been to increase the risk estimate by 10%. In this example, the impact on the original estimate is relatively small, especially considering that the epistemic uncertainties associated to this value have usually an error factor of 2 or 3.

3.2.2 Numerical Example (Passive System)

The numerical example of the previous section shows that a detailed analysis, such as the one proposed in Figure 16, is not adding useful detail to the PRA for the LOCA sequence of a current PWR. However, it is possible to identify sequences where the inclusion of functional failures will have an important impact on the PRA results.

---

[14] While we include the impact of functional failures, we neglect the impact of the functional success. This is due to the fact that the probability of success with no emergency cooling systems available is assumed to be zero. The choice of not including functional successes results in a more conservative estimate of the plant risk.

Figure 19 considers the example of a passive cooling system. The passive system probability of failure is negligible, because it has no active mechanical equipment; therefore the frequency of occurrence of core damage, without considering functional failures is equal to

$$P = 10^{-4} \cdot 10^{-5} = 10^{-9} \tag{3.4}$$

However, the inclusion of functional failures changes completely the results. Considering a value of functional failures equal to 10^{-2} (realistic considering the uncertainty associated with passive systems [Burgazzi, 2003, 2004, and Marques 2004]) the frequency of occurrence of core damage increases to

$$P = 10^{-4}\left(10^{-5} + (1-10^{-5})F_1\right) \approx 10^{-6} \tag{3.5}$$

The increase in the failure frequency has been 1000-fold. In this case the inclusion of functional failures in the plant PRA would have certainly added additional information.

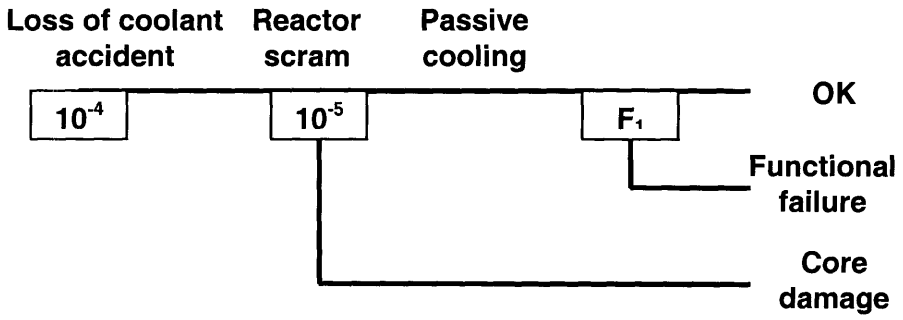

Figure 19 Simplified event tree for a passive cooling system

3.3 Filtering Criterion

A criterion to determine the importance of the impact of functional failures in a sequence can be developed as follows (Figure 20).

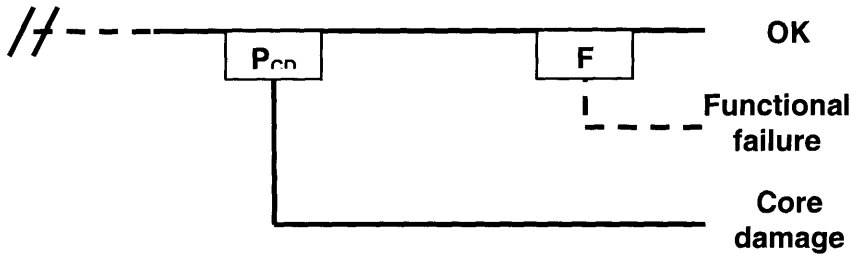

Figure 20 Filtering criterion to determine the importance of functional failures

Figure 20 shows the ET to the right of a generic cut point. The sequence is supposed to lead to a success if no additional failures occur. The branch leading to core damage is supposed to represent the collapsed branches leading to core damage in the original ET. Therefore, the probability P_{CD} is equal to the probability of having core damage (regardless of the subsequence followed). It is then possible to determine the impact of the functional failure and to compare it to the original result to determine its importance. The impact of the functional failure will be negligible if

$(1 - P_{CD})F << P_{CD}$ or, using the rare event approximation $F << P_{CD}$

(3.6)

Therefore, the probability of functional failure associated with a branch has to be compared with the probability of core damage due to all other causes (hardware failures and human failures). Calculating the probability of core damage (P_{CD}) from the PRA, and obtaining a first estimate of the probability of functional failure with a simplified

analysis such as the one proposed in Appendix C, it is possible to find branches, i.e. sequences, that have a large impact. For these sequences a detailed analysis can be performed to estimate a realistic value of functional failure probability.

From (3.6) it appears that for sequences that rely heavily on active components (have large P_{CD} values) functional failure impact will likely be negligible. On the other hand, for those reliable systems that have low P_{CD} value and at the same time have a large uncertainty, the impact of functional failures can be important. An example is given by passive systems that are very reliable, from the hardware point of view, and at the same time can suffer from high state of knowledge uncertainty.

3.4 Epistemic Uncertainty and Functional Failures

In this section we investigate how epistemic uncertainties propagate whenever functional failures are included into PRA. We are going to analyze the three different cases plotted in Figure 21. The first case represents a generic event tree where functional failures are neglected. The second case represents an event tree where functional failures are considered. The third case represent an event tree where, in addition to functional failures, also the possibility of success if the acceptance criteria are not met is considered. We will call this event a functional success. In all three cases we assume that the initiating event happened, i.e. we are interested in the conditional core damage probability.

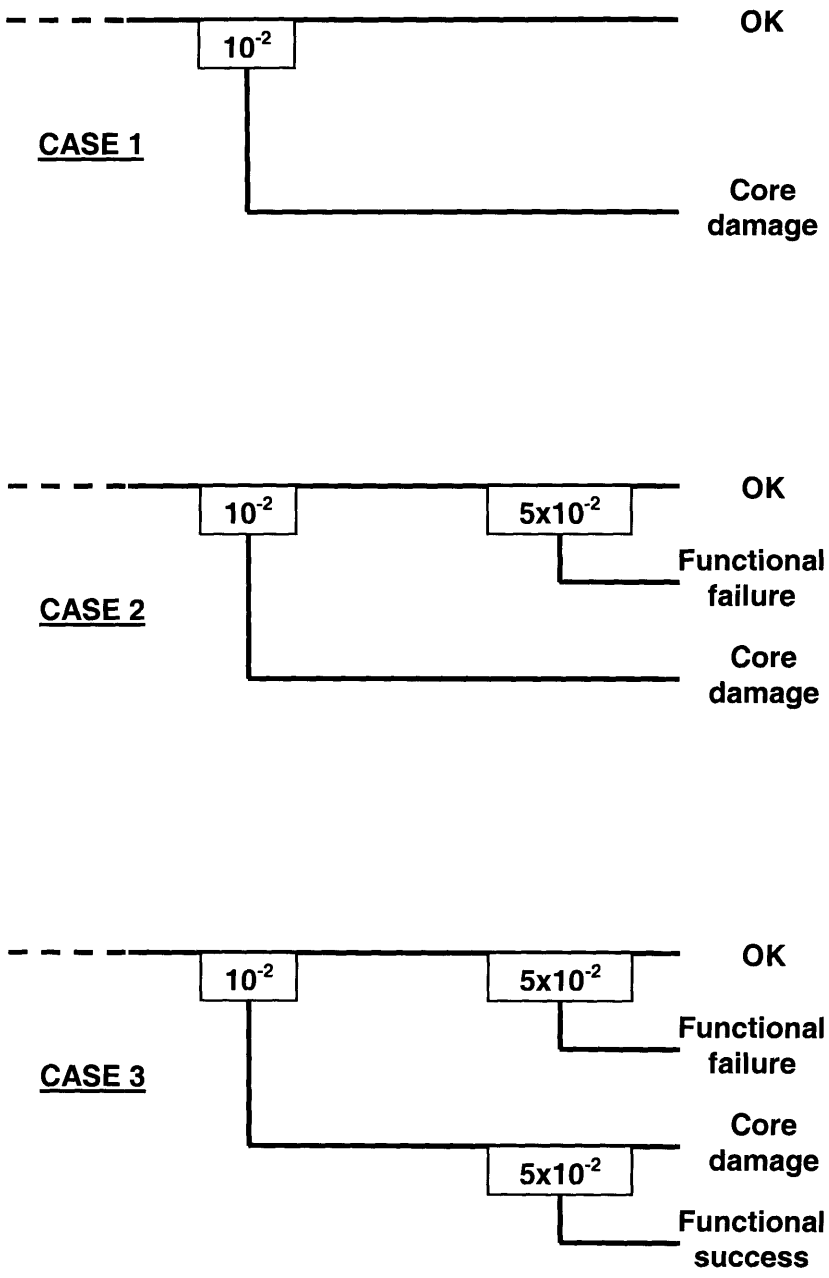

Figure 21 Event trees used for the uncertainty propagation analysis

There are two types of epistemic uncertainty that affect the results of the PRA. The first epistemic uncertainty is on the numerical values of the components failure probabilities or on the initiating events frequencies. This is quantified with distributions describing the current state of knowledge. The second uncertainty is on the final event tree outcomes. The possible outcomes of the sequences are success or core damage. Whenever acceptance criteria are met it is assumed that success will occur, while if acceptance criteria are not met it is assumed that core damage will occur. This is equivalent to say that the outcome point estimate for acceptance criteria that are met is success and the point estimate for not meeting acceptance criteria is core damage. However, we have seen in the previous chapters that there is always the possibility that even if acceptance criteria are met core damage will ensue and vice versa. To take this uncertainty into account functional failures and functional successes have to be included. Therefore, the inclusion of functional failures is actually the result of propagating the epistemic uncertainty on the outcomes. The relationship between initiating event frequencies, component failure probabilities and outcomes is summarized in Table 5.

	Initiating Event	**Hardware Failure**	**Functional Failure**	**Functional Success**
Point estimate	Frequency (e.g. 10^{-4} per year)	Component failure probability (e.g. 10^{-2})	Success	Core damage
Possible values	Any positive numerical value	Any value in the interval [0,1]	- Success - Core damage	- Success - Core damage
Epistemic uncertainty	Distribution of positive values	Distribution of values between [0,1]	Probability of the core damage event (functional failure probability)	Probability of the success event (functional success probability)

Table 5 Relationship between epistemic uncertainty on initiating event, hardware failure, functional failure, and functional success.

Let us now calculate the resulting conditional core damage probability for the three cases plotted in Figure 21 and see how the epistemic distributions on the core damage probability look like. The point estimate for the safety system failure probability is assumed to be 10^{-2}; we further assume the epistemic uncertainty on this value to be described with a lognormal distribution with error factor equal to 2 and a value for the functional failure and functional success probabilities equal to 5%. By performing a Monte Carlo simulation to propagate these uncertainties we obtain the histogram plotted in Figure 22.

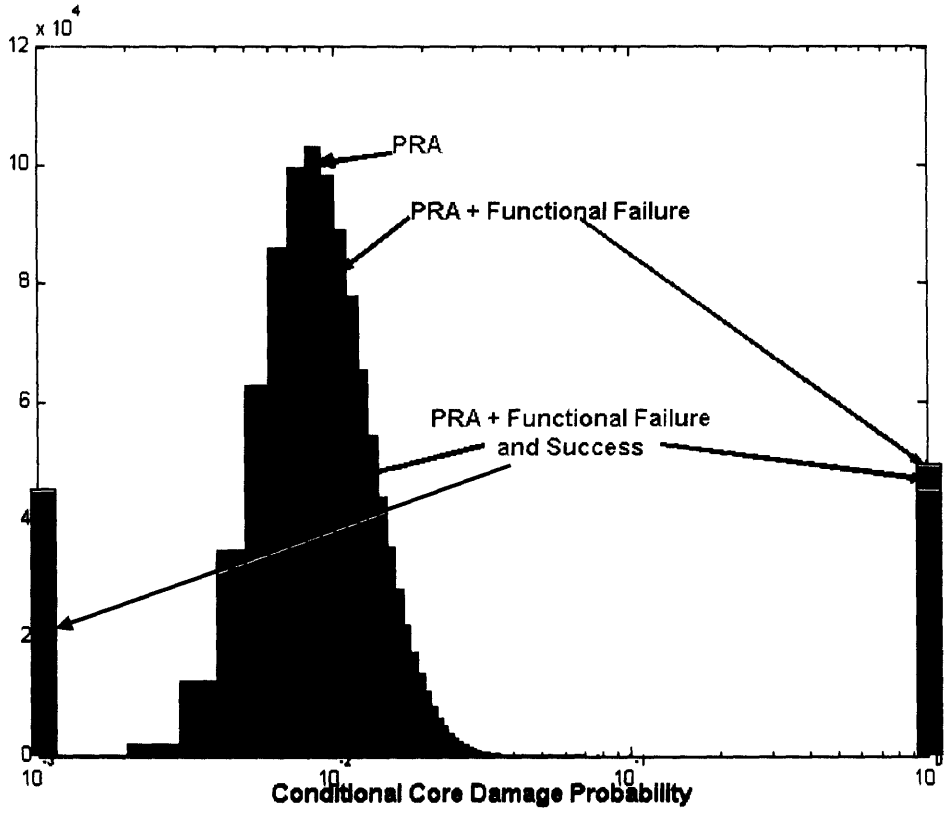

Figure 22 Histogram results of 1,000,000 Monte Carlo simulations propagating the epistemic uncertainty with functional events included

The histograms in Figure 22 represent the epistemic distribution on the condition core damage probability value. The area under the three curves is the same, but the inclusion of functional failures and successes introduces spikes at the zero and unity values.

For case 1 (PRA), the conditional core damage probability is continuously distributed around the value 10^{-2} as expected. If we include the functional failure (case 2, or PRA + Functional Failure), then we are considering the possibility that even if the safety system works there could be core damage. This possibility results in a conditional core damage probability value that can assume the value of unity (in case core damage results even if acceptance criteria are met). The spike in the histogram represents this event. Finally, in case 3 (PRA + Functional Failure and Success), also the functional success is considered, therefore, it is also possible that there will never be core damage (in case success results regardless of the fact that acceptance criteria are met or not). This is represented by the additional spike at the value of zero in the histogram.

PART IV: FUNCTIONAL FAILURES IN A PASSIVE SYSTEM

4.1 Introduction

In this part of the thesis a case study regarding the quantification of functional failures in a cooling passive system for a Gas-cooled Fast Reactor (GFR) is presented. The results of this chapter are also presented in a paper by Pagani et al. [2004a].

In this chapter, a case study involving natural convection cooling in a GFR under post-LOCA condition is analyzed to quantify the role of functional failures. After the introduction, the model used in the case study is presented, and the numerical results from the methodology presented in Part II are shown. These results are obtained by propagating the uncertainties through the Monte Carlo method with importance sampling presented in Appendix A. A discussion of the numerical results, including a comparison between the passive design and an active design is provided at the end of the chapter.

4.2 System description and operating conditions (Step 1)[15]

The reactor used in the case study is a 600MW GFR cooled by helium flowing through separate channels in a silicon carbide matrix core. This design has been the subject of study in the last several years at the Massachusetts Institute of Technology within the framework of the I-NERI project "Development of GEN IV Advanced Gas-Cooled Reactors with Hardened/Fast Neutron Spectrum". The studies by Okano et al. [2002], Eapen et al. [2002], and Williams et al. [2003] have confirmed the possibility of using natural circulation to remove the decay heat in case of an accident. A number of identical loops have been considered in the analysis. In addition to the passive system, which

[15] The step number in reported in parenthesis refers to the methodology presented in Part II and diagrammed in Figure 16

operates in natural convection at 1.65MPa, an active version with blowers providing the necessary flow rate and operating at atmospheric pressure has also been considered.

In case of a LOCA, long-term heat removal is assured by forced (in the active system) or natural (in the passive system) circulation in each loop. To achieve the high pressure necessary for natural circulation, the primary system is contained in a guard containment designed to maintain the necessary pressure.

A GFR decay heat removal configuration is shown schematically in Figure 23, where only one loop out of N is shown. The hot gas (helium) from the reactor core proceeds through a top reflector and chimney to the inner coaxial duct and then upwards to the hot plenum of the Emergency Cooling System (ECS) Heat Exchanger (HX), where it transfers heat to naturally circulating water on the secondary side. Cold gas from the HX flows down through a check valve to the outer coaxial duct, which brings it back to the reactor vessel where it proceeds through the downcomer back to the core as indicated by arrows. A check valve is installed (item 15 in the figure) to prevent backflow through the ECS HX during normal operation. A blower is mounted in the downcomer below the HX to provide cooling during shutdown since the safety grade ECS HX is used for both shutdown cooling and post LOCA heat removal. The blower can also be used for forced circulation in post LOCA scenarios, but is not credited for passive decay heat removal.

To achieve a sufficient decay heat removal rate by natural circulation, it is necessary to maintain an elevated pressure even after LOCA. This is accomplished by a guard containment, which surrounds the reactor vessel and power conversion unit and holds the pressure at a level that is reached after the depressurization of the system.

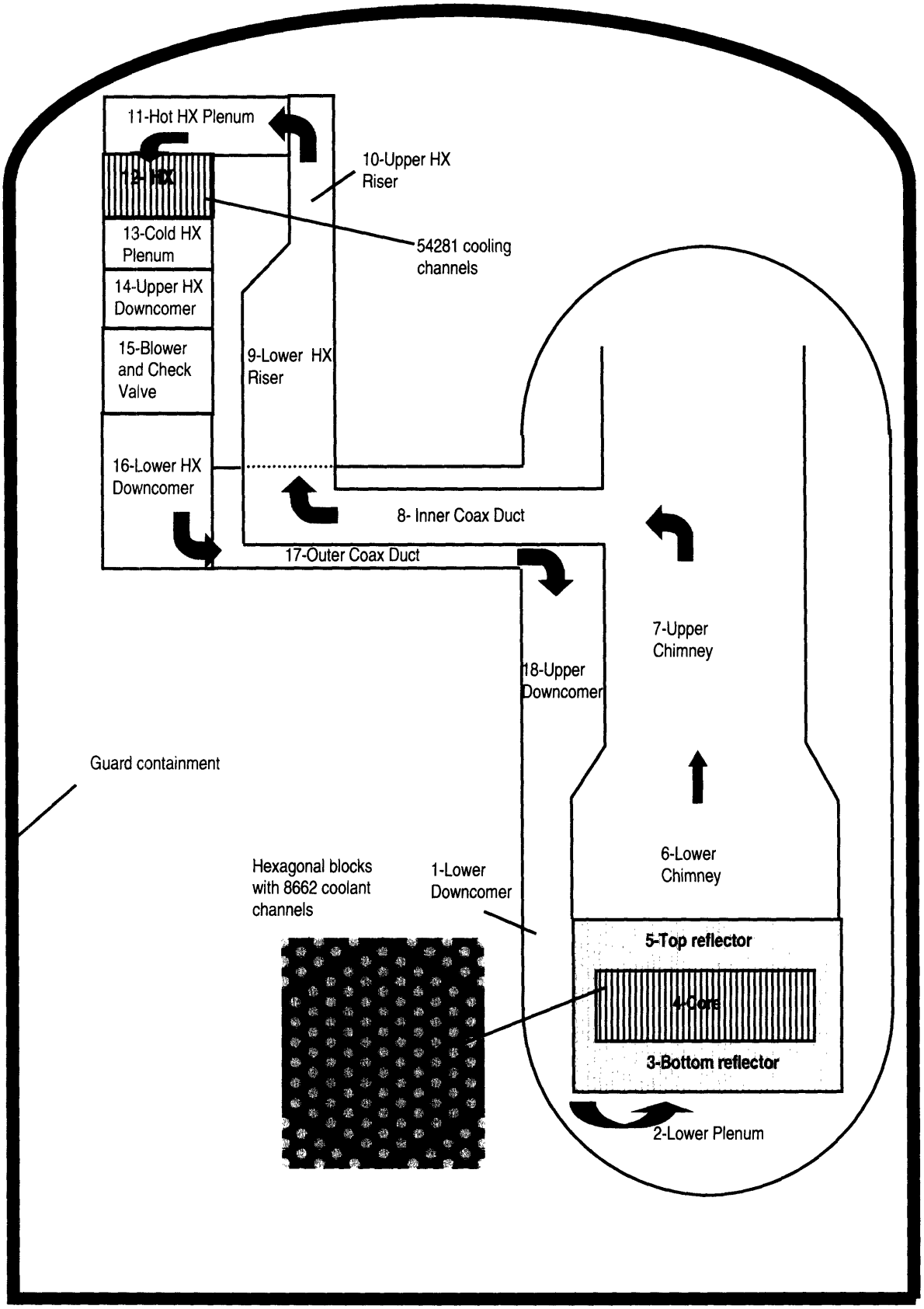

Figure 23 Schematic of GFR Decay Heat Removal Loop

The average core power to be removed is assumed to be 12 MW, equivalent to 2% of full reactor power (600 MW). Thus, significant reduction in decay heat would have to happen before reaching this scenario[16]. To guarantee natural circulation cooling at this power level, a pressure of 1,650kPa is required[17].

The multiple loops are identical in geometry and characteristics. The secondary side of the cooler is assumed to have a constant wall temperature of 90°C.

The design is dimensioned so that only two loops will be sufficient to cool the core (50% loops). The loop dimensions have been selected so that the design satisfies the requirements to keep the calculated outlet temperature below 1,200°C in the hot channel and 850°C in the average channel. The geometry of the design is reported in Table 6, where section numbers in the first column correspond to the flow path numbers on Figure 23.

It is important to note that the subject of the analysis will be the quasi-steady state natural convection cooling (or active if blowers are used) that takes place after the LOCA transient has occurred. The measures that will be calculated in the following sections refer to this steady state period and are conditional on the successful inception of natural convection. Therefore, the analysis does not take into account the failure probability of not starting natural convection or the probability of failure to build up and maintain a high pressure level in the guard containment.

---

[16] This reduction will be due to heat storage in core materials, helium from accumulators and a short time cooling safety system, before natural circulation can be established.

[17] During normal operations there is atmospheric pressure inside the guard containment.

Section	Hydraulic Diameter [m]	Flow Area [m^2]	Length [m]	Height [m]	K-loss coefficient	Roughness [m]
1	0.6	7.2571	7.7	-5.3	1	4.50E-05
2	7.4	43.008	1	0.5	0	4.50E-05
3	0.0145	1.65E-04	1	1	0.5	1.00E-05
4	0.0145	1.65E-04	1.7	1.7	0.25	1.00E-05
5	0.0145	1.65E-04	1	1	1	1.00E-05
6	7.4	4.30E+01	3	3	0	4.50E-05
7	5.4	2.29E+01	6	6	0.1	4.50E-05
8	0.8	5.03E-01	4	0	1.23	4.50E-05
9	1	2.24E+00	2	2	0	4.50E-05
10	1.6364	5.40E+00	1.5	1.5	0.1	4.50E-05
11	0.15	1.35E+00	1.25	-0.5	0.23	4.50E-05
12	0.003055	9.81E-06	0.3	-0.3	1.23	1.00E-05
13	0.15	1.35E+00	1.25	-0.2	1	4.50E-05
14	1.526	8.20E+00	1	-1	0	4.50E-05
15	1	3.76E+00	3	-3	13.23	4.50E-05
16	1.526	8.20E+00	1	-1	0	4.50E-05
17	0.25	3.63E-01	3	0	1	4.50E-05
18	2.0253	2.29E+00	5.4	-5.4	0.5	4.50E-05

Table 6 Geometry of the system

The loop geometry begins at section #7 and ends at section #18

4.3 Thermal Hydraulic Model (Step 3)

To simulate the steady state behavior of the system a thermal hydraulic code developed at MIT [Williams et al. 2003] has been used[18]. This code treats all multiple loops as identical. The whole loop is subdivided in sections that are defined by their length, hydraulic diameter, area, height, form loss coefficient, and roughness. The heater (reactor core) and cooler (heat exchanger) sections have been further subdivided into separate nodes to calculate the temperature and flow gradient with sufficient detail (40 nodes have been used for this analysis). Both the average and hot channel are modeled in the core, so that the increase in temperature in the hot channel due to the radial peaking factor can be calculated.

To obtain a steady state solution, the code balances the pressure losses around the loop so that friction and form losses are compensated by the buoyancy term, while at the same time maintaining the heat balance in the heater and cooler. The heat balance between the inlet and outlet of every node is calculated through equation (4.1)

$$\dot{Q}_i = \dot{m}_i c_{p,i} (T_{out,i} - T_{in,i}) = S_i h_i (T_{wall,i} - T_{bulk,i}) \tag{4.1}$$

where $\dot{Q}_i$ is the heat transferred [kW], $\dot{m}_i$ is the mass flow rate [kg/s], $c_{p,i}$ is the specific heat at constant pressure [kJ/kg°K], T_i is the temperature in degrees Kelvin (measured at the outlet, at the inlet, at the wall channel, and at the coolant bulk), S_i is the heat exchanging surface [m^2], and h_i is the heat transfer coefficient [kW/m^2°K]. The index i refers to the different sections. Equation (4.1) states the equality between the enthalpy increase between the flow at the inlet and the flow at the outlet in any section (first

[18] The original thermal hydraulic code was developed in Fortran. The author has modified and improved the code using MatLab. The MatLab version can be found in Appendix.

equality) and the heat exchange between the channel wall and the bulk of the coolant (second equality).

The heat transfer coefficient (h) is a function of fluid characteristics and geometry and is calculated through appropriate correlations covering forced, mixed, and free convection regimes in both turbulent and laminar flow including transitions between individual regimes and flows, as reported in Williams et al. [2003 and 2004]. Different Nusselt number correlations are used in the different regimes to obtain a value for the heat transfer coefficient[19].

The mass flow rate is determined by a balance between buoyancy and pressure losses following equation (4.2)[20]

$$\sum_i [\rho_i g H_i + f_i \frac{L_i}{D_i} \frac{\dot{m}^2}{2\rho_i A_i^2} + K_i \frac{\dot{m}^2}{2\rho_i A_i^2}] = 0 \qquad (4.2)$$

The index i refers to the different sections, ρ is the coolant density [kg/m^3], H is the height of the section [m], f is the friction factor, L is the length of the section [m], D is the hydraulic diameter of the section [m], $\dot{m}$ is the mass flow rate [kg/s], A is the flow area of the section [m^2], and K is the form loss coefficient.

Equation (4.2) states that the sum of buoyancy (first term), of friction losses (second term), and of form losses (third term) should be equal to zero along the closed loop.

---

[19] The correlations are reported in Williams et al. [2003] pages 24-39.

[20] Acceleration losses are not considered in the equation because they cancel out over a closed loop. They are considered only to determine the flow split between the hot and the average channel.

The summation is carried over all sections and over individual nodes for the heater and cooler. The friction factor (f) is a function of the fluid characteristics and geometry and is calculated using appropriate correlations [Williams et al. 2003, pages 15-24]. An iterative algorithm is used to find a solution that satisfies simultaneously the heat balance and pressure losses equations.

4.4 Uncertainties (Step 4 and 5)

The thermal-hydraulic model used to find the steady-state solution is a simplified description of what happens in reality. The correlations it uses are subject to prediction errors. That is, the results of the correlations are subject to errors

$$y = f(x)\varepsilon \tag{4.3}$$

where y is the real value of the quantity to be predicted (h or f), $f(x)$ is the result of the correlation, and ε is the prediction error. This error is modeled as being normally distributed with mean value equal to unity and standard deviation to be determined below. This error represented in equation (4.3) is commonly classified as *model uncertainty* [Apostolakis, 1999]. It is present because the correlations are approximate. Also, some uncertainty exists regarding the value of *parameters* such as the power level, the pressure in the guard containment, and the wall temperature in the cooler. Both model and parameter uncertainties are epistemic (or, state-of-knowledge) uncertainties, and are meant to describe our current state of knowledge through probability distributions [Apostolakis, 1990, 1995, 1999, and Winkler 1996]. The epistemic probability distributions used in our study are normal distributions whose mean value corresponds to

the nominal value and whose standard deviation is proportional to the estimated uncertainty[21].

The uncertainties regarding parameter values are the following:

- Power, with an estimated standard deviation of 1%
- Pressure, with an estimated standard deviation of 7.5%
- Cooler wall temperature, with an estimated standard deviation of 5%

The factor ε that represents model uncertainties is assumed to be normally distributed with mean value equal to unity (as stated above) and standard deviation as follows:

- Nusselt number in forced convection: standard deviation equal to 5%
- Nusselt number in mixed convection: standard deviation equal to 15%
- Nusselt number in free convection: standard deviation equal to 7.5%
- Friction factor in forced convection: standard deviation equal to 1%
- Friction factor in mixed convection: standard deviation equal to 10%
- Friction factor in free convection: standard deviation equal to 1.5%

The choices are elaborated on below.

4.4.1 Power

According to industry practice and experience, an error of 2% is usually considered in the determination of the power level, due to uncertainties in the measurements. Assuming

---

[21] The choice of normal distributions is mainly driven by the fact that the calculations involved in the particular Monte Carlo algorithm we use are simplified using normal distributions. However, one problem of using normal distributions is that negative values of the parameters are possible. We overcome this difficulty by cutting off the tail of the distribution so that only positive values are considered. This trick does not affect the results because negative values are at least ten standard deviations removed from the mean.

that this error defines the 95% confidence interval[22] we have accordingly set the standard deviation equal to 1%.

4.4.2 Pressure

The system pressure before the accident is kept by the control system within a small percentage of the nominal value. However, the post-LOCA conditions are determined not only by the pressure level in the primary system and guard containment before the accident but also by the energy stored before the accident, the energy absorbed by surrounding materials, the dynamics of the accident, and by the leakage rate of the gas from the guard containment. All these uncertainties accumulate in the final pressure value in the guard containment. Therefore, its uncertainty in post-LOCA conditions should be relatively large and the 95% confidence interval has been set to ±15%.

4.4.3 Cooler Wall Temperature

The model uses the inner wall temperature in the cooler as a boundary condition. Water with inlet and outlet temperatures of 25°C and 85°C, respectively is proposed as the secondary cooling medium. The design of secondary cooling system has not been finalized, hence a uniform inner wall temperature of 90°C was used in the model as a first approximation. Independently of the detailed design of the water cooling system, this wall temperature will carry uncertainties stemming from fouling of heat transfer surfaces and from the heat transfer coefficient on the water side, as well as uncertainties in the inlet water temperature, which arrives from the water storage tank outside guard containment and is affected by ambient conditions in the reactor building. Considering the secondary system uncertainties, a 95% confidence interval of ±10% on this value has been considered.

---

[22] For a normal distribution, the two-sided 95% confidence interval lies at ±1.96 standard deviations from the mean value, therefore an error of ±2% corresponds roughly to a standard deviation of 1%.

4.4.4 Nusselt Number and Friction Factor

Correlations used to calculate values for the Nusselt number and friction factor are obtained from experimental databases. They have a different functional form depending on the geometry, fluid characteristics, boundary conditions (uniform heat or uniform temperature), and regime (forced, natural or mixed convection). Heating in vertical piping and the forced flow regime has been extensively studied because of its practical importance in power production, and the correlations involved are quite precise. On the other hand, natural and especially mixed convection correlations are not supported by extensive experimental results, and the resulting correlations suffer from larger uncertainty. Starting from correlation errors available in the open literature [Churchill 1998, and Gnielinski 1976], and depending on the applicability of the correlation used, we have estimated the error on the Nusselt number to range from a minimum of 10% (forced convection) to a maximum of 30% (mixed convection). Similarly, the error in the friction factor ranges from a minimum of 2% (forced convection) to a maximum of 20% (mixed convection).

4.5 Nominal Conditions Results

4.5.1 Failure Limits

By using nominal values[23] for all parameters, the outlet temperatures under nominal conditions can be calculated. The limits imposed on the coolant outlet temperature are 850°C for the average channel and 1,200°C for the hot channel. "Failure" occurs whenever the calculated temperature value is larger than the limit. The limit of 850°C on the core-average outlet temperature is driven by concerns of unacceptably high thermal stresses in the cooler and in the stainless steel cross ducts connecting the reactor vessel and the cooler. This limit is rather arbitrary and is based on designers' concerns. No

[23] In our example, given the choice of normal uncertainty distributions, nominal values happen to be both mean values and median values.

stress calculations have been performed to support its value at this feasibility study level. Future mechanistic analyses could show that the 850°C limit may have to be corrected. The rationale for the hot channel limit derives from the need to limit the fuel temperature to avoid excessive release of fission gases. A limit of 1,600°C is commonly accepted for SiC coated fuel pellets in Modular High Temperature Gas Reactors (MHTGR). However, the type of fuel in the GFR differs from that of the MHTGR and a 1,200°C limit on the coolant outlet temperature for the hot channel has been imposed conservatively[24]. An additional rationale behind the hot channel limit is given by the limit on thermal stresses on above-core structures due to non-mixed flow.

4.5.2 Results

In Table 7, the calculated nominal values for different numbers of loops are reported. Safety margins defined as the difference between the limit and the outlet temperature are reported in parentheses. With the exclusion of the single loop case[25], all other designs provide a positive safety margin both for the hot and for the average channel. For comparison, the margins of the actively cooled system (with blowers) are shown. The active system has an identical design for each loop, but uses blowers placed in the cold leg (section 15 in Figure 23). The active system operates at atmospheric pressure so that there is no need for backup pressure and the blower power has been chosen to have the same margin for the hot channel as the passive system in the 2-loop design.

---

[24] The 1,200°C has been imposed as a conservative limit believed to lie below the real failure point for the fuel. A complete probabilistic risk assessment should also quantify the uncertainties on the limits and propagate them in a way similar to what is done for the calculated maximum temperatures. However, data about the relevant uncertainties are quite difficult to obtain and, in the present study, we limit ourselves to the propagation of uncertainties in the calculated maximum temperatures and use as limits conservative values.

[25] Unsatisfactory performance of the single loop case is expected, since the system is designed to satisfy the limits for 2x50% loops in operation.

	1 Loop	2 Loops	3 Loops	4 Loops	5 Loops
Passive design	1,085	616	489	438	413
Average channel	(N/A)	(234)	(361)	(412)	(437)
Passive design	1,226	871	620	529	492
Hot channel	(N/A)	(329)	(580)	(671)	(708)
Active design	1,158	562	428	390	371
Average channel	(N/A)	(288)	(422)	(460)	(479)
Active design	1,227	870	520	457	432
Hot channel	(N/A)	(330)	(680)	(743)	(768)

Table 7 Calculated outlet temperature for nominal conditions. Safety margins are in parentheses.

4.6 Probabilistic Calculations (Step 6 and 8)

Even if the nominal calculations show that the multiple-loop designs are capable of performing their cooling function, the uncertainties associated both with the model and with the parameters do not rule out the possibility that the system will behave differently from the simulated one and will possibly fail to cool the reactor core. This event will lead to a *functional failure* of the system.

To better highlight the fact that uncertainty in the coolant outlet temperature is present, Figure 24 plots an histogram of the outlet temperature in the hot channel for a 4-loop design. The histogram is the result of 1,000 simulations. For each individual simulation random values for the uncertain parameters and for the correlation errors have been

extracted from the relative epistemic distributions as defined above. The figure shows the large uncertainty[26] of the result around its nominal value of 529°C.

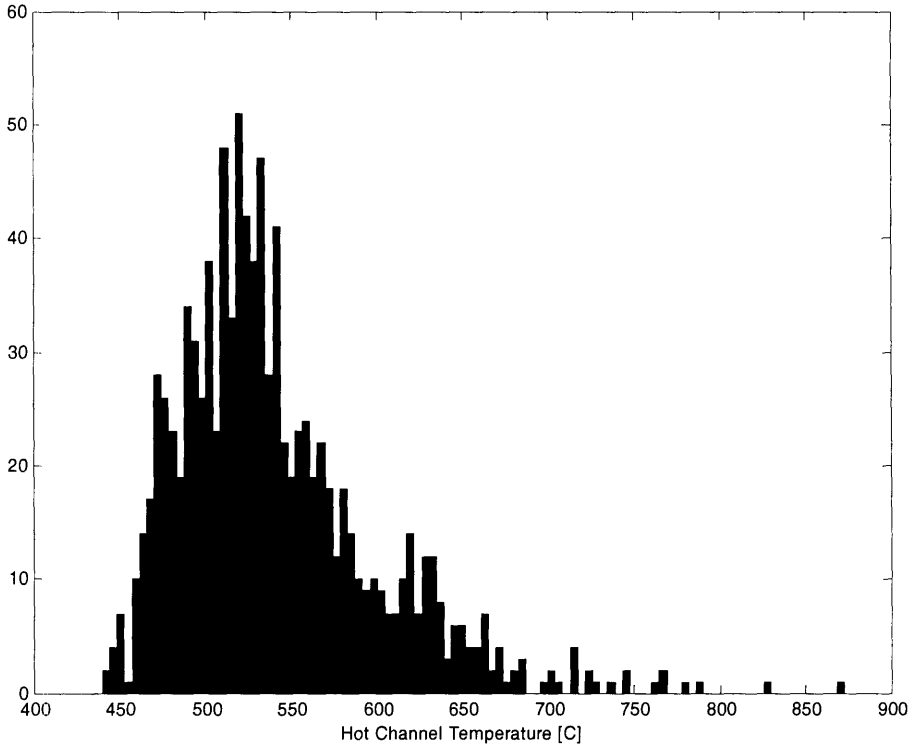

Figure 24 Temperature distribution in the hot channel for a 4-loop design

To calculate the probability of functional failures (as defined by the limits given above in Section 4.1), 10,000 Monte Carlo simulations have been performed for each design[27].

---

[26] It is interesting to note that the shape of the temperature distribution is not normal and shows positive skewness. The fact that the distribution is not normal impedes the possibility of using the simplified method presented in Appendix C in Step 2 of Figure 16.

[27] By performing Monte Carlo simulations, it is possible to propagate model and parameter uncertainties and calculate the distribution of the outlet temperatures, thus the probability of observing a temperature value above the defined limit. The application of a simple-sampling Monte Carlo algorithm would require a prohibitively large number of simulations to obtain low

The calculated failure probabilities and their errors (corresponding to a 95% confidence level) are reported in Table 8.

Probability of failure	1 Loop	2 Loops	3 Loops	4 Loops	5 Loops
Passive design	9.93E-1 ±3.39E-2	4.76E-2 ±2.24E-3	4.05E-4 ±4.02E-5	7.19E-6 ±8.72E-7	9.58E-7 ±8.40E-8
Active design	9.92E-1 ±2.95E-2	< 1E-11	< 1E-11	< 1E-11	< 1E-11

Table 8 Probabilities of functional failure

As previously stated, the values in Table 8 are conditional on the fact that natural (or forced in the active design) convection has already been established and do not take into account the initial transient phase. For instance, the 2-loop design steady state in its passive configuration has a probability of 4.76% to have temperatures above the limits. This failure event is due to epistemic uncertainties in the values of parameters and correlation results.

---

errors for estimated values in the order of 10^{-5} or even lower. Therefore, it was necessary to use a variance reducing technique such as importance sampling to obtain small errors on the results with a limited number of simulations.

Parameter	Passive design		Active design	
	Hot channel	Avg channel	Hot channel	Avg channel
Power	0.011763	0.008732	0.02333	0.011279
Pressure	0.011245	0.010583	-	-
Cooler temperature	0.003594	0.003807	0.004362	0.00289
Nusselt number (free convection)	-	-	-	-
Nusselt number (mixed convection)	0.002055	0.002057	-	-
Nusselt number (forced convection)	0.000236	0.000273	0.003979	0.002374
Friction factor (free convection)	-	-	-	-
Friction factor (mixed convection)	0.00541	0.002565	-	-
Friction factor (forced convection)	6.96E-05	0.000356	0.010267	0.003633

Table 9 One way sensitivity analysis for the 2-loop design. Relative variation of the outlet temperature for a 1% variation of the uncertain parameter

The failure probabilities for the passive design, although lower than the estimates provided in the examples by Burgazzi [2003] and Jafari et al. [2003], are far from being negligible. These results show that, together with hardware failures, functional failures should be explicitly considered in evaluating the reliability of the overall system. On the other hand, the results for the active system show that, for multiple-loop designs, the functional failure probabilities are negligible and they can be ignored. Very low values for the active design are due to the fact that the system is less sensitive to uncertainties as

the results from Table 9 show. Table 9 shows the result of a one-way sensitivity analysis. It shows the relative variation of the maximum temperatures for a 1% variation in parameter value. For example, a 1% change in the pressure will change the maximum temperature by a factor of 1.011245 to 881°C.

The active design is not subjected to pressure uncertainty (because it operates at atmospheric pressure) and to uncertainties associated with mixed convection (because it operates in the forced regime); therefore the total uncertainty on the outlet temperature and correspondingly the functional failure probability are smaller.

The single most important uncertainty is the one on the pressure value that affects the final result both because of the large sensitivity (Table 9) and because of the associated standard deviation. For the hot channel the effect of this uncertainty is about 7% larger than for the average channel, and, in fact, the observed failure mode is due exclusively to a hot channel outlet temperature above the limit. This behavior is observed even if actually the safety margin for the hot channel appears to be larger than the safety margin for the average channel (Table 7). This is because of the large sensitivity of hot channel flow rate to kinematic viscosity. Due to small helium flow rates under natural circulation, the flow in the core channels is in the laminar regime, where friction factor is inversely proportional to Reynolds number and thus strongly dependent on kinematic viscosity. Kinematic viscosity ($\nu = \mu / \rho$) increases strongly with temperature (roughly as $T^{3/2}$) and because temperature in the hot channel is higher than in the average channel, friction factor in the hot channel is increased, reducing the flow. The smaller the flow in the hot channel, the higher coolant temperature rise will be, leading to earlier attainment of the hot channel temperature limit.

4.7 Safety Margins Are Not a Reliable Measure of System Performance

Large safety margins are commonly used to enhance safety. Their importance lies in the fact that they are simple and measurable. They are often interpreted as an indirect measure of the unquantified system performance, i.e., the larger the margin, the safer the system is considered to be. However, this interpretation is not always accurate. It is possible to have two systems with the same safety margin, which have different probabilities of failure and vice versa. The results from Table 8 show that indeed the probability of failure for the 2-loop active design and the 2-loop passive design are completely different, even if the hot channel margins are the same[28]. Also, despite the fact that for all designs the margins for the average channel are smaller than the margins for the hot channel, the hot channel is the cause of failure in all designs.

While the above observation is fairly well known in reliability physics [Rao, 1992], it is useful to highlight the fact that safety margins are a measure of the "distance" between load and capacity (Figure 25). While this measure provides a first approximation of functional reliability, ranking different systems on safety margins alone can lead to erroneous results. The knowledge of the distance from failure in terms of safety margins is not sufficient to evaluate the risk of a system; the breadth of the uncertain distribution is the other important part of the assessment.

---

[28] As discussed in Section 4.2, the failure mode is the hot channel temperature being above the limit, thus the margin on this value is to be considered an appropriate measure of the safety margin.

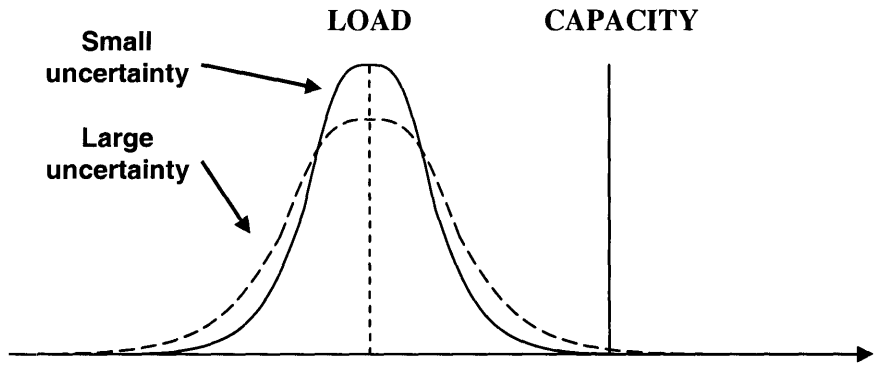

Figure 25 Uncertainty on load. In the case study only uncertainty on the load is considered; the capacity is described by a point estimate value.

4.8 Effects of Redundancy on Functional Failures

Employing redundancy is a common way to reduce the probability of system failure. The effect of redundancy on hardware failures can be modeled using analytical tools such as fault trees. The dependence among component failures is taken into account using appropriate common cause failure (CCF) models [Marshall et al. 1995]. On the other hand, functional failures are due to uncertainties that can affect different components at the same time and depend on the overall system sensitivity to these uncertainties. Uncertainties that affect all loops in the same way (such as power and pressure levels) reduce the benefits due to redundancy[29], while changes in system sensitivity could both improve or reduce them. The gain in functional reliability due to redundancy follows completely different rules and can be substantially different from the corresponding gain in hardware reliability.

---

[29] A discussion on the correlations that epistemic uncertainties introduce in the analysis of redundant components can be found in Apostolakis et al.[1981].

In the case of hardware failures, the largest reduction in failure probability can be achieved with ideal independence among components. In this special case, the reduction of the failure probability with the number of redundant components is

$$P_{n,i} = p^n \qquad (4.4)$$

where $P_{n,i}$ is the probability of failure of the system with n independent components and p is the probability of failure of a single component. This value constitutes a lower bound on the failure probability of a redundant system. However, this lower bound for reduction in failure probability does not apply to functional failures. Let us consider the results of Table 8. For the case of a single loop, the probability of failure is 0.993, while for the redundant system with two loops the probability of failure is 0.0476. The decrease in failure probability due to the additional loop is larger than in the ideal case of perfect independence, in fact $p^2 = 0.993^2 = 0.986 > 0.0476 = P_2$[30]. In Table 10 the results for all the configurations are compared with the theoretical results calculated assuming perfect independence and treating functional failures as if they were hardware failures. For the 1-, 2- and 3-loop configurations, the decrease in failure probability obtained by adding an additional loop is larger than the gain that would have resulted assuming independence.

---

[30] This result should not be unexpected; in fact, the system has been designed so that a single 50% loop is expected to fail its mission, while 2 or more loops will be able to accomplish it. This example is intended to stress the fact that probabilities associated with functional failures cannot be treated in the same fashion as probabilities of hardware failures.

		1 Loop	2 Loops	3 Loops	4 Loops	5 Loops
Probability of Failure	From Simulations	9.93E-1 [P_1]	4.76E-2 [P_2]	4.05E-4 [P_3]	7.19E-6 [P_4]	9.58E-7 [P_5]
	Assuming Independence	-	9.86E-1 [P_1^2]	1.04E-2 [$P_2^{3/2}$]	2.99E-5 [$P_3^{4/3}$]	3.72E-7 [$P_4^{5/4}$]

Table 10 Comparison of failure probabilities obtained from simulations and calculated assuming independence.

4.9 Inclusion of functional failures in PRA

The objective of a PRA is to identify all possible accident scenarios and quantify their frequencies. To achieve this result, a logic model of the system is developed, in the form of event trees and fault trees, which describes the system as a function of its components. By assigning frequencies to accident initiators (initiating events) and failure probabilities to components, it is possible to quantify the failure frequency of the overall system. While hardware failures are naturally included in the model as probabilities of failure of the individual components, functional failures should be dealt with at the success criteria level as it has already been discussed in Part III.

Success criteria are normally defined on the basis of deterministic analyses that rely on the concept of sufficient safety margins. Satisfying these requirements can theoretically imply a small functional failure probability; however, they are usually treated as full successes in PRA, assuming implicitly a negligible probability of functional failure. The reason for this assumption is that active redundant safety systems, like the ones installed in nuclear plants, are not sensitive to uncertainties to such a degree as to worry about

functional failures. The results of Table 8 show that indeed functional failure probabilities for the active system (blowers operating) are negligible (below 10^{-11}).

A completely different approach should be taken for passive systems. Recent studies by Burgazzi [2003 and 2004] and Jafari et al. [2003] have shown that functional failures can be important in risk assessment involving passive systems.

To show how much functional failure can affect the risk assessment of a passive system, let us quantify the risk of a 2-, 3- and a 4-loop design considering functional failures. The passive system design has no hardware components that can fail[31], therefore only functional failures due to epistemic uncertainty contribute to its unreliability.

For each given configuration, there is a probability of functional failure, F_i, given by the results of Table 8. F_i is the conditional failure probability given that natural convection has occurred and is due to epistemic uncertainty. Including these functional failures we can write the total failure probabilities of the systems as

$$P_{2,F} = F_2 = 4.76 \cdot 10^{-2}$$
$$P_{3,F} = F_3 = 4.05 \cdot 10^{-4}$$
$$P_{4,F} = F_4 = 7.19 \cdot 10^{-6}$$

where $P_{2,F}$, $P_{3,F}$ and $P_{4,F}$ are the total failure probabilities of the 2-loop, 3-loop and 4-loop designs, respectively.

---

[31] The check valves are the only hardware component that can fail. However, check valve failure probability should be considered during the transient leading to natural convection (failure to open the check valve). During the steady state operation once the check valve has opened the component cannot fail.

Given the previous estimates it is possible to make a comparison with the actively cooled system (with blowers operating). In this case blower failures have to be included, while functional failures are negligible.

Let us assume a mission time of 72 hours and a failure to run frequency ranging from 10^{-5} to 10^{-4} per hour[32]. To take into account common cause failures the Multiple Greek Letter (MGL) model has been used. Realistic values for the parameters have been estimated from Marshall et al. [1995] and are the following[33]

$$\beta = 0.035$$
$$\gamma = 0.65$$
$$\delta = 0.7$$

Using the rare event approximation, the total probability of failure of the 3- and 4-loop systems is given by the formulae

$$P_{2,A} = 2(1-\beta)q + \beta q$$
$$P_{3,A} = 3[(1-\beta)q]^2 + \frac{3}{2}\beta(1-\gamma)q + \beta\gamma q \qquad (4.5)$$
$$P_{4,A} = 4[(1-\beta)q]^3 + 4\beta(1-\beta)(1-\gamma)q^2 + \frac{4}{3}\beta\gamma(1-\delta)q + \beta\gamma\delta q$$

where q is the probability of failure of the blower, β, γ and δ are the MGL factors for the blowers, and $P_{2,A}$, $P_{3,A}$ and $P_{4,A}$ are the total failure probabilities of the 2-loop, 3-loop, and 4-loop active designs, respectively.

---

[32] These values are assumed to be the 5th and 95th percentiles of the parameter epistemic distribution. The distribution used is lognormal.

[33] Epistemic uncertainty has been modeled with lognormal truncated distributions with error factor equal to 3. The truncation is necessary to avoid parameter values above unity.

The epistemic uncertainties have been distributed through Monte Carlo and the results are summarized in Table 11. The failure probability of the active system is dominated by the common cause failures of the blowers. In fact an increase in redundancy from 3 to 4 loops does not improve the reliability of the system significantly.

		2 Loops	3 Loops	4 Loops
Passive design	**Mean**	4.76E-2	4.05E-4	7.19E-6
Active design	**Mean**	5.70E-3	1.58E-4	7.85E-5
	Median	3.00E-2	1.82E-3	1.14E-3
	5th percentile	3.00E-3	1.68E-4	1.06E-5
	95th percentile	5.70E-2	3.48E-3	2.18E-3

Table 11 Probability of failure results for the passive and active systems

The reliability results are summarized in Table 11. While the passive system is always more reliable than the active one when functional failures are not considered (because it has a zero failure probability), this is not the case if their impact is included in the analysis. Comparing the mean values[34] shows that the active system is actually more reliable than the passive one for the 2- and 3-loop designs. An increase in redundancy, as discussed in Section 5.2, is more effective for functional reliability (affecting the passive system) than for hardware reliability (affecting the active system), therefore for the highly redundant 4-loop design the passive system seems to be better than the active one.

[34] Mean values have to be compared to assess the more reliable system because uncertainty is present. Uncertainty on the hardware reliability value is described by the 5th and 95th percentile values, while uncertainty on the functional reliability comes from the fact that the possible outcomes are success (corresponding to a functional failure realization of zero) and failure (corresponding to a functional failure realization equal to unity).

It should finally be stressed that the calculated failure probability refers to the 72 hours steady state period after the initial transient. The results are conditional on the successful inception of natural (or forced) convection.

4.10 Sensitivity Analysis (Step 7)

The epistemic distributions used to quantify uncertainties on parameters and on the model are meant to represent all available information. It would however be interesting to perform the calculation of functional failures assuming different epistemic distributions to assess the value of additional information. Let us suppose for instance that, with additional experimental results it is possible to halve the uncertainty on the mixed flow correlation errors or, with a different type of guard containment it is possible to halve the uncertainty on the pressure level. The calculation of functional failure probability for these different scenarios would allow the assessment of the value of information and would help in allocating resources to either program.

The functional failure probability has been calculated for the 2-loop design for the following three scenarios:

1. Uncertainties on the mixed flow correlations are halved
2. Uncertainty on the pressure level is halved
3. Both uncertainties on the mixed flow correlations and uncertainty on the pressure level are halved

The results are reported in Table 12. They show that the value of information due to a reduction of uncertainty on the pressure is larger than the one due to a reduction in correlation error. If the resources are limited this information can help the project manager in making a decision about resource allocation.

Also, a reduction in both these uncertainties (scenario 3) will increase the reliability of the passive design above the reliability of the active design. Again, this shows the strict relationship between functional failures and the state of knowledge and how this latter affects them (Figure 15).

Scenario	1	2	3
Functional Failure Probability	3.35E-2 ±2.23E-3	6.51E-3 ±1.32E-3	3.48E-4 ±4.28E-5

Table 12 Sensitivity Analysis

4.11 Conclusions

Functional failures are not taken into account in risk assessments explicitly. By satisfying deterministic criteria such as large safety margins, we presume that the probability of functional failures is sufficiently low. An analysis of the role and characteristics of functional failures has been performed in the case of passive cooling in a gas-cooled fast reactor using a simplified steady-state model to perform the necessary calculations. The results can be summarized in the following points:

1. Deterministic safety measures alone such as safety margins can provide a misleading evaluation of the failure probability of a passive system. Systems with the same safety margin can have different probabilities of functional failure. Additional information should be used together with safety margins to determine the safety of a system.
2. The analysis of multiple-loop systems has shown that redundancies impact hardware and functional failures in different ways. Functional failures depend on the behavior of the system with respect to uncertainties and a change in the system such as the addition of a redundant loop can decrease the functional failure

probability in a different way than the corresponding change in hardware failure probability.

3. The combination of large uncertainties and high hardware reliability, typical of passive safety systems, makes it necessary to include functional failures in the PRA explicitly. Failure to do this would lead to optimistic results. Also, due to the functional failure effect, passive systems are not necessarily more reliable than active systems, as is commonly believed.

Some simplifications have been assumed in the paper.

- The model considers only steady-state behavior. A detailed analysis should include a transient analysis to understand the dynamics of inception of natural convection.
- The estimates of uncertainties, i.e., standard deviations, were based on expert opinion and are rough estimates for the real values. Also, the shape of the epistemic distributions has been chosen so that the calculations could be simplified. The functional failure probability is very sensitive to the tails of the epistemic distributions; therefore, the values of the standard deviations and the shape of the distributions can affect the final results. A detailed study of a real system should focus on the determination of epistemic uncertainties.

Finally, it needs to be noted that in addition to PRA outcome, the economic aspects will play an important role in the final selection of the design. Although the PRA results indicate that passive decay heat removal having more than three loops could achieve substantial reduction in failure probability, it would be more costly because of the large size of the heat exchangers required to compensate for low heat transfer rates associated with natural convection, and the need for a guard containment to maintain relatively high backup pressure. Considering both the PRA results and economics, for this particular example, the 3(x50%)-loop active emergency cooling system appears to be the preferred

choice because it exhibits smaller failure probability than the 3-loop passive system and is expected to have appreciably lower capital cost than the 4(x50%)-loop passive system with a high-pressure guard containment. Moreover, the active system can function safely in a passive mode should sufficiently high pressure be maintained in non-LOCA accidents. Thus, a passive system that does not require safety-grade power trains may not necessarily be more economical than an active system, as commonly believed.

PART V: HIGH BURNUP FAILURE LIMIT

5.1 Introduction

In the previous part of the thesis the uncertainty on the load (outlet temperature) has been quantified to calculate the probability of functional failure in a passive cooling system. The uncertainty on the capacity was not modeled. In this part of the thesis we will focus on capacity and show an example of quantification of its uncertainty. The case study describes an example of quantification of uncertainty for the capacity, i.e., the failure limit. We analyze the failure limit in a rod ejection accident in a PWR with Zr-4 cladding at different burnup levels. This case study shows a practical example of quantification of uncertainty in the capacity, and it is also interesting because of the importance of the issue in current research programs worldwide. The results are presented also in a paper by Pagani et al. [2004b].

There are economic incentives for using high burnup fuel in commercial reactors. Raising the burnup limit as high as possible allows for a more efficient utilization of the fuel, thus decreasing the associated costs. For this reason, the burnup level of commercial fuel has increased from 33 GWd/MTU up to 47 GWd/MTU by mean assembly [Schmitz et al. 1998]. The mechanical properties of cladding and fuel differ substantially with the level of burnup leading to similar fuel behavior in accident conditions. We focus our attention on a Reactivity-Initiated Accident (RIA) corresponding to a rod ejection in a PWR. Issues arise because safety limits that were initially defined on the basis of databases containing only data coming from low burnup fuel are no longer applicable to current levels. Experimental programs in France, Japan, and Russia in the 1990s have revealed new phenomena occurring at burnup levels larger than 40 GWd/MTU. These decrease the fuel failure limit. It is, therefore, necessary to redefine the failure limits making use of the new experience.

Traditionally, failure limits have been defined in a conservative way by setting a limit value low enough to guarantee a low probability of failure, if the limit is not exceeded. In this paper, we propose a probabilistic approach to the definition of a limit that includes the information about the uncertainty in the data. This limit can, then, be used directly to better assess the risk of a RIA in terms of failure probability.

After a brief review of the current limits and the results of experimental programs, the sources of uncertainty in the data are identified. The Frapcon and Fraptran computer codes are, then, used to simulate the behavior of the fuel during a rod ejection accident and to propagate the uncertainties previously identified. The data obtained are, then, fitted to obtain a probabilistic limit giving the probability of failure as a function of enthalpy and burnup. Finally an example of failure probability calculation is presented and conclusions are drawn.

5.2 Overview of Existing Data and Uncertainties

5.2.1 Failure Modes and High Burnup Effects on Fuel Performance

The rod ejection accident is based on the assumption that a control rod assembly is expelled by the internal core pressure because of a mechanical failure of the housing of the drive mechanism. The ejection induces a positive reactivity increase that causes a local power pulse that will be terminated by negative reactivity fuel feedback. During the accident sequence, the energy deposition on the fuel rod can be significant and may lead to failure due to several mechanisms. Failures of the cladding can develop, and fuel particles can be expelled into the coolant. Understanding the failure modes and the high-burnup fuel behavior in accident conditions is important in order to determine the fuel's capacity to withstand the accident. Detailed discussion of high burnup phenomena and failure modes in a RIA can be found in Schmitz et al.[1995, 1998], Fuketa et al. [1996, 1997], Lemoine [1997], Chung et al. [1998], Diamond [2002], and USNRC [2004]. They can be summarized in the following points:

- Thermal crisis. Departure from Nucleate Boiling (DNB) can challenge the cladding. Because this failure mechanism is important for low burnup (at medium and high burnup, other failure mechanisms dominate), it is unlikely that this will result in a release of fuel particles [Montgomery et al. 2002].

- Molten fuel. Fuel melting and excessive thermal expansion of the fuel pellet can occur at high enthalpy levels. The sudden expansion of the pellet can fail the cladding and result in molten fuel dispersal and small steam explosions that can damage the pressure boundary. This phenomenon can occur at all burnup levels and is especially important at low burnup when other phenomena do not dominate.

- Pellet cladding mechanical interaction. For high burnup rods, the gap between the fuel and the cladding narrows and eventually closes. In this case, the pellet-cladding mechanical interaction (PCMI) during the transient can lead to excessive stresses in the cladding resulting in its failure.

- Oxidation and hydrogen absorption. In general, this failure mechanism is more likely for medium and high burnup levels because of the thicker oxidation layer on the cladding surface. The oxidation process releases hydrogen that is partly absorbed by the cladding alloy. At high concentrations, the excess hydrogen precipitates as zirconium hydrides that make the metal more brittle and reduce the capacity of the cladding.

- Spallation. For large oxide layer thicknesses, oxide blisters can detach from the cladding and disperse in the coolant. This phenomenon is called spallation. Locations affected by spallation also have very high hydride content and have been preferential failure locations during experiments.

- Rim effect. At high burnup levels, fuel microstructures form. These microstructures, known as rim effect, develop at the outer surface of the fuel and are due to a very high local burnup level caused by neutron shielding. Fission gas accumulates in the grain boundaries in this outer fuel region and the high fission gas pressure achieved during the transient can lead to prompt fuel dispersal in case of cladding failure.

From the above summary, it appears that the failure of the cladding can be caused by several mechanisms ranging from DNB to mechanical stresses due to PCMI to molten fuel. The high strains and stresses resulting in the cladding can lead to cladding failures. Cladding failures are more likely whenever oxidation (and, eventually, spallation) is present because of the reduction in cladding ductility due to consequent hydride formation. However, the failure of the cladding is not by itself sufficient to determine a catastrophic failure. It has to be coupled with fuel dispersal. At low burnup levels, fuel dispersal can be caused by fuel melting; at higher burnup levels, it is caused by sudden explosion of the rim structure in the outer pellet.

5.2.2 Current Limit Criterion

The current limit criteria for the rod ejection accident require that the accident neither damage the pressure boundary nor impair the cooling capabilities. A quantitative criterion states a limit of 280 cal/gm [870 J/gm] on the radial average fuel rod enthalpy at the location in the core where this enthalpy is maximum. The limit has been set to assure the avoidance of fuel melting, thus ensuring pressure boundary integrity and core coolability.

The experimental programs on high-burnup fuel rods showed the important role of the oxidation layer thickness, of the spallation phenomenon, and the development of fuel microstructures as large quantities of fission gas accumulated in the grain boundaries. The experiments showed that these phenomena could lead to failure for enthalpy levels

much lower than the current regulatory limit. Figure 26 shows the experimental results as failures (solid points) and non-failures (empty points). The horizontal axis represents the average burnup level of the fuel rod used in the experiment; the vertical axis represents the value of radial average enthalpy measured during the experiment. For non-failures, the enthalpy value corresponds to the maximum value reached during the experiment while, for failure points, the enthalpy value corresponds to the enthalpy level at which failure is reported. It appears that the failure limit is decreasing with the burnup level and that there is considerable scatter in the results[35], especially at higher burnup. This scatter is the result of uncertainty in relevant parameters at a fixed burnup level such as the cladding oxidation and its hydrogen content.

[35] By scatter, we mean the mix of non-failure points with failure points with no clear separation between the failure and non-failure regions.

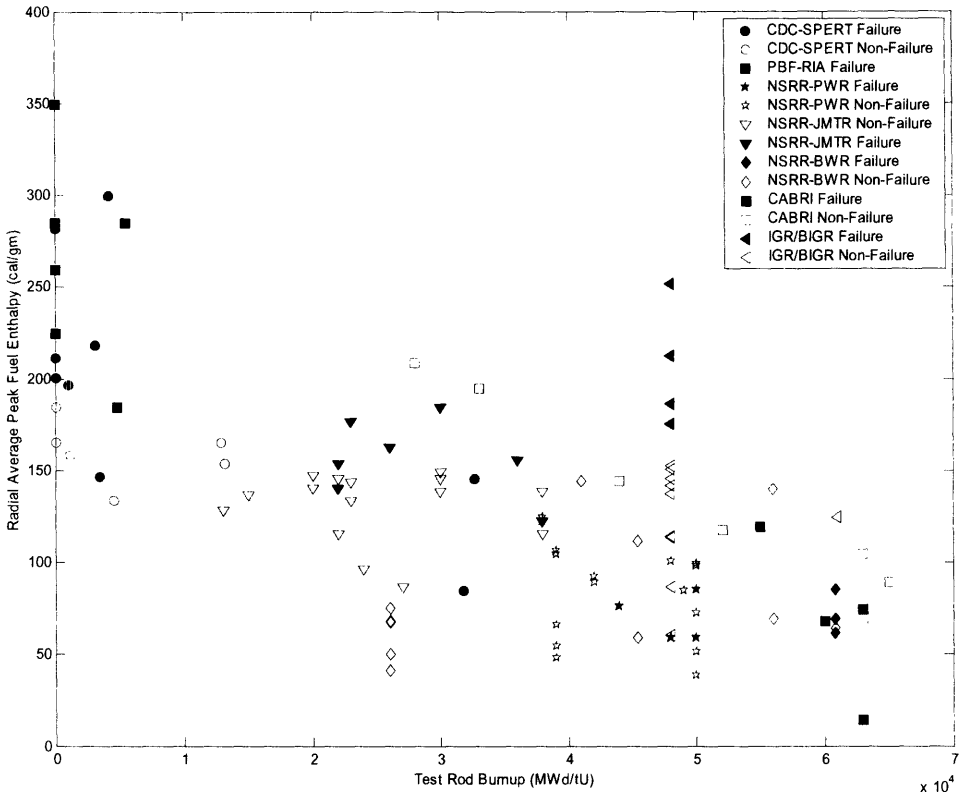

Figure 26 Results from experiments of simulated rod ejection accidents. The data are a collection of several experimental programs (CDC-SPERT: from USA; PBF: from USA; NSRR: from Japan; CABRI: from France; IGR/BIGR: from Russia)

The enthalpy limit also appears to be much lower than the regulatory limit; this is due partly to the fact that the conditions at which the experiments were conducted differ from the conditions in a commercial reactor and among experiments (Table 13). The lower temperature and a narrower power pulse used in the experiments compared to normal reactor conditions contribute to decrease the failure limit.

PWR Operating Condition	– Coolant: water at 290-330ºC and 15.5MPa – Rods: commercial reactors, some are mixed oxide fuels (MOX) – Pulse width around 100ms
CABRI (France)	– Coolant: hot sodium (280°C) at 0.5MPa – Rods: commercial reactors, some are MOX – Pulse width ranging from 10 to 80ms
NSRR (Japan)	– Coolant: stagnant water at 25°C – Rods: commercial reactors (PWR and BWR), experimental reactor (JMTR) – Pulse width ranging from 4 to 7ms
IGR/BIGR (Russia)	– Coolant: water or air at 20°C at atmospheric pressure or 16MPa – Rods: from VVER reactors. Differences from other programs: • Zr - 1% Nb cladding material, very resistant to oxidation • Central hole in fuel column – Pulse width ranging from 3 to 800ms

Table 13 Environmental conditions of PWR and experimental programs

5.2.3 Sources of Uncertainty

To determine the failure limit, it is important to understand the fuel behavior at different burnup levels and to model the relevant phenomena leading to cladding failure. The burnup level affects the oxidation layer thickness, while the oxidation history of the rod affects the hydrogen content of the cladding and, therefore, its mechanical resistance. Whereas a relationship can be determined between burnup and oxidation, this relationship depends on the cladding alloy, on the power history of the rod, and on the chemical environment and is affected by considerable uncertainty [Montgomery et al. 2002]. The uncertainty on the oxidation is such that a representation of the failure limit as a function of burnup only will inevitably present scatter in the results because data

points that have the same burnup level can have very different levels of oxidation, thus different failure limits. To model this uncertainty, a ±35% uniform uncertainty has been assumed around the average value. This uncertainty is consistent with the scatter measured in Zr-4 cladding [Montgomery et al. 2002]. Furthermore, the oxide layer thickness is not by itself the main cause of decreased resistance in the cladding. The hydrogen absorbed in the cladding, corresponding on average to 15% of the hydrogen produced in the oxidation process, determines the formation of hydrides and the consequent reduction in ductility. But this hydrogen amount is also uncertain [Limback 1994], and this uncertainty adds to that of the oxide layer to contribute to scatter in the data. This uncertainty has been modeled with a uniform distribution on the interval 10% to 20% for the percentage of absorbed hydrogen.

5.3 Probabilistic Limit for a PWR

In this part, we obtain the distribution of the failure limit for a Zr-4 rod subjected to a rod ejection accident in a PWR. To do so, the uncertainties in relevant parameters identified above are modeled and propagated using, with some minor modifications, the Fraptran [Cunningham et al. 2001] and Frapcon [Lanning et al. 1997] computer codes. A large number of virtual experiments[36] will be performed to propagate the uncertainties and to obtain sufficient data to derive a probabilistic failure limit.

5.3.1 Definition of Failure Modes

The regulatory failure limit is defined with the objective of avoiding pressure pulses that challenge the primary boundary and avoiding core coolability problems. These problems depend on two events: the failure of the cladding and the release of fuel particles in the coolant. To simplify the approach and to define conservatively the failure point, we identify the failure limit with the cladding failure, without further investigating whether

---

[36] By virtual experiments, we mean that the data are not obtained from a real experiment but from a computer simulation of the accident sequence.

fuel dispersal happens or not. Since cladding failure is a necessary condition for the pressure pulses and core coolability problems, this simplified approach will provide a conservative answer.

The computer code used to simulate the transient (Fraptran) does not calculate explicitly failures of the cladding; therefore the failure event must be determined from the analysis of other parameters contained in the code output. We have defined two competing types of failure modes:

- Thermal failure: the cladding is assumed to fail whenever its average temperature exceeds 800°C. This criterion is used as a proxy for the departure from nucleate boiling.

- Mechanical failure: following the approach of Montgomery et al. [2002], the cladding is assumed to fail whenever the Strain Energy Density (SED) exceeds the Critical Strain Energy Density (CSED). The CSED has to be defined from experimental results. Correlations reported by Montgomery et al. [2002] have been used. The CSED is assumed to be a function of the oxide layer thickness ratio (used as a proxy for the hydrogen content that is the real parameter affecting cladding resistance). Two different correlations are used depending on the spallation state of the rod:
  For non-spallated cladding, the correlation is given by

$$CSED = 41.5e^{-6.6R_{ox}} \tag{5.1}$$

  For spallated cladding, the correlation is given by

$$CSED = 0.371R_{ox}^{-1.24} \tag{5.2}$$

where R_{ox} is the ratio of oxide layer thickness to total cladding thickness. The correlations have been obtained by fitting data points from experiments. To take into account the scatter of data points around the correlation prediction, an error of ±50% has been modeled with a uniform distribution.

5.3.2 Virtual Simulation Process

The simulations are performed following the process represented in the diagram of Figure 27.

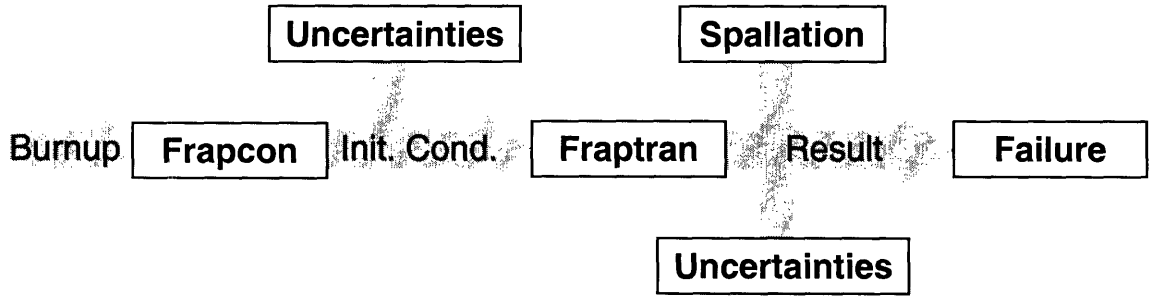

Figure 27 Virtual simulation process

Frapcon (version 3.2) is used to obtain the initial conditions of the rod at a given burnup level. The power history is assumed to be linear and decreasing with time to model the decreasing fuel rod reactivity, as plotted in Figure 28. The condition simulated is the Hot Zero Power (HZP) condition deemed to be the most challenging condition for this type of accident [Diamond et al., 2002].

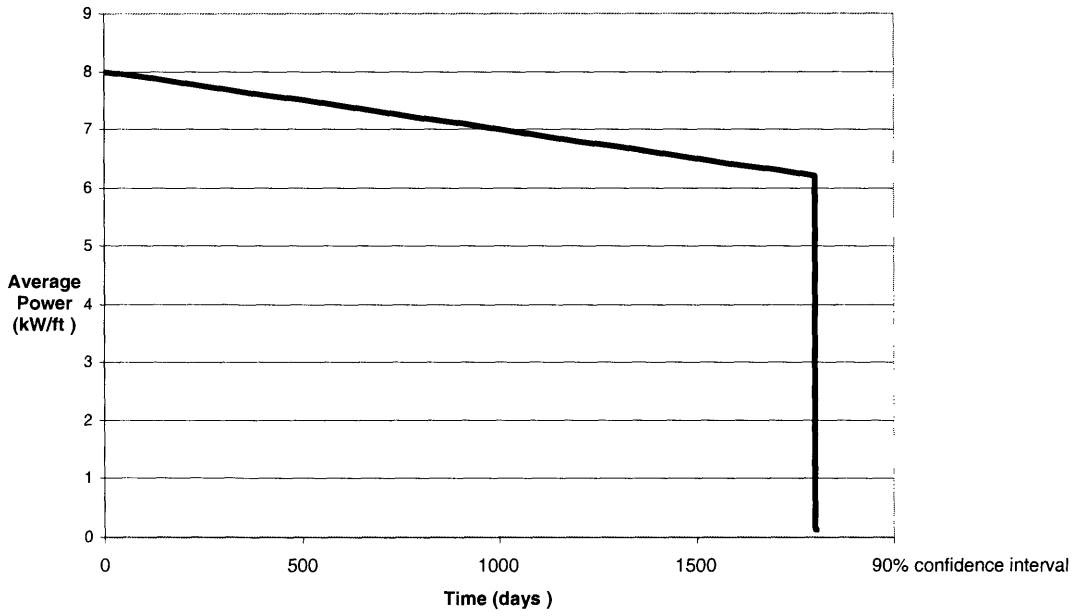

Figure 28 Power history

The initial estimates of oxide layer thickness and hydrogen content obtained from Frapcon are adjusted to take into account their uncertainty. Fraptran (version 1.2) is then used to perform the accident simulation and to obtain the time evolution of temperature and strain energy density in the rod. During the accident transient, the sudden local increase in reactivity results in a power pulse that is sufficient for the reactor to go prompt critical and may result in a linear power several times higher than the nominal value. The sudden increase in temperature in the fuel will result in a decrease in reactivity due to Doppler feedback. The shape of the power pulse is thus determined by the initial reactivity insertion, which depends on the worth of the control rod assembly, and by the Doppler feedback contribution. The shape of the pulse has been determined in an ideal case by Lewins [1995]. The dependence of the pulse width on energy has been studied in realistic cases [Diamond et al. 2002, USNRC 2004] and results in an inverse proportionality relationship between the two parameters. This relationship has been taken into account to analyze the effect of power pulses with different heights on the

capacity. Once the Fraptran code simulation is performed, a simple model is used to determine the spallation state of the cladding to choose the correlation to be used for the critical strain energy density and to compare the correlation result with the calculated SED to determine whether the rod has failed or not.

5.3.3 Spallation Model

The spallation phenomenon has been observed in samples whose oxide layer thickness exceeded 100 microns. For a large oxide layer thickness, oxide blisters tend to detach from the cladding surface and disperse in the coolant. This yields a local decrease in the total cladding thickness that can help the development of cracks during the accident transient. Spallation locations correspond also to very high local concentration of hydrogen. It is not clear whether the high hydrogen concentration is actually the cause for spallation or is a result of spallation. In the first case, if spallation does not affect the hydrogen concentration, then the failure data points should be fitted using a unique CSED correlation regardless of their spallation state. On the other hand, if spallation accelerates the hydrogen absorption process, then it is correct to identify two different regimes and use two separate correlations depending on the spallation state. We have chosen to perform the analysis following the approach of Montgomery et al. [2002] using two different correlations.

The Frapcon and Fraptran computer codes do not model local phenomena such as spallation; therefore, it is necessary to modify the results of the code to take spallation into account. The model that we developed uses the following assumptions derived from observations:

1. Spallation only occurs for an oxide layer thickness to total cladding thickness ratio above 0.1 (the threshold).
2. If the threshold is exceeded locally, then there is a probability for the location to be spallated.
3. Among samples exceeding the threshold, i.e., those whose maximum oxide layer thickness ratio exceeds the value 0.1, about half of them undergo spallation.

The fuel has been modeled with 12 axial nodes. Whenever a node has an oxide layer value above the threshold, there is a fixed probability for that axial node to be spallated. This determines the type of CSED correlation to be used. To have consistency with bullet 3 above, the value of the spallation probability defined in bullet 2 is the same for all the 12 axial nodes and has been calibrated so that the probability of observing spallation in the whole rod, i.e., of having at least one node spallated, is equal to 0.50.

5.3.4 Virtual Experimental Results

In Figure 29, the data from the virtual experiments are plotted. Failures are plotted in solid symbols. The plot differentiates between non-spallated samples (circles) and spallated samples (triangles). In the case of no failures, the enthalpy value refers to the maximum enthalpy reached during the transient, while, in the case of failures, the enthalpy value refers to the enthalpy level where failure began occurring. The figure shows the failure points as a function of enthalpy and burnup level.

The data points show a decrease in the failure limit with burnup, as expected. The decrease is smooth until around 35 GWd/MTU, at which point the spallation phenomenon begins taking place. This event further reduces the limit, making it possible to observe failures at enthalpy levels smaller than 50 cal/gm. Because of the uncertainties, the data are very scattered, showing non-failure points interspersed with failure points all over the burnup range. The definition of a conservative limit would, then, be possible, but it would be a value well below 50 cal/gm for high-burnup fuel rods.

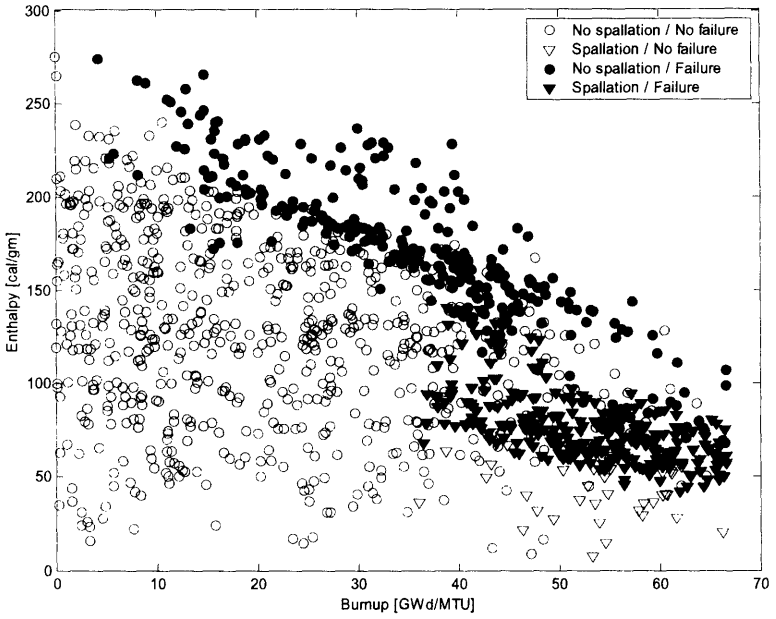

Figure 29 Results of the virtual experiments.

5.3.5 Statistical Analysis

To utilize the above data, instead of defining a conservative limit, we define a cumulative distribution function Φ(h/B) of the enthalpy at which failure occurs as a function of burnup, i.e.,

$$\Phi \equiv \Phi(h/B) \tag{5.3}$$

where h is the enthalpy level and B is the burnup level.

Being a cumulative distribution function, Φ(h/B) has the following properties (for a fixed value of B):

- Its value for zero enthalpy is zero
- Its value for infinite enthalpy is unity
- It is monotonically non-decreasing

The interpretation of $\Phi(h/B)$ is as follows: For a fixed burnup level B, there is a probability distribution of the enthalpies at which the fuel fails. For a value h^*, the probability that the enthalpy at which failure occurs (for the fixed burnup level B) is less than h^* is $\Phi(h^*/B)$ or, equivalently, the probability of fuel failure is $\Phi(h^*/B)$.

Because it is skewed to the right and is analytically easy to work with, we choose the cumulative lognormal distribution function for the enthalpy, with its parameters μ and σ depending linearly on burnup, i.e.,

$$\Phi(h/\mu,\sigma) = \int_0^h \frac{1}{x\sqrt{2\pi}\sigma}\exp[-\frac{(\log x-\mu)^2}{2\sigma^2}]dx$$
$$\mu = \mu_0 + \mu_1 B \qquad (5.4)$$
$$\sigma = \sigma_0 + \sigma_1 B$$

where μ_0, μ_1, σ_0, and σ_1 are constant parameters.

The function $\Phi(h/B)$ depends on these four parameters, which must be determined from the data points. The point values of these parameters are determined by fitting the function to the data points of Figure 29 using the Maximum Likelihood Estimate (MLE) method. The optimal value of the parameters is such as to maximize the logarithmic likelihood function, i.e.,

$$L(\mu_0,\mu_1,\sigma_0,\sigma_1) = \qquad (5.5)$$
$$= \sum_{i=\text{failures}} \log[\Phi(h_i/\mu_0+\mu_1 B_i, \sigma_0+\sigma_1 B_i)] + \sum_{i=\text{non failures}} \log[1-\Phi(h_i/\mu_0+\mu_1 B_i, \sigma_0+\sigma_1 B_i)]$$

where the index i refers to the data points corresponding to failures in the first sum and corresponding to non-failures in the second sum.

Because of the regime shift due to spallation, two different sets of parameters are determined: one set for spallated samples and one set for non-spallated samples. The results are reported in Table 14. Figure 30 and Figure 31 show graphically the median failure limit, i.e., the enthalpy level at which the probability of failure is equal to 50% and the lower and upper bounds whose enthalpy levels correspond to a probability of failure of 5% and 95% respectively.

	Non-spallated	Spallated
μ_0	5.6315	4.9684
μ_1	-0.0184	-0.0195
σ_0	0.0471	-0.0880
σ_1	0.0035	0.0047

Table 14 MLE parameter values

The curves show a failure limit decreasing (negative value of μ_1) with burnup and uncertainty increasing (positive value of σ_1) with burnup. For example, for a burnup level of 47 GWd/MTU, a failure probability of 0.05 corresponds to an enthalpy level of 89 cal/gm for non-spallated fuel (Figure 30), and to an enthalpy level of 46 cal/gm for spallated fuel (Figure 31).

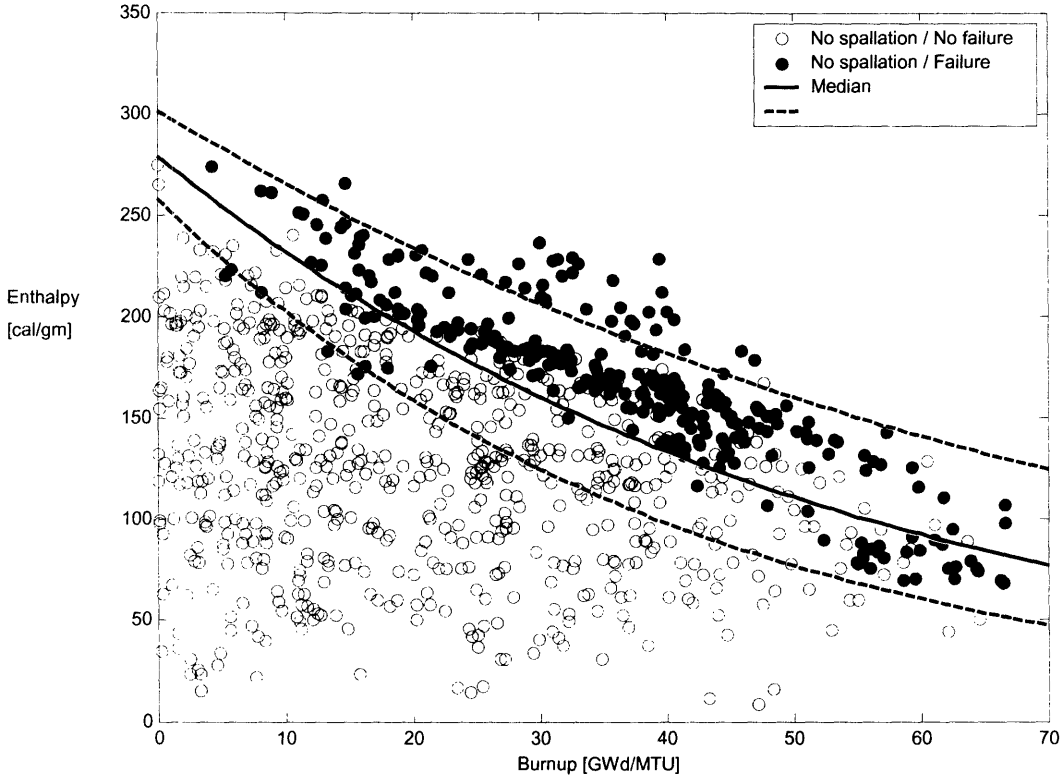

Figure 30 Data fitting for non–spallated samples.

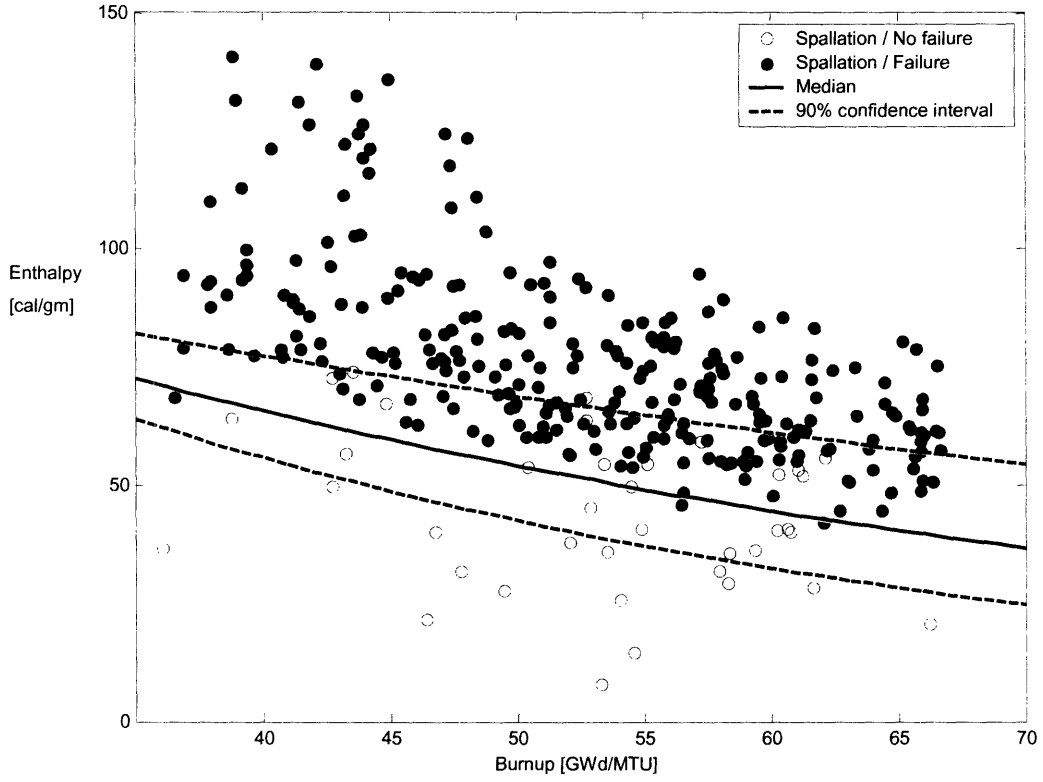

Figure 31 Data fitting for spallated samples

To obtain a unique failure limit regardless of the spallation state, it is necessary to combine the information about the spallated data with the information about the non-spallated data. To do this, it is necessary to calculate the probability of spallation for a given burnup level. The spallation probabilities obtained from the data points are plotted in Figure 32. The simulated data have been grouped according to their burnup level. Each group contains data that have burnup levels within a 5GWd/MTU interval. The line shows the linear fit to the data points and has been used in the calculation. The linear fit is constrained so that the probability of spallation is zero below 35GWd/MTU, in agreement with the results of simulations (Figure 29 and Figure 31).

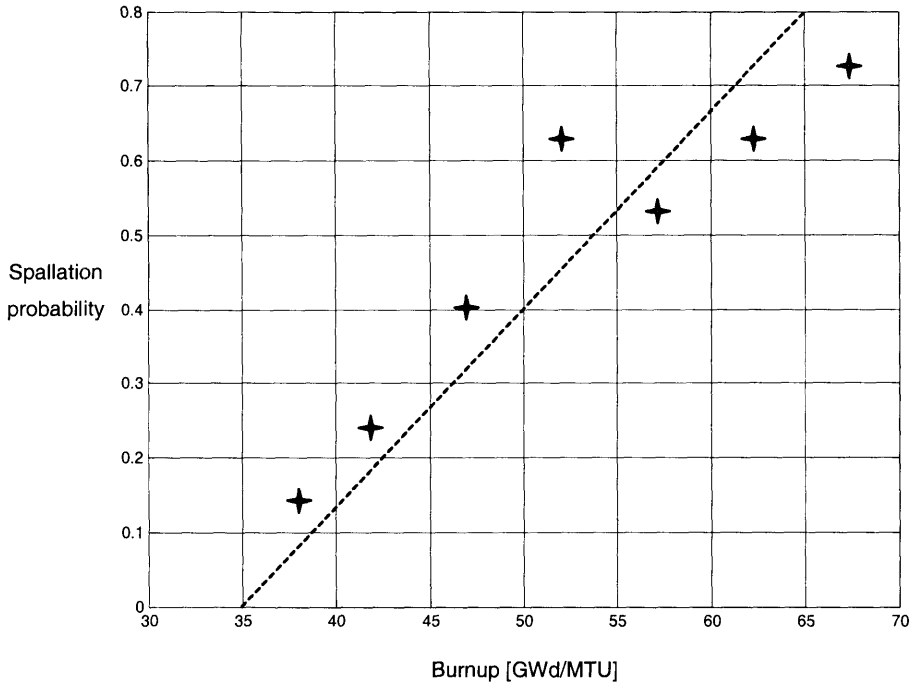

Figure 32 Spallation probabilities.

The failure limit can then be written as

$$\Phi(h/B) = [1 - p(B)]\Phi_{non\text{-}spallated}(h/B) + p(B)\Phi_{spallated}(h/B)$$

$$p(B) = \begin{cases} 0 \text{ if } B < 35 \\ 0.0266B - 0.9333 \\ 1 \text{ if } B > 72.5 \end{cases} \tag{5.6}$$

$$\Phi_{non\text{-}spallated}(h/B) = \int_0^h \frac{1}{x\sqrt{2\pi}(0.0471 + 0.0035B)} \exp[-\frac{[\log x - (5.6315 - 0.0184B)]^2}{2(0.0471 + 0.0035B)^2}]dx$$

$$\Phi_{spallated}(h/B) = \int_0^h \frac{1}{x\sqrt{2\pi}(-0.0880 + 0.0047B)} \exp[-\frac{[\log x - (4.9684 - 0.0195B)]^2}{2(-0.0880 + 0.0047B)^2}]dx$$

where $p(B)$ is the spallation probability as a function of burnup, Φ(h/B) is the failure limit, while $\Phi(h/B)_{non\text{-}spallated}$ and $\Phi(h/B)_{spallated}$ are the previously calculated specific failure limits for spallated and non-spallated data respectively.

5.3.6 Probabilistic Failure Limit

The results of the analysis are shown graphically in Figure 33. In the first figure, limits corresponding to different failure probabilities are shown, while in the second plot, the data points are shown together with the limit corresponding to a failure probability of 10%. Table 15 shows the value of the 5th, 50th, and 95th percentiles for different burnup levels.

We obtain the probability density function of h by taking the derivative of Φ(h/B) with respect to h. This result represents the distribution of the capacity. This information can be used coupled with a distribution of the load (the power pulse calculated by a neutronic code) to obtain the probability of failure, defined as the probability of the load exceeding the capacity. A design would, then, be satisfactory, if it implied a low failure probability. A similar formulation would allow the quantification of risk in terms of failure probabilities without the need to introduce non-quantified conservative margins.

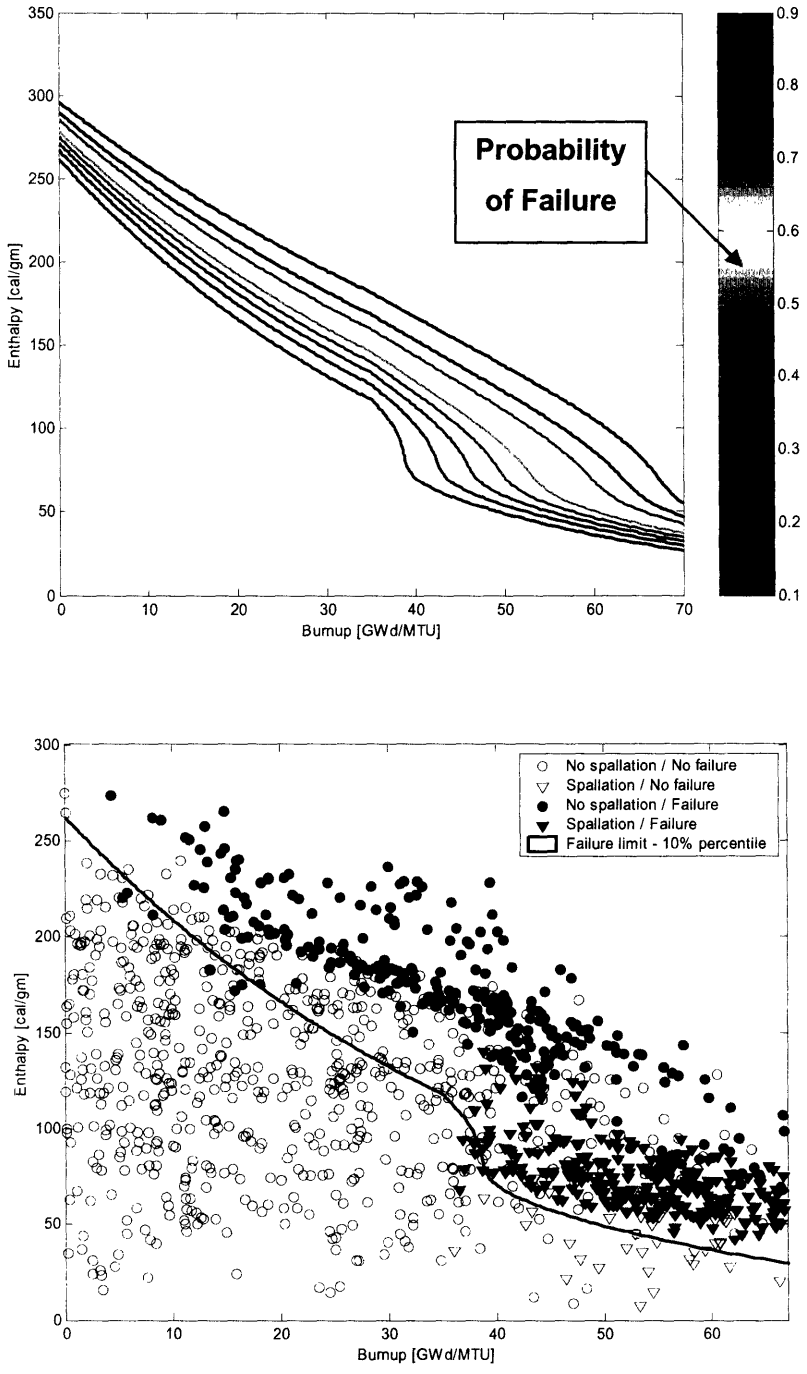

Figure 33 Failure limit

Burnup [GWd/MTU]	5th percentile [cal/gm]	50th percentile [cal/gm]	95th percentile [cal/gm]
0	258	279	302
10	203	232	266
20	159	193	234
30	125	161	206
40	64	129	180
50	46	90	151
60	34	51	121
70	25	38	68

Table 15 Characteristic values of the probability distributions of the failure limit

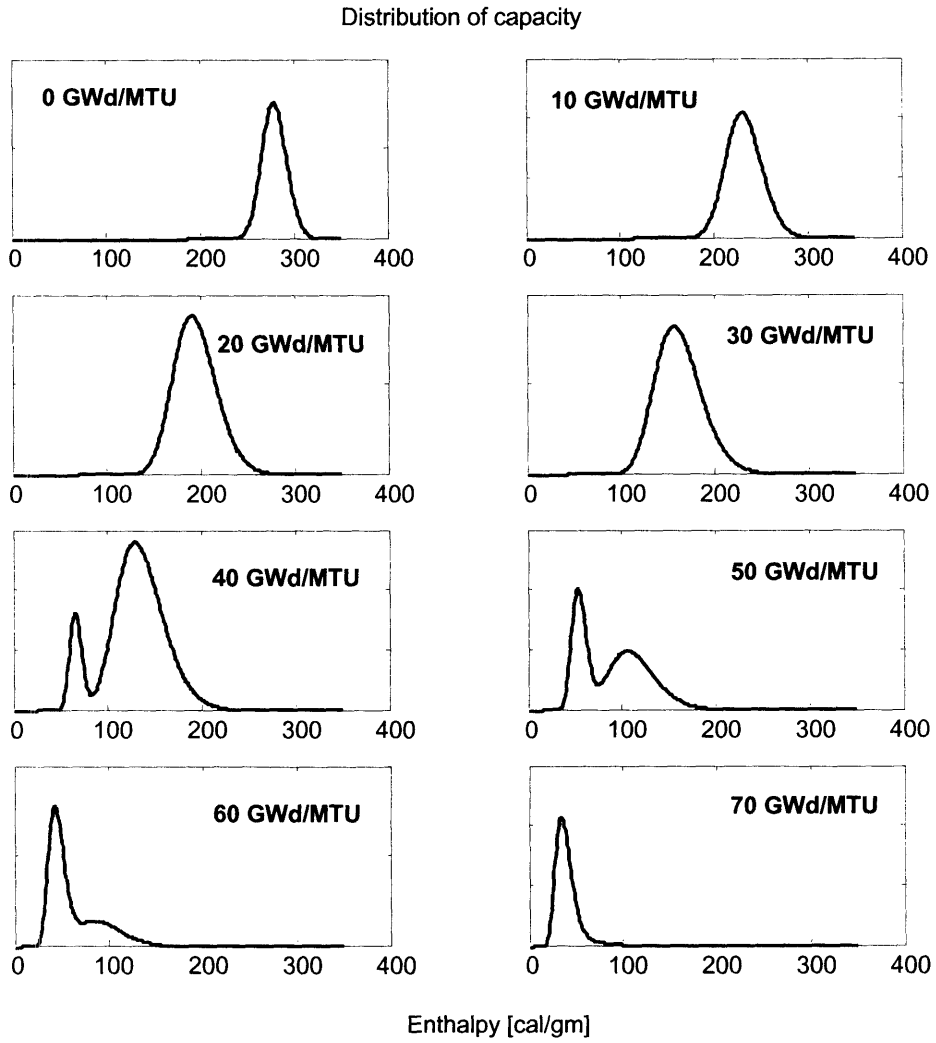

Figure 34 Probability density functions of the failure enthalpy for given values of the burnup.

The results are plotted in Figure 34 for different burnup levels. Figure 34 and Table 15 clearly show that the failure limit decreases as the burnup level increases. The effect of spallation is also shown. For low burnup (0-30 GWd/MTU), the failure distribution is unimodal (lognormal), because spallation is not possible. With the increase in burnup, spallation becomes important and the failure distribution is composed by two lognormal

distributions, one for the spallated samples and the other for the non-spallated samples. For this reason, the distribution is bimodal between 40 and 60 GWd/MTU. For higher burnup (70 GWd/MTU), the spallation probability increases and the distribution for spallated samples dominates and the distribution is unimodal again.

5.3.7 Example of Failure Probability Calculation

As a simple example let us consider an hypothetical rod ejection that induces an increase in enthalpy of 50 cal/gm.[37] We further assume a burnup of 50 GWd/MTU and an uncertainty in the maximum enthalpy value modeled with a normal distribution with a standard deviation equal to 5 cal/gm. The probability density functions of the load (maximum peak enthalpy) and the capacity (failure limit) are graphically represented in Figure 35.

The failure probability is given by the probability of the load to exceed the capacity and can be calculated using eq. (2.1). The calculation gives a result of 0.1268. This means that there is a conditional probability of failure equal to 0.1268 given that a rod ejection accident results in a 50 cal/gm power pulse. This result can be coupled in a PRA with the frequency of such a rod ejection accident to obtain the contribution of this accident to the frequency of cladding failure. If the frequency of a rod ejection accident is equal to 10^{-6} yr^{-1} (as reported in Diamond [2002]), then the frequency of this sequence will be equal to $1.2x10^{-7}$ yr^{-1}.

The main advantage of calculating explicitly failure probabilities is that they provide a quantification of the safety margins and can be used in a PRA. Having a quantitative measure of margin allows us to assess whether the margin is sufficient or not.

---

[37] To select a realistic value of enthalpy in case of an accident, we have chosen the value provided by Boyack et al. [2001].

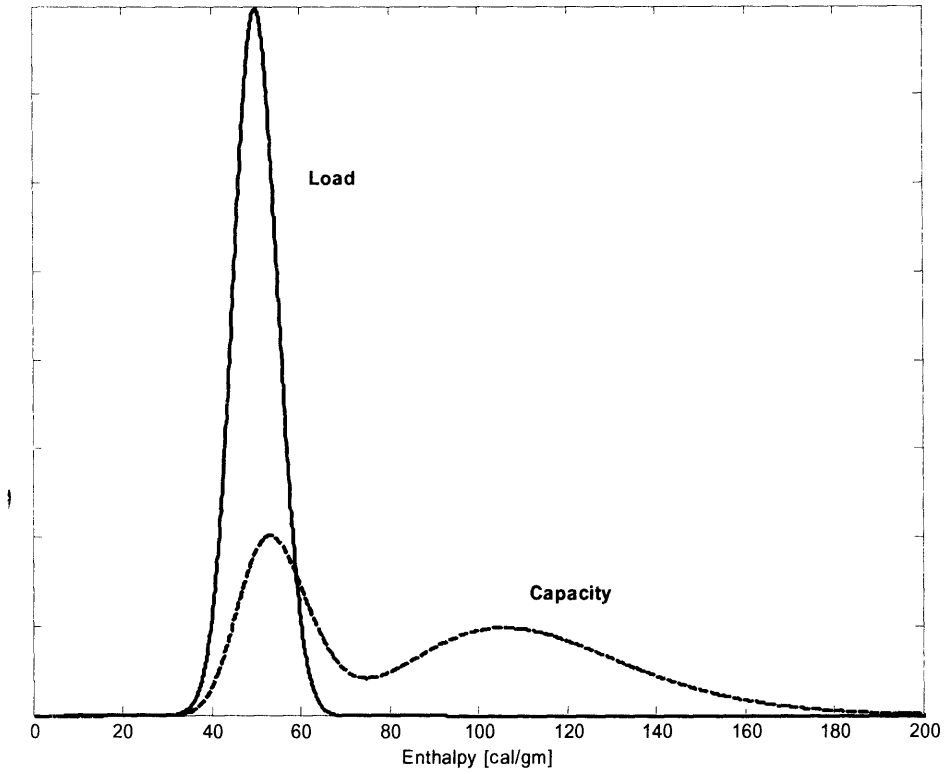

Figure 35 Load and capacity probability density functions for a 50 cal/gm power pulse at 50 GWd/MTU

5.4 Conclusions

The probabilistic analysis reported in this paper describes a process for the derivation of the distribution of the failure limit as a function of burnup and enthalpy. The main results of the analysis can be summarized as follows:

- The failure limits show considerable uncertainty (Figure 34 shows an uncertainty of around 100 cal/gm). This uncertainty derives from uncertainties in relevant quantities such as the hydrogen content in the cladding and justifies a probabilistic approach rather than the more traditional conservative approach.

- The failure limit for high-burnup levels is considerably lower than the current limit. The results show that at 70 GWd/MTU and 25 cal/gm, there is already a 0.10 probability of failure. This confirms the necessity to better understand the underlying phenomena and to update the failure limits.

- The probabilistic approach used in this paper is generic and can be applied to other types of failures. The types of failure that can benefit the most from such an approach are those where large uncertainties are present, and where very conservative limits can imply unnecessary burden. The calculated failure limit distributions can be used in a PRA to quantify the frequency of a given scenario.

In the interpretation of the above results, the underlying assumptions have to be taken into account. The results are derived from data points obtained through a virtual experiment, and their realism depends on the realism of the computer models and the assumptions utilized. In particular, the spallation effect has been modeled in a very simplified way, and the definition of cladding failure relies on the SED/CSED approach and on the correlations used in Montgomery et al. [2002]. To include these model uncertainties [Apostolakis 1995] in the analysis would require additional information regarding the accuracy of these models possibly using expert judgment [Budnitz et al. 1998]. Our results are not more reliable than their underlying assumptions. A more realistic failure limit can be obtained applying the probabilistic analysis to real experimental results or using more detailed computer codes.

CONCLUSIONS

We have developed a methodology for the calculation of functional failures. We have investigated the impact of these failures on PRA and found that they affect the way acceptance criteria are defined. Although PRA is a probabilistic approach, the way acceptance criteria are defined is deterministic and does not contain any quantitative information regarding uncertainties. Current PRAs therefore neglect the role of functional failures by assuming that their value is equal to zero. Although this approach is satisfactory for most of the accident scenarios in current LWRs, there are cases, e.g., passive systems and high burnup fuels, in which a detailed evaluation of the load-capacity interference is required. A complete PRA should then include the information about functional failures. The application of the methodology requires epistemic distributions for loads and capacities.

A numerical example of this reliability physics approach has been shown in the first case study, where the analysis of a gas-cooled fast reactor passive cooling system has been analyzed. The focus was in the uncertainties of the "load." The results show that functional failures are an important contributor to the overall failure probability of the system and, therefore, should be included in PRAs. Otherwise, deterministic safety margins can provide a misleading evaluation of the performance of a passive system. A comparison with an alternative active design has been considered also. The results show that the active design can have, for this particular application, better reliability than the passive one.

The second case study shows how to derive the epistemic distribution on the capacity, i.e., on the failure limit, from experimental data. We analyzed the failure limit for the rod ejection accident in a current PWR for different burnup levels. This case study has been chosen not only because of its relevance to the present research, but also for its importance in current research programs worldwide. Results show that uncertainties in

relevant parameters, e.g., cladding oxide layer thickness and hydrogen content, contribute substantially to the uncertainty in the final failure limit value. This finding suggests that a probabilistic approach would be more appropriate than a traditional conservative one. Also, this confirms the necessity to better understand high burnup fuel behavior and to update the current failure limits.

The results of the research show the necessity to better model uncertainties and to include them in the PRA especially for those types of failure scenarios in which large uncertainty is present. Most of the accident sequences in PRAs for LWRs model active systems whose behavior is well understood; therefore, the quantification of safety margins will not impact the PRA results. On the other hand, for some accident sequences characterized by large uncertainty (RIA with high burnup fuel, or new designs relying on passive systems), the impact of safety margin should be included in the PRA.

The inclusion of safety margins in PRA, using an approach such as the one introduced in the thesis, will allow better risk-informed decision making and could eventually reduce the need for excessive conservatism, thus avoiding unnecessary burden.

FUTURE WORK

In the following list, we highlight opportunities of further research.

- **Calculation of functional failure probability.**

  The methodology presented in Part III shows how to perform the calculation of the probability of functional failures. The efficiency of the method can benefit from the development of advanced Monte Carlo techniques (step 6 of Figure 16) and a sound filtering criterion (step 2) to reduce the computational burden. Also, the development of a formal procedure to identify and quantify uncertainties (step 4 and 5) would be useful.

- **Passive system reliability.**

  The analysis of the passive cooling system has been performed with a simplified thermal hydraulic model and for steady-state condition only. It would be useful to perform a complete analysis that takes into account both the initial transient when the natural convection is established and the following phase, when the decay heat decreases over time. This would permit a realistic evaluation of the system risk to be used in the design of such a reactor.

- **High-burnup fuel limits.**

  The analysis performed in the high-burnup case relies on the results of the Frapcon and Fraptran computer codes. To improve the realism of the results, it would be desirable to derive the failure limit from actual experimental data. However, because of different conditions between experiments and commercial reactors, data adjustments are necessary, which can introduce an additional source of error. The realism of the results can also be improved using better models for the fuel behavior. It appears to be especially important to model local phenomena such as hydride formation and spallation.

- **Inclusion of safety margins in existing PRAs.**

  While the impact of safety margins on existing PRAs is probably not a major issue, it would be interesting to apply the methodology to an existing PRA. This exercise would show the real impact of margins upon different accident scenarios

and would provide useful information. Also, the modified PRA could be used to calculate the impact on safety margins of licensing basis changes and the resulting impact on CDF and LERF.

REFERENCES

Apostolakis, G. and Kaplan, S., 1981. "Pitfalls in risk calculations." *Reliability Engineering*, 2, 135-145.

Apostolakis, G., 1990. "The concept of probability in safety assessments of technological systems." *Science*, 250, 1359-1364.

Apostolakis, G., 1995. "A commentary on model uncertainty." in Mosleh A., Siu N., Smidts C., and Lui C. (eds.), *Proceedings of Workshop on Model Uncertainty: its Characterization and Quantification,* Center for Reliability Engineering, pp. 13-22, University of Maryland, College Park, MD, (also published as Report NUREG/CP-0138, US Nuclear Regulatory Commission, Washington, DC, 1994)

Apostolakis, G., 1999. "The distinction between aleatory and epistemic uncertainties is important: an example from the inclusion of aging effects into PSA." In *Proceedings of the PSA '99 International Topical Meeting on Probabilistic Safety Assessment*, Washington, DC, 22-26 August.

Apostolakis, G.E., Koser, J.P., and Sato, G., 2004. "Decision analysis and its application to the frequency of containment integrated leakage rate test." *Nuclear Technology*, 146, 181-198.

Ardillon E., Barthelet B. and Meister E., 2000. "Probabilistic approaches as methodological support to industrial codification in nuclear engineering." In *Proceeding of PVP00: Joint JSME/ASME Pressure Vessel and Piping Conference*, Seattle, 23-27 July.

Boyack B., Duffey R., Griffith, P., Lellouche, G., Rohatgi, U., Wilson, G., Wulif, W.,and Zuber, N., 1989. "Quantifying reactor safety margins. Application of code scaling, applicability, and uncertainty evaluation methodology to a large-break, loss-of-coolant accident." NUREG/CR-5249, US Nuclear Regulatory Commission, Washington, DC.

Boyack B., Motta A.,Peddicord K, Alexander C, Deveney R, Dunn B, Fuketa T, Higar K., Hochreiter L, Langenbuch S., Moody F, Nissley M., Papin J., Potts G., Pruitt D., Rashid J., Risher D., Rohrer R., Tulenko J., Valtonen K., Waeckel N., and Wiesnack W., 2001. "Phenomenon identification and ranking tables (PIRTs) for rod ejection accidents in pressurized water reactors containing high burnup fuel." NUREG/CR-6742, US Nuclear Regulatory Commission, Washington, DC.

Budnitz, R.J., Apostolakis, G.E., Boore, D.M., Cluff, L.S., Coppersmith, K.J., Cornell, C.A., and Morris, P.A., 1998. "Use of technical expert panels: Applications to probabilistic seismic hazard analysis." *Risk Analysis*, 18, 463-469.

Burgazzi L., 2003. "Reliability evaluation of passive systems through functional reliability assessment." *Nuclear Technology*, 144, 145-150.

Burgazzi L., 2004. "Evaluation of uncertainties related to passive systems performance." *Nuclear Engineering and Design*, 230, 93-106.

Chelemer H., Boman L.H., and Sharp D.R., 1975. "Improved thermal design procedure." Report WCAP-8568, Westinghouse Electric Corporation, Pittsburgh, PA.

Chung, H.M., and Kassner, T.F., 1998. "Cladding metallurgy and fracture behavior during reactivity-initiated accidents at high burnup." *Nuclear Engineering and Design* 186, 411-427.

Churchill, S.W., 1998. *Heat Exchanger Design Handbook*, ed. Hewitt, G.F., Begell House, Inc. New York.

Cunningham, M.E., Beyer, C.E., Medvedev, P.G., and Berna, G.A., 2001. "FRAPTRAN: a computer code for transient analysis of oxide fuel rods." NUREG/CR-6739, (also PNNL-13576), US Nuclear Regulatory Commission, Washington, DC.

Depisch F., Seeberger G., and Blank S., 1998. "Application of best-estimate methods to LOCA in a PWR." In *Seminar Proceedings of Best Estimate Methods in thermal Hydraulic Safety Analysis* (NEA/CSNI/R(99)10), Ankara, Turkey June 29 – July 1.

Diamond, D.J., Bromley, B.P., and Aronson, A.L., 2002. "Studies of the rod ejection accident in a PWR." Brookhaven National Laboratory Technical Report W-6382, Upton, NY.

Eapen, J., Hejzlar, P., and Driscoll, M.J., 2002. "Analysis of a natural convection loop for post-LOCA GCFR decay-heat removal." MIT Department of Nuclear Engineering Report MIT-GCFR-002. Cambridge, MA.

Ellingwood, B.R., and Yasuhiro, M., 1993. "Probabilistic methods for condition assessment and life prediction of concrete structures in nuclear power plants." *Nuclear Engineering and Design*, 142, 155-166.

Fishman G., 1996. *Monte Carlo: Concepts, Algorithms, and Applications*. Springer-Verlag, New York.

Fuketa, T. Mori, Y., Sasajima H., Ishijima K., and Fujishiro T., 1996. "Behavior of high burnup PWR fuel under a simulated RIA condition in the NSRR." In *Specialist Meeting*

on Transient Behaviour of High Burnup Fuel (September 12-14, 1995), NEA/CRNI/R(95)22, 1996 59-85. Cadarache, France.

Fuketa, T., Sasajima, H., Mori, Y., and Ishijima, K., 1997. "Fuel failure and fission gas release in high burnup PWR fuels under RIA conditions." *Journal of Nuclear Materials* 248, 249-256.

Gelman A., Carlin J.B., Stern H.S., and Rubin D.B., 1995. *Bayesian Data Analysis.* Chapman and Hall, London.

Gnielisnki, V., 1976. "New equations for heat and mass transfer in turbulent pipe and channel flow." *International Chemical Engineering*, Vol. 16, 2, 359-368

Hammersley J., and Hanscomb D., 1964. *Monte Carlo Methods.* Chapman and Hall, London.

Idelchik, I.E., 1993. *Handbook of Hydraulic Resistance.* 3rd ed., CRC Press, p.752.

Jafari, J., D'Auria, F., Kazeminejad, H., and Davilu, H., 2003. "Reliability evaluation of a natural circulation system." *Nuclear Engineering and Design*, 224, 79-104.

Kalos M., and Whitlock P., 1986. *Monte Carlo Mehods, Volume I: Basics.* John Wiley and Sons, New York.

Lanning, D.D., Beyer, C.E., and Painter, C.L., 1997. "FRAPCON-3: modifications to fuel rod material properties and performance models for high-burnup application." NUREG/CR-6534, (also PNNL-11513), US Nuclear Regulatory Commission, Washington, DC.

Lemoine, F., 1997. "High burnup fuel behavior related to fission gas effects under reactivity initiated accidents (RIA) conditions." *Journal of Nuclear Materials* 248, 238-248.

Lewins J., 1995. "The adiabatic Fuchs-Nordheim model and non-dimensional solutions." *Annals of Nuclear Energy*, 22:10, 681-686.

Limback, M., 1994. "Corrosion and hydriding performance of Zircaloy-2 and Zircaloy-4 cladding materials in PWRs." In *ANS/ENS International Topical Meeting on Light Water Reactor Fuel Performance*, West Palm Beach, Florida, p.286.

Long M.W., Narciso J.D., 1999. "Probabilistic design methodology for composite aircraft structures." Report DOT/FAA/AR-99/2, *Office of Aviation Research*, Washington, DC.

Madsen H.O., Krenk K. Lind N.C., 1986. *Methods of Structural Safety*. Prentice-Hall, Inc., Englewood Cliffs, New Jersey, USA.

Marques M., Pignatel J.F., D'Auria F., Burgazzi L.,Muller C., Bolado-Lavin R., Kirchsteiger C., La Lumia V., Ivanov I., and Kalchev B., 2004. "Reliability methods for passive systems." *Proceedings of ICAPP '04*, Pittsburgh, PA, USA, 13-17 June.

Marseguerra M., and Zio E., 2002. *Basics of the Monte Carlo Method with Application to System Reliability*. LiLoLe – Verlag GmbH, Hagen, Germany.

Marshall, F., and Rasmuson, D., 1995. "Common-Cause Failure Data collection and Analysis System Volume 6 – Common-Cause Failure Parameter Estimations", Idaho National engineering Laboratory, Report INEL-94/0064. Idaho Falls, ID.

Montgomery R.O., Waeckel N., and Yang, R., 2002. "Topical report on reactivity initiated accident: Bases for RIA fuel rod failure and core coolability criteria." Electric Power Research Institute Report 1002865. Palo Alto, CA.

Mosleh A., Apostolakis G., 1985. "The development of a generic data base for failure rates." In *Proceedings of the International ANS/ENS Topical Meeting on Probabilistic Safety Methods and Applications*, San Francisco, CA, USA, 24-28 February.

Mosleh A., Apostolakis G., 1986. "The assessment of probability distributions from expert opinions with an application to seismic fragility curves." *Risk Analysis* 6, 447-461.

Okano, Y., Hejzlar, P., and Driscoll, M.J., 2002. "Thermal hydraulics and shutdown cooling of supercritical CO_2 GT-GCFRs." MIT Department of Nuclear Engineering Report. MIT-ANP-TR-088. Cambridge, MA.

Pagani, L.P., Apostolakis, G.E., and Hejzlar, P., 2004a. "The Impact of Uncertainties on the Performance of Passive Systems." To appear in *Nuclear Technology*.

Pagani, L.P., and apostolakis, G.E., 2004b. "the probability distribution of the failure limit of high-burnup fuels with Zr-4 cladding." Submitted to *Nuclear Technology* in August 2004.

Pagani, L.P., Smith, C.L., and Apostolakis, G.E., 2004c. "Making decision for incident management I nuclear power plants using probabilistic safety assessment." To appear in *Risk, Decision and Policy*.

Rao, S.S., 1992. *Reliability-based Design*. McGraw-Hill, Inc., New York.

Rasmussen N. et al., 1975. "Reactor safety study, an assessment of accident risks in U.S. commercial nuclear power plants." WASH-1400 Report (NUREG-75-014). US Nuclear regulatory Commission, Washington, DC.

Schmitz, F, Papin J., Haessler M., Nervi J., and Permezel P., 1995. "Investigation of the behaviour of high-burnup PWR fuel under RIA conditions in the CABRI test reactor." In *Proceedings 22nd WRSM*, NUREG/CP-0140 vol.2 329-349. US Nuclear Regulatory Commission, Washington, DC.

Schmitz, F., and Papin, J., 1998. "High burnup effects on fuel behaviour under accident conditions: the tests CABRI REP-Na." *Journal of Nuclear Materials* 270, 55-64.

Siu N., and Kelly D., 1998. "Bayesian parameter estimation in probabilistic risk assessment." *Reliability Engineering and System Safety* 62, 89-116.

Smith, C.L., Shah, V.N., Kao, T., and Apostolakis, G.E., 2001. "Incorporating aging effects into probabilistic risk assessment – A feasibility study utilizing reliability physics models." Report 83415-3850, Idaho National Engineering and Environmental Laboratory, Idaho Falls, ID. (also NUREG/CR-5632. US Nuclear Regulatory Commission, Washington, DC.)

USNRC, 1998. "An approach for using probabilistic risk assessment in risk-informed decisions on plant-specific changes to the licensing basis." NUREG-1.174, US Nuclear Regulatory Commission, Washington, DC.

USNRC, 2004. " An assessment of postulated reactivity-initiated accidents (RIAs) for operating reactors in the U.S." Report ML040920189, US Nuclear Regulatory Commission, Washington, DC.

Westinghouse, 2004. "AP1000 Probabilistic Risk Assessment. Revision 6" Report APP-GW-GL-022 Revision 6, Westinghouse Electric Corporation, Pittsburg, PA.

Williams, W., Hejzlar, P., Driscoll, M.J., Lee, W.J., and Saha, P., 2003. "Analysis of a convection loop for GFR post-LOCA decay heat removal from a block-type core." MIT Department of Nuclear Engineering. MIT-ANP-TR-095. Cambridge, MA.

Williams, W. C., Hejzlar, P., and Saha, P., 2004. "Analysis of a Convectional Loop for GFR Post-LOCA Decay Heat Removal." In *Proceedings of ICONE12, 12th International Conference on Nuclear Engineering*, Arlington, VA.

Winkler, R.L., 1996. "Uncertainty in probabilistic risk assessment." *Reliability Engineering and System Safety* 54, 127-132.

Zio E., Apostolakis G., 1996. "Two methods for the structured assessment of model uncertainty by experts in performance assessments of radioactive waste repositories." *Reliability Engineering and Safety Systems* 54, 225-241.

APPENDIX A: MONTE CARLO ANALYSIS

A.1 Problem Description and Definitions

The problem of estimating low probability events in the order of 10^{-5} or 10^{-6} events per year is very difficult to tackle, both from a theoretical and from an experimental point of view. Still, this kind of probabilities is encountered in failure events of reliable engineering systems such as nuclear plants and is of primary importance for the assessment of risks involved in the operations of such systems.

From the experimental point of view the estimate of these probabilities is usually not feasible because of the difficulty of observing a sufficient number of failure events within a reasonable limited time, nevertheless, theoretical models can be developed and used to simulate the phenomena that lead to failure modes and to estimate their probability of occurrence.

Functional failures of an engineering system come from the fact that we are unable to determine its current state or its future evolution with absolute precision. The **state** is given by a complete description of all the characteristics of a system (set of operating conditions) that are relevant to its modeling. Such characteristics could be for instance operating pressure, fluid temperature, flow rate, and rotor velocity for a simple model of a water pump. A set of numerical values for the operating pressure, fluid temperature, flow rate, and rotor velocity will uniquely define the state of the pump in the simplified model. If these numerical values were known with certainty then the model capability of describing the behavior of the real system would depend only on the level of details included into the model itself. However, the numerical values of the parameters are subject to uncertainties and their values will be known up to a given error.

Every system is designed to perform one or multiple functions. The objective of a model is then to be able to describe the behavior of a system given its initial operating conditions and to determine whether or not it will be able to perform the specified functions. In case the system will not be able to perform the specified function a **functional failure** will have occurred.

In mathematical terms, if we call x_1, x_2, ... the system parameters, then we can then define for every system a failure function such that

$$\begin{cases} F(x_1, x_2, ...) = 1 & \text{if the system fails} \\ F(x_1, x_2, ...) = 0 & \text{otherwise} \end{cases} \qquad \text{(A.1)}$$

The failure function will divide the parameter space into two regions, depending on whether it assumes a value of unity (**failure region**) or zero (**reliable region**). The surface at the interface of the regions is called failure surface.

A.2 Introduction to Monte Carlo Methodology

During the Second World War, the scientists working on the Manhattan project to the development of the atomic bomb discovered that complex mathematical problems about neutron transport theory could be solved through probabilistic "games" simulating the physical phenomena. The methodology, developed mainly by Von Neumann, Fermi, Ulam and Metropolis, was called Monte Carlo, referring to the small European city famous for its Casino.

The methodology is used in a variety of problems to estimate characteristic values that cannot be obtained analytically or where more conventional methods like numerical calculations are too cumbersome. The basic methodology, often referred to as crude Monte Carlo sampling, consists in performing simulations of the phenomenon at hand

several times and obtaining a set of observations of the desired values. The simulations are often performed using mathematical models reproducing the behavior of the system under consideration. An estimate[38] of the desired value is then obtained evaluating ensemble averages of the observed values. The observed values are independent random variables identically distributed; this means that regardless of the complexity of their distribution the sample average will converge with probability 1 to the average value of their distribution for the strong law of large numbers[39]. Also, because of the central limit theorem[40], the sample average will converge in distribution to a normal distribution

---

[38] It should be noted the difference existing between estimate and estimator. If we have a set of observed values $y_1, y_2, \ldots$ we can define a mathematical function of these variables $t(\mathbf{y})$. This function is called an *estimator*. For instance an estimator for the mean value is $\sum_i \frac{y_i}{N}$ where N is the total number of observations. On the other hand, when we take the observed values of $\mathbf{y}$ and calculate the actual value of t we speak of *estimate*.

[39] The Law of Large Numbers (LLN) states the following.

Let $S_n = X_1 + \ldots + X_n$ where $X_1, X_2, \ldots$ are IID random variables with a finite mean $\overline{X}$. Then for any $\varepsilon > 0$,

$$\lim_{n\to\infty} P\left(\sup_{m\geq n} \left| \frac{S_m}{m} - \overline{X} \right| > \varepsilon \right) = 0$$

This type of convergence is called convergence with probability 1.

[40] The Central Limit Theorem (CLT) states the following

Let $S_n = X_1 + \ldots + X_n$ where $X_1, X_2, \ldots$ are IID random variables with a finite mean $\overline{X}$ and finite variance σ^2, then

$$\lim_{n\to\infty} \left[P\left(\frac{S_n - n\overline{X}}{\sqrt{n}\sigma} \leq y \right) \right] = \int_{-\infty}^{y} \frac{1}{\sqrt{2\pi}} \exp\left(\frac{-x^2}{2} \right) dx$$

whose mean is the expected value of the sample mean and whose standard deviation depends on the standard deviation of a single experiment and decreases with the number of samples as

$$\sigma_t = \frac{\sigma}{\sqrt{N}} \tag{A.2}$$

Given the above dependency on the number of observations it is ideally possible to calculate the estimate at any desired level of accuracy simply by increasing the number of simulations performed.

To show a simple application of the methodology let us consider the classic example of inferring the value of π from the following experiment. Suppose we throw a needle several times onto a board ruled with parallel straight lines and calculate the number of intersections between needle and lines. The probability of the needle intersecting any line is equal to

$$P = \frac{L/d}{\pi/2} \tag{A.3}$$

where L is the needle length and $d > L$ is the distance between parallel lines.

Let us define a "dummy" random variable that takes the value unity whenever the needle intersects a line and the value of zero otherwise. We are going to run the experiment several times and collect the observed values of the random variable.

This type of convergence is called convergence in distribution.

The values of the random variable for every toss are independent and identically distributed.

In the example the relevant distribution is a Bernoulli

$$\begin{cases} X = 1 \text{ with probability P} \\ X = 0 \text{ with probability 1 - P} \end{cases} \qquad \text{(A.4)}$$

Whose mean is equal to the value in (A.3) and whose standard deviation is given by

$$\sigma = \sqrt{P(1-P)} \qquad \text{(A.5)}$$

Taking the sample average we can then estimate the value of P. Different estimates are reported in

Table 16 for d equal to 1 and L equal to 0.5.

Number of simulations	Sample mean [0.3183]	Sample standard deviation [0.4658]	95%-confidence interval
10	0.3000	0.4830	0.0006-0.5994
100	0.2300	0.4230	0.1471-0.3129
1,000	0.3240	0.4682	0.2950-0.3530
10,000	0.3080	0.4617	0.2990-0.3170
100,000	0.3195	0.4663	0.3166-0.3224
1,000,000	0.3187	0.4660	0.3178-0.3196

Table 16 Buffon experiment results. Theoretical values are reported in brackets [].

The evaluation of the error is performed using the sample standard deviation defined as

$$s = \sqrt{\frac{\sum_i [y_i - m]^2}{n-1}} \tag{A.6}$$

Therefore, assuming a normal distribution from the Central Limit Theorem, the 95% confidence level interval is defined as

$$m \pm 1.96 \cdot s \tag{A.7}$$

As the number of simulations increases the estimate approaches the real value (reported in the table header in square brackets). However, equation (A.2) shows that to decrease the error by a factor of 2 it is necessary to increase the number of simulations by a factor of 4. Whenever the time required for an individual simulation is significant, as is often the case for realistic models, it becomes almost impossible to use the simple crude Monte Carlo method.

To empirically show the issue of low probability estimation through crude Monte Carlo sampling let us calculate the probability that a given parameter, whose uncertainty is described by a standard normal distribution, has a value larger than 4.5. This probability can be numerically calculated with the following formula

$$P = \int_{-\infty}^{4.5} \frac{1}{\sqrt{2\pi}} \exp\left(-\frac{x^2}{2}\right) dx = 3.4 \cdot 10^{-6} \tag{A.8}$$

To obtain the same result with a relative error of 10% using crude Monte Carlo the number of simulations necessary would be given by

$$0.1 \cdot 3.4 \cdot 10^{-6} = \frac{\sigma}{\sqrt{n}} = \frac{\sqrt{P(1-P)}}{\sqrt{n}} = \frac{0.0018}{\sqrt{n}} \Rightarrow n = 2.9 \cdot 10^{7} \qquad \text{(A.9)}$$

Thus, about 30 millions simulations would have been necessary to perform the estimate within a 10% error bound. If each simulation required only one second to be performed then the whole calculation would require one year of CPU time.

After an initial enthusiasm about the Monte Carlo method, due to its flexibility and capability to simulate complex uncertain distributions and models, the crude sampling version of it has been almost entirely abandoned mainly because of the previous issue. To overcome this problem, some improvements, called variance reducing techniques, have been developed to increase the efficiency of the method. A complete description of different techniques is beyond the scope of this research[41]. The next section will focus instead on a particular type of variance reducing technique developed to tackle the problem of functional failure probability estimation.

---

[41] For a detailed treatment of variance reducing techniques and Monte Carlo method in general the interested reader can refer to the following texts.
Hammersley and Hanscomb [1964] provide a concise but complete description of the method and some applications. Kalos and Whitlock [1986] provide an updated discussion of similar material, while Fishman [1996] goes into detailed description of advanced topics like Gibbs sampling and Markov chain sampling. Marseguerra and Zio [2002] describe applications of Monte Carlo to reliability calculations.

A.3 Importance Sampling Technique

A.3.1 Introduction

Let us focus on the problem of determining the failure probability of a system given uncertainties on its parameters. Given the conditional distribution $f(\mathbf{x})$ describing the uncertainties on the parameters and the failure function $F(\mathbf{x})$ as defined in equation (A.1), we can write the probability of failure as

$$P = \int F(x_1, x_2, ...) f(x_1, x_2, ...) d\mathbf{x} \tag{A.10}$$

The mathematical form of the failure function is usually not known, and Equation (A.10) should be evaluated through Monte Carlo sampling.
Unfortunately, the number of simulations needed with the crude algorithm is extremely large. It is however possible to reduce the number of necessary simulations by an appropriate transformation.

We can rewrite equation (A.10) as

$$P = \int F(x_1, x_2, ...) f(x_1, x_2, ...) d\mathbf{x} = \int \frac{F(x_1, x_2, ...)}{g(x_1, x_2, ...)} f(x_1, x_2, ...) g(x_1, x_2, ...) d\mathbf{x} \tag{A.11}$$

If we restrict functions $g(\mathbf{x})$ such that $f(x_1, x_2, ...) g(x_1, x_2, ...)$ is still a probability density function and we extract the uncertain parameters from this new distribution then, from equation (A.11), the estimator $\frac{F(x_1, x_2, ...)}{g(x_1, x_2, ...)}$ has expectation equal to P and its variance is equal to

$$\sigma_{Fg}^2 = \int \left(\frac{F(x_1, x_2, ...)}{g(x_1, x_2, ...)} - P \right)^2 f(x_1, x_2, ...) g(x_1, x_2, ...) d\mathbf{x} \tag{A.12}$$

This variance should be compared with the variance of the crude Monte Carlo estimator

$$\sigma_F^2 = \int (F(x_1, x_2, ...) - P)^2 f(x_1, x_2, ...) d\mathbf{x} \qquad \text{(A.13)}$$

The object is to find a function $g(\boldsymbol{x})$ so as to minimize the variance in equation (A.12). This is achieved by choosing a function $g(\boldsymbol{x})$ that mimics as much as possible $F(\boldsymbol{x})$[42]. This corresponds in practice to concentrating the sample points in the parts of space that are more important and not spreading them evenly all over the space.

A.3.2 Numerical Example

Let us consider for example the case of a single parameter whose uncertainty is described by a standard normal distribution[43]. Let us define the failure function to be equal to unity if the parameter value happens to be larger than 4.5. The probability of failure can be calculated analytically using equation (A.10) and is equal to 3.4e-6.

Let us first define a function $g(x)$ such that it is piecewise constant

$$g(x) = \begin{cases} a & \text{if } x \le 4 \\ 1000 \cdot a & \text{otherwise} \end{cases} \qquad \text{(A.14)}$$

---

[42] For a detailed explanation of this fact refer to Hammersely and Handscomb [1964] pages 57-59.

[43] In the discussion of the methods we limit ourselves to standard normal distributions because they are most commonly used to describe epistemic uncertainty and to avoid unnecessary complications. Note that it is always possible through appropriate transformations to transform a normally distributed random variable into another random variable from any distribution. Also, for the same reason, in the case of multiple random variables we limit the discussion to the case of independent variables, being possible to obtain dependent random variables from independent ones through appropriate transformations.

And such that

$$\int \frac{1}{\sqrt{2\pi}} g(x)\exp(-\frac{x^2}{2})dx = 1 \qquad \text{(A.15)}$$

Thus, $f(x_1, x_2, ...)g(x_1, x_2, ...)$ still is a probability density function. Its shape is plotted in Figure 36.

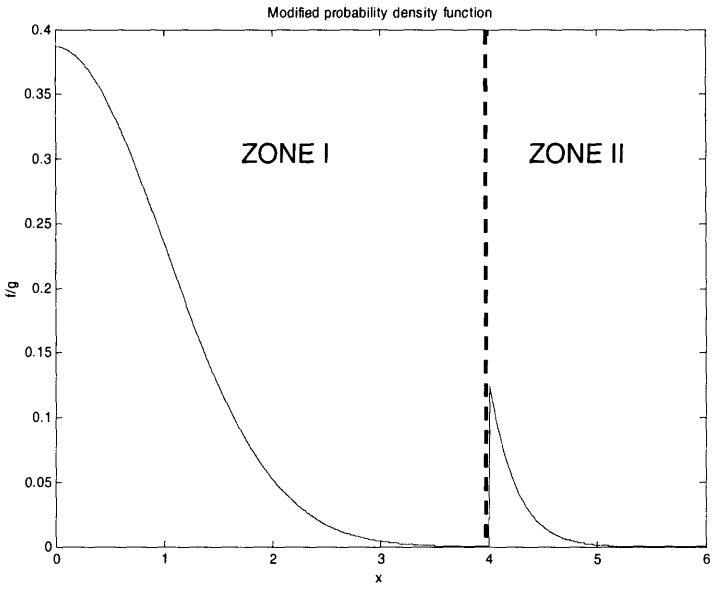

Figure 36 Transformed probability density function

As it appears from the plot, the transformation is such that parameters near the failure zone (i.e. parameter values larger than 4.5) have an increased probability of being extracted.

The results of different samplings are reported in Table 22. 1,000 simulations should be sufficient to determine the order of magnitude of the real value (3.4e-6) and 10,000

simulations already give an estimate with a 95% confidence level within 35% of the real value.

By comparison, performing the same number of calculations with the crude Monte Carlo method there were no observations of failure, and it was therefore impossible to give an estimate to the failure probability.

Number of simulations	Sample mean [3.4e-6]	Error
10	0	
100	1.0e-5	±2.0e-5
1,000	4.1e-6	±4.0e-6
10,000	3.7e-6	±1.2e-6

Table 17 Importance sampling results for a piecewise constant transformation function

The increase in efficiency compared to the crude method is evident; however, some care is necessary in the application of importance sampling using the described step transformation function. The increased efficiency depends on the relative position of the step compared to the failure point (i.e. 4.5).

In Table 18 the results of the 10,000 simulations made with different step positions are reported. Shifting the step position to the right, the efficiency stays almost constant until it passes the failure point; then there is a sudden decrease in efficiency and the result is no longer reliable.

Step position	4.0	4.3	4.4	4.5	4.6	4.7	4.8	4.9
Estimate	3.7e-6	3.2e-6	3.4e-6	2.5e-6	1.6e-6	1.0e-6	5.0e-7	4.0e-7
Error [±]	1.2e-6	1.1e-6	1.1e-6	9.8e-7	7.8e-7	6.2e-7	4.4e-7	3.9e-7

Table 18 Step position sensitivity analysis for a piecewise constant transformation function. 10,000 simulations have been performed. The failure point position is at 4.5. (The real value is 3.4e-6).

In fact, from Figure 36 it is possible to see that if the step is to the right of the failure point then all the extractions in zone II will be leading to failure while almost all the ones in zone I will not. The estimate will tend to return the same value as if the actual failure point were in the same position as the step[44].

The above issue is of primary practical importance, because in estimating the probability of failure of a system the position of the failure point (i.e. the shape of the failure surface in more than one dimension) is not known a priori. For this reason it is more desirable a smoother transformation function that is more robust to the relative position of the failure point.

[44] Note that if the number of simulations were increased sufficiently then the few extractions falling in zone I leading to failure would drive the final result to its real value of 3.4e-6. However, the number of simulations necessary to achieve this result is comparable to the one needed with the crude Monte Carlo method.

A.4 Exponential Transformation Function

A.4.1 One Dimensional Case

For the same problem of the previous section let us define the transformation function $g(x)$ to be an exponential function

$$g(x) = \exp(a + bx) \tag{A.16}$$

where we have

$$\begin{cases} a = -\dfrac{\mu^2}{2} \\ b = \mu \end{cases} \tag{A.17}$$

The new probability density function $f(x)g(x)$ is then equal to

$$f(x)g(x) = \frac{1}{\sqrt{2\pi}} \exp(-\frac{x^2}{2} + a + bx) = \frac{1}{\sqrt{2\pi}} \exp(-\frac{(x-\mu)^2}{2}) \tag{A.18}$$

The performance of the algorithm as a function of the number of simulations has been calculated performing simulations for a value of μ equal to 4 (Table 19).

Number of simulations	Sample mean [3.4e-6]	Error
10	5.7e-7	±7.5e-5
100	5.5e-6	±2.1e-6
1,000	3.4e-6	±5.3e-7
10,000	3.4e-6	±1.7e-7

Table 19 Importance sampling results for an exponential transformation function

The results reported in Table 19 show that the efficiency of the transformation function is superior to the piecewise constant function (Table 17).

To verify the robustness of the algorithm to changes in the value of the parameter μ, an analysis similar to the one performed in Table 18 has been performed. The results are reported in Table 20.

	μ value	2.5	3.5	4.0	4.5	5.0	5.5	6.5
10,000	Estimate	3.1e-6	3.3e-6	3.4e-6	3.3e-6	3.4e-6	3.3e-6	3.5e-6
	Error [±]	4.7e-7	2.1e-7	1.7e-7	1.5e-7	1.6e-7	1.9e-7	4.0e-7
1,000	Estimate	3.5e-6	2.9e-6	3.4e-6	3.2e-6	3.6e-6	3.1e-6	2.8e-6
	Error [±]	1.6e-6	6.2e-7	5.6e-7	4.5e-7	5.3e-7	5.8e-7	1.1e-6

Table 20 μ value sensitivity analysis for an exponential transformation function (the real value is 3.4e-6).

The range explored spans a region far from the failure point by as much as two standard deviations (2.5 – 6.5) and the results show that the final estimate does not suffer sudden changes within the specified region.

A.4.2 Multi Dimensional Case – Minimum Distance Point

We are now going to introduce the multidimensional case where more than one parameter is uncertain. We assume that the uncertainties are still described by standard normal distributions and further that the parameter uncertainties are independent.

Let us consider the case of two uncertain parameters with failure function defined in (A.19).

$$\begin{cases} F(x_1, x_2) = 1 & \text{if } x_1 + x_2 \geq 6.36 \\ F(x_1, x_2) = 0 & \text{otherwise} \end{cases} \qquad \text{(A.19)}$$

The real value of the failure probability can be calculated to be equal to 3.4e-6[45].
The exponential transformation function used is simply the product of two exponentials previously defined in (A.16). μ_1 and μ_2 will be the parameters of the two exponentials.

[45] The failure function has been chosen so that the value of the failure probability is the same as the one calculated in the one dimensional case.

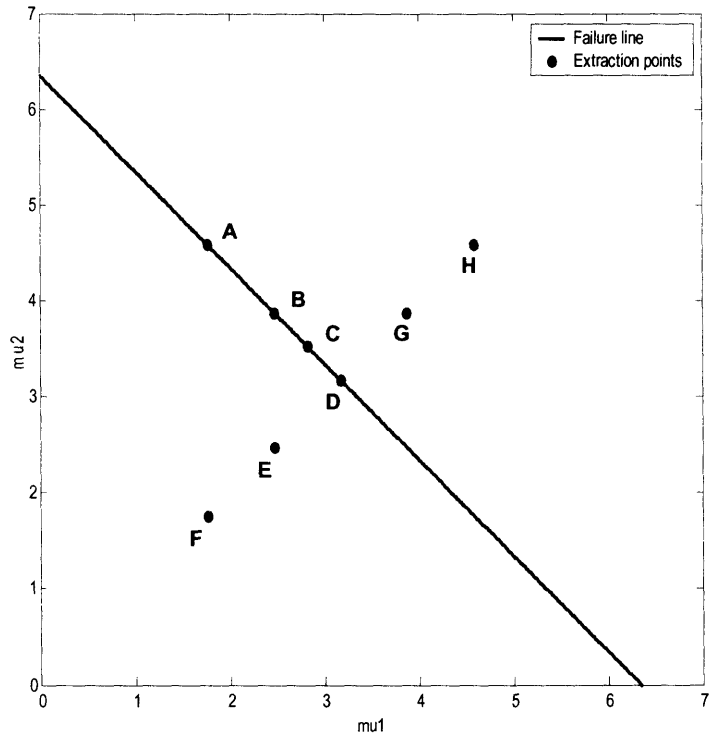

Figure 37 Extraction points

The role of the transformation function is to shift the sampling core near the failure surface. This is achieved through the choice of the parameters μ_1 and μ_2. The values of the parameters explored correspond to points on the failure surface for the first four columns of Table 21 (points A-D), while the last four columns correspond to points outside (points E-F) and inside (points G-H) the failure region as shown in Figure 37. The range explored is up to two standard deviations away from the point on the failure surface that has minimum distance[46] (point D) from the origin. The result of 1,000 and 10,000 simulations are reported in Table 21.

---

[46] The distance defined here is the Euclidean distance between two points. If x_i are the coordinates of the first point and y_i the coordinates of the second point, then their relative distance is defined as

	Point	A	B	C	D	E	F	G	H
	μ_1 value	**1.77**	**2.48**	**2.83**	**3.18**	**2.48**	**1.77**	**3.88**	**4.59**
	μ_2 value	**4.59**	**3.88**	**3.53**	**3.18**	**2.48**	**1.77**	**3.88**	**4.59**
10,000	Estimate	3.1e-6	3.4e-6	3.4e-6	3.4e-6	3.4e-6	3.5e-6	3.8e-6	4.1e-6
	Error [±]	5.8e-7	2.5e-7	1.7e-7	1.5e-7	2.1e-7	5.1e-7	6.6e-7	1.5e-6
1,000	Estimate	3.0e-6	3.1e-6	3.6e-6	3.5e-6	3.2e-6	3.0e-6	3.4e-6	2.9e-6
	Error [±]	1.2e-6	7.3e-7	5.6e-7	4.8e-7	6.6e-7	1.4e-6	1.9e-7	3.6e-7

Table 21 Sensitivity analysis in two dimensions (the real value is 3.4e-6).

The results in Table 21 show that the smaller error is achieved for the minimum distance point (D). This highlights the fact that points at a larger distance from the origin have a smaller probability, and thus contribute to a lesser degree to the final result. Also, Table 21shows that as long as the core of the sampling is within a couple of standard deviations from the minimum distance point the estimates are still reliable; however, if the core of the sampling is further removed away from the minimum distance point, then the

---

$$d = \sqrt{\sum_i (x_i - y_i)^2}$$

This simple definition can be used when the distributions describing the uncertainties are the same. If the distributions were different we should include additional information about the uncertainties in the parameters to take into account the parameter probabilities to lay at different standard deviations from the origin. An approximated definition of distance including this information can be written as

$$d \approx \sqrt{\sum_i \left(\frac{x_i - y_i}{\sigma_i} \right)^2}$$

Where, σ_i is the standard deviation of the i-th uncertain parameter.

estimates cease to be reliable. This last fact is shown in Table 22, where different estimates have been calculated for points laying on the failure surface far from the minimum distance point at different multiples of standard deviations. The results show that the reliability of the calculation decreases dramatically when the distance is larger than 4 standard deviations.

σ	0	1	2	3	4	6	8
Estimate	3.4e-6	3.4e-6	3.2e-6	4.3e-6	1.2e-6	2.1e-8	4.2e-13
Error [±]	1.5e-7	2.4e-7	6.0e-7	2.5e-6	8.5e-7	2.9e-8	2.6e-13

Table 22 Sensitivity analysis in two dimensions (10,000 simulations). Sensitivity to the distance from the minimum distance point (the real value is 3.4e-6).

From the above discussion it appears that the optimal point to be used as sampling core is the minimum distance point. Still, in practical cases the position of the minimum distance point is unknown. Therefore, it is necessary to introduce an algorithm to perform the search for the minimum distance point at the same time as the extraction process proceeds. This algorithm is presented in the next section.

A.5 Stochastic Search

A simple, yet efficient algorithm to explore the parameter space for the minimum distance point on the failure surface consists in updating the sampling core point (i.e. the parameters μ_i) during the extraction process with the failure point that has the minimum distance among all the samples so far. The steps of the algorithm are then the following[47]:

---

[47] A MatLab code implementing the algorithm can be found in appendix

1) Start with an initial value for the sample core point.
2) If the current number of sampling is equal to the total number then calculate the final result and stop.
3) Extract a new sample point from the transformed distribution centered on the current sample core and store its information (zero if in the reliable region, unity otherwise).
4) If the newly extracted point is a failure point then calculate its distance. If its distance is smaller then the distance of the current sample core then modify the transformed distribution setting the new point to be the sample core. Return to step 2.

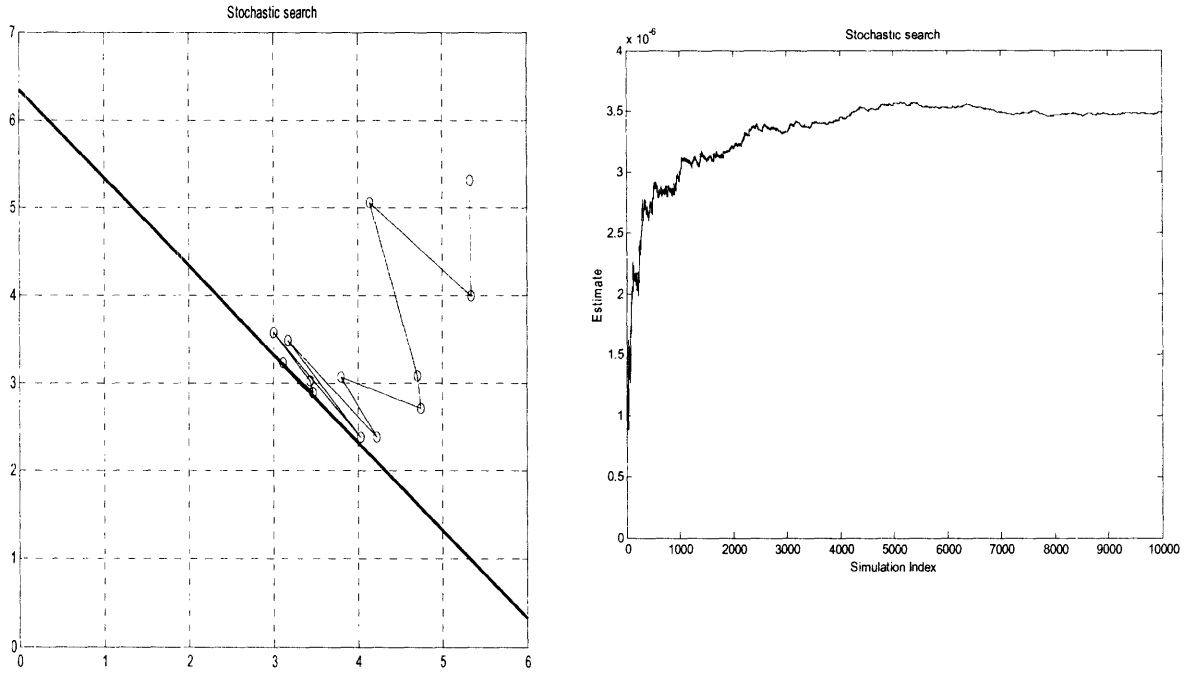

Figure 38 Sample core trajectory and estimate evolution (the real value is 3.4e-6).

Coupling the search algorithm to the importance sampling method for the example defined by (A.19) an estimate for the failure probability has been calculated. The initial core sampling point has been defined by setting μ_1 and μ_2 both equal to 5.3267. The trajectory of the core sampling point is plotted in Figure 37 together with a plot of the estimate value as a function of the total number of simulations for a given stochastic trajectory.

To calculate the error of the estimate for the stochastic search algorithm it is no longer possible to use (A.2), because the sample core changes during the extraction process, therefore the points are no longer extracted from the same distribution. Therefore, to have an estimate of the error 100 different stochastic searches have been performed and the ensemble standard deviation is used in (A.6). The results are reported in Table 23.

Simulations	10	100	1,000	10,000
Estimate	1.8e-6	4.5e-6	3.4e-6	3.4e-6
Error	±8.0e-6	±2.2e-6	±5.1e-7	±1.5e-7

Table 23 Stochastic search results (the real value is 3.4e-6).

The algorithm converges quickly to the optimal extraction point, and after 1,000 simulations the error on the estimate is relatively small[48].

[48] The excellent result obtain in the example is in part due to the fact that the number of dimensions involved were only two. When more parameters are to be extracted then an increased number of simulations would be necessary.

A.6 Summary of Monte Carlo Method

Monte Carlo method in its crude form is not efficient enough to provide reliable results with a reasonable number of simulations. To obtain an estimate of probabilities as small as 10^{-6} at least 10^{7} simulations are necessary. Variance reducing techniques have to be implemented; among these we have analyzed the case of importance sampling using an exponential transformation function whose objective is to shift the effective sampling core toward more efficient regions of the parameter space. The optimal extraction point appears to be the minimum distance point. The position of this point is a priori unknown; therefore, to find the minimum distance point a stochastic search algorithm that explores the parameter space has been developed and coupled with the importance sampling technique. The algorithm updates the sampling core during the extraction process. The implementation of this technique enables the calculation of reliable results in a limited number of simulations.

APPENDIX B: CORRELATIONS USED IN THE GFR MODEL

The correlations used in the model have been chosen among a multitude presented in the scientific literature. This appendix is supposed to present only a brief summary of the correlations and decision procedures to determine which one to use. A complete review of the existing literature and a discussion of the chosen correlations can be found in Williams [2003].

B.1 Friction Factor

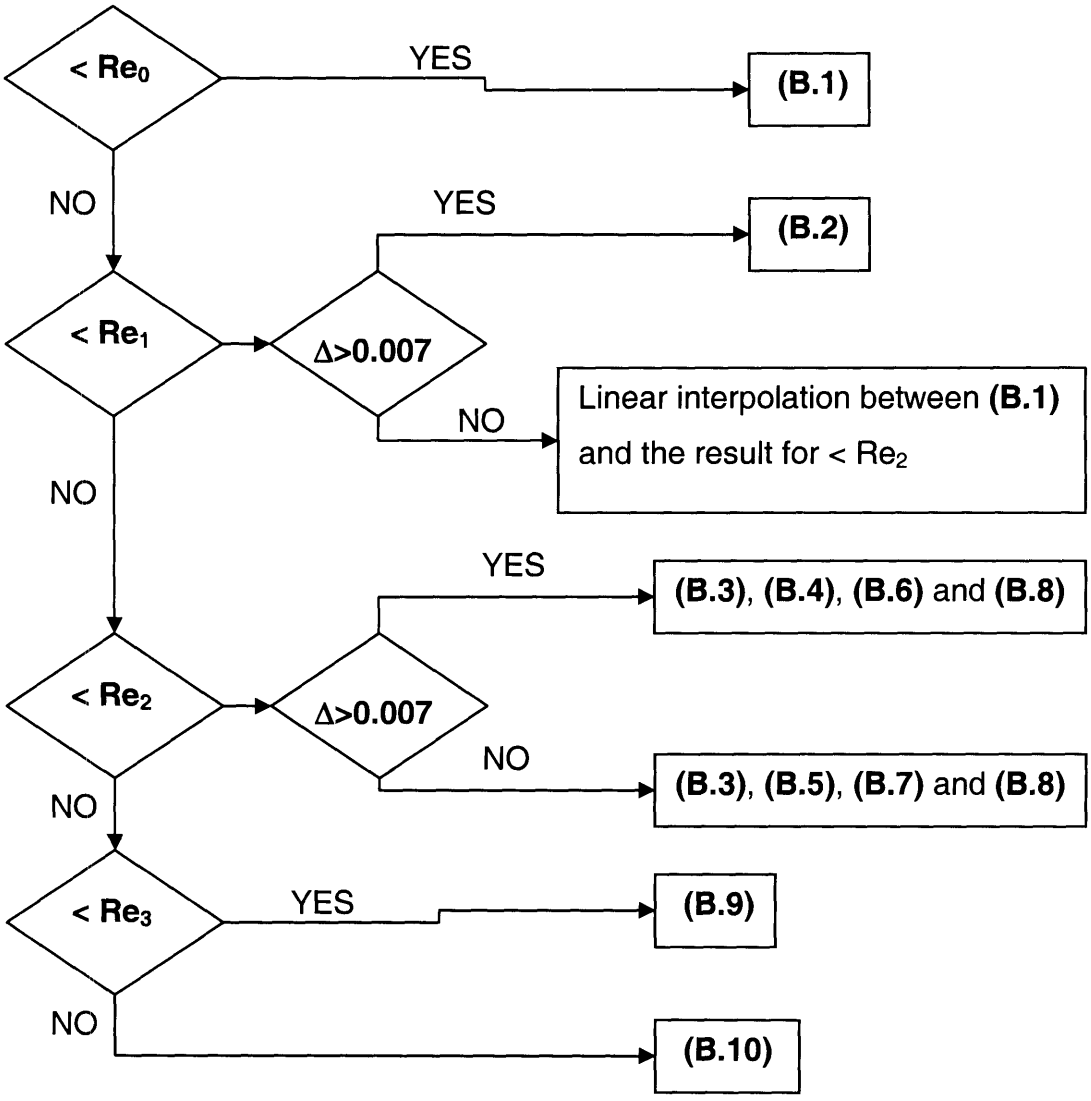

Figure 39 Friction factor decision diagram

$$f = \frac{64}{\mathrm{Re}} \tag{B.1}$$

$$f = 4.4\,\mathrm{Re}^{-0.595}\exp(\frac{0.00275}{\Delta}) \tag{B.2}$$

$$f = (f_2 - f^*)\exp(-[0.0017(\mathrm{Re}_2 - \mathrm{Re})]^2) + f^* \tag{B.3}$$

$$f^* = f_1 - 0.0017 \tag{B.4}$$

$$f^* = f_1 \tag{B.5}$$

$$f_1 = 0.0775 - \frac{0.0109}{\Delta^{0.286}} \tag{B.6}$$

$$f_1 = 0.032 \tag{B.7}$$

$$f_2 = \frac{1}{[2\log_{10}(\frac{2.51}{\mathrm{Re}_2\sqrt{f_2}} + \frac{\Delta}{3.7})]^2} \tag{B.8}$$

$$f = \frac{1}{[2\log_{10}(\frac{2.51}{\mathrm{Re}\sqrt{f}} + \frac{\Delta}{3.7})]^2} \tag{B.9}$$

$$f = \frac{1}{[2\log_{10}(\frac{3.7}{\Delta})]^2} \tag{B.10}$$

$$Re_0 = 754 \exp(\frac{0.0065}{\Delta}) \tag{B.11}$$

$$Re_1 = 1160(\frac{1}{\Delta})^{0.11} \tag{B.12}$$

$$Re_2 = 2090(\frac{1}{\Delta})^{0.0635} \tag{B.13}$$

$$Re_3 = 441.19(\frac{1}{\Delta})^{1.1772} \tag{B.14}$$

The reference for the above formulae is Idelchik [1993].

B.2 Nusselt Number

REGIME	Laminar	Transitional	Turbulent
Forced	Direct Solution	Weighted Average of Forced Laminar and Turbulent	Gnielinski
Mixed	Churchill	Greater Value of Laminar Mixed and Turbulent Mixed	Churchill
Natural	Churchill	Greater Value of Laminar Natural and Turbulent Natural	Churchill

Gnielinski Friction Factor Formula	$\frac{1}{\sqrt{f}}=1.8\cdot\log_{10}(\mathrm{Re})-1.5$
LM=Log Mean b = bulk w = wall L = axial length D = Tube Diameter h = heat transfer coefficient	$\mathrm{Ra}_{LM}=\frac{g\rho^2 c_p \beta D^3 (T_w - T_f)_{LM}}{\nu k}$ $\mathrm{Ra}^* = \frac{g\beta\rho^2 c_p D^4}{\nu k}\left(\frac{dT_f}{dL}\right)$ $\mathrm{Re}=\frac{Du_b\rho}{\nu}\quad Nu=\frac{hD}{k}$

Uniform Wall Heat Flux

REGIME	Laminar	Transitional	Turbulent
Forced	$Nu_{FL}=48/11$	$\left[Nu_{FT}(\text{at } 5000)-Nu_{FL}\right]\cdot\frac{(\mathrm{Re}-2300)}{(5000-2300)}+Nu_{FL}$	$Nu_{FT}=\frac{(f/2)(\mathrm{Re}-1000)\mathrm{Pr}}{1+12.7(f/2)^{1/2}(\mathrm{Pr}^{2/3}-1)}$
Mixed	$Nu_{ML}=\sqrt[6]{Nu_{FL}^6+Nu_{NL}^6}$	IF $Nu_{ML}\le Nu_{MT}$ THEN Nu_{ML} ELSE Nu_{MT}	$Nu_{MT}=\sqrt[3]{Nu_{FT}^3-Nu_{NT}^3}$
Natural	$Nu_{NL}=0.846\mathrm{Ra}^{*1/4}$	IF $Nu_{NL}\le Nu_{NT}$ THEN Nu_{NL} ELSE Nu_{NT}	$Nu_{NT}=\frac{0.15\cdot\mathrm{Ra}^{1/3}}{\left[1+(0.492/\mathrm{Pr})^{9/16}\right]^{16/27}}$

Constant Wall Temperature

REGIME	Laminar	Transitional	Turbulent
Forced	$Nu_{FL}=\overline{Nu_{FL}}=3.657$	$\left[Nu_{FT}(\text{at } 5000)-Nu_{FL}\right]\cdot\frac{(\mathrm{Re}-2300)}{(5000-2300)}+Nu_{FL}$	$Nu_{FT}=\frac{(f/2)(\mathrm{Re}-1000)\mathrm{Pr}}{1+12.7(f/2)^{1/2}(\mathrm{Pr}^{2/3}-1)}$
Mixed	$Nu_{ML}=\overline{Nu_{ML}}=\sqrt[3]{Nu_{FL}^3+Nu_{NL}^3}$	IF $Nu_{ML}\le Nu_{MT}$ THEN Nu_{ML} ELSE Nu_{MT}	$Nu_{MT}=\sqrt[3]{Nu_{FT}^3-Nu_{NT}^3}$
Natural	$\overline{Nu_{NL}}=\frac{0.75(\mathrm{Ra}\cdot\mathrm{D/L})^{1/4}}{\left[1+(0.492/\mathrm{Pr})^{9/16}\right]^{4/9}}$	IF $\overline{Nu_{NL}}\le Nu_{NT}$ THEN Nu_{NL} ELSE Nu_{NT}	$Nu_{NT}=\frac{0.15\cdot\mathrm{Ra}^{1/3}}{\left[1+(0.492/\mathrm{Pr})^{9/16}\right]^{16/27}}$

Table 24 Heat transfer correlations

APPENDIX C: LINEAR SENSITIVITY APPROXIMATION

We will present the methodology as it appears in Chelemer et al. [1975] where it was originally developed and applied to estimate the probability of failure associated with Departure from Nucleate Boiling Ratio (DNBR) variations.

The methodology can be applied to estimate the probability density function of continuous system parameters. The failure of the system is defined whenever the interesting parameter exceeds a pre-specified limit value.

Suppose that a system is defined to be failed whenever its temperature is above a given limit value. Through a model it is possible to simulate the behavior of the system and calculate the temperature value as a function of other system parameters. However, because of uncertainties in the parameters, the calculated temperature value will be uncertain and we can define an uncertainty factor by the following equation

$$y = \frac{T(\text{real})}{T(\text{calculated})} \tag{C.1}$$

The uncertainty factor is supposed to depend on the uncertainties of the input parameters, and at a first order approximation[49] this dependence can be written as

$$\frac{dy}{y} = s_1 \frac{dx_1}{x_1} + s_2 \frac{dx_2}{x_2} + \ldots + s_n \frac{dx_n}{x_n} \tag{C.2}$$

The factor s_i represents the sensitivity factor associated with the i^{th} parameter. Integrating this equation we obtain

---

[49] The approximation consist is that the sensitivity factors are assumed to be constant.

$$y = Cx_1^{s_1} x_2^{s_2} \ldots x_n^{s_n} \tag{C.3}$$

If all parameters except the i[th] are held constant and are assumed to be independent, then the value of s_i can be interpreted as representing the percentage change in temperature resulting from a one percent change in x_i, all other parameters being held constant.

$$s_i = \frac{\partial y}{y} \Big/ \frac{\partial x_i}{x_i} = \frac{\partial(\ln y)}{\partial(\ln x_i)} \tag{C.4}$$

Considering each parameter x_i as being distributed around a mean value μ_i, it is possible to expand y in a Taylor's series about the μ_i

$$y - \mu_y = \frac{\partial y}{\partial x_1}(x_1 - \mu_1) + \frac{\partial y}{\partial x_2}(x_2 - \mu_2) + \ldots + \frac{\partial y}{\partial x_n}(x_n - \mu_n) + \text{higher order terms} \tag{C.5}$$

From (C.3) we have

$$\mu_y = C\mu_1^{s_1} \mu_2^{s_2} \ldots \mu_n^{s_n} \tag{C.6}$$

If the perturbations around the mean values are small, the higher order terms in (C.5) can ignored, and the variance of y results in the following expression

$$\sigma_y^2 = (\frac{\partial y}{\partial x_1})^2 \sigma_1^2 + (\frac{\partial y}{\partial x_2})^2 \sigma_2^2 + \ldots + (\frac{\partial y}{\partial x_n})^2 \sigma_n^2 \tag{C.7}$$

Using (C.3), (C.6), and (C.7), we have

$$(\frac{\sigma_y^2}{\mu_y})^2 = s_1^2 (\frac{\sigma_1^2}{\mu_1})^2 + s_2^2 (\frac{\sigma_2^2}{\mu_2})^2 + \ldots + s_n^2 (\frac{\sigma_n^2}{\mu_n})^2 \tag{C.8}$$

(C.8) is the main result of the methodology. Given the uncertainties of each parameter and the sensitivities it is possible to calculate the uncertainty in the temperature uncertain factor. Also, the central limit theorem of statistic indicates that the probability distribution function of y will approach a normal distribution even if the distributions of the individual parameters are not[50]. Once the distribution of y is known it is then possible to calculate the probability that the real temperature value will be above the limit using the normal cumulative distribution function.

The above procedure is simple and provides a quick first estimate for the failure probability value. It should be noted that the assumptions involved are sometimes very strict and cannot be fully applied in practice. First, the system sensitivities to the parameters can vary widely from the operating condition point to a point near the limit surface. Second, the first order approximation involved in discarding the higher order terms in (C.5) cannot be valid because of synergic effects between different parameters. Third, it is possible that a limited number of parameters, maybe only one or two, dominates thus determining the non normality of the distribution of y. Finally, and probably most important for the estimation of low probability events, the central limit theorem guarantees the normality of the distribution near the mean value, but not so much in the tails of the distribution whose shape actually affects the final result. For the above reasons the methodology should be used to provide a first estimate of the results, but not entirely relied upon without additional evidence.

---

[50] Provided there are sufficient uncertain parameters and no one dominates the others.

APPENDIX D: MATLAB CODE FOR GFR THERMAL HYDRAULIC MODEL

```
function [Data_heater,Data_cooler,Data_sections] =
GFR_single_loop(Riser_geometry,Loop_geometry,...

Heater_input,Cooler_input,Fluid_type,Peaking_factor,Press,Nu_error_force
d,Nu_error_mixed,Nu_error_free,f_error_forced,f_error_mixed,f_error_free
)

%function [Data_heater,Data_cooler,Data_sections] =
GFR_single_loop(Riser_geometry,Loop_geometry,...
%
Heater_input,Cooler_input,Fluid_type,Peaking_factor,Press,Nu_error,f_err
or)
%
%Calculates the steady state cooling regime of a GFR
%
%OUTPUT
%
%Data_heater, Data_cooler are the output matrices for heater and cooler
%they have N rows (N is the number of nodilization cells)
%and 12 columns arranged as follows
%Z(m) Q(kW/m2) T_bulk(C) T_wall(C) h(kW/m2-K) Press(kPa) Rho(kg/m3) Re
V(m/s) dP(Pa) Nu Pr
%Data_heater has also a third dimension so that Data_heater(:,:,1) are
the
%values of the hot rod and Data_heater(:,:,2) are the values of the
average rod
%
%Data_sections has as many lines as the different sections and 12
columns of average values
%Dh(m) A(m2) L(m) H(m) K R(m) T(C) Rho(kg/m3) V(m/s) Press(kPa) dP(Pa)
Re
%
%
%INPUT
%
%Riser_geometry is a matrix containing data relative to the common part
of the plant
%it has as many lines as the different sections, usually 5
%vessel lower space, bottom reflector, heater, upper reflector and
vessel upper space
%it has 6 columns arranged as follows
%Dh(m) A(m2) L(m) H(m) K R(m)
%where L is the length of the section while H is the heigth
%K is the concentrated loss and R is roughness
%
%Loop_geometry is a matrix containing data relative to the loop part of
the plant
%it has as many lines as the different sections, usually 5
%inclined ducting, cooler upper plenum, cooler, ducting, horizontal
ducting
%Dh(m) A(m2) L(m) H(m) K R(m)
%where L is the length of the section while H is the heigth
%K is the concentrated loss and R is roughness
%
%Heater_input contains data for the heater, it is a vector with 4 lines
```

```
%[heater position as line in Riser_geometry, number of nodalization
points, average Q(kW/m2), number of channels]'
%
%Cooler_input contains data for the cooler, it is a vector with 5 lines
%[cooler position as line in Loop_geometry, number of nodalization
points, wall temperature(C), number of channels, number of loops]'
%
%Fluid type is a flag =1 for CO2; =2 for He
%
%Peaking_factor is a vector [axial peak, radial peak]'
%
%Press is the operating pressure (kPa) at the lower vessel plenum
%Nu_error and f_error are the error coefficient of the correlations
%
%
%%%%%%%%%%%%%%%%%%%%%%%%%%%%%%%%%%%%%%
%%                                    %
%%  Written by L. Pagani - Nov 2003 %
%%  Modified Feb 2004               %
%%                                    %
%%%%%%%%%%%%%%%%%%%%%%%%%%%%%%%%%%%%%%



global Heater_index Cooler_index Number_of_sections Heater_nodalization
Cooler_nodalization Hot_flow_fraction Mass_flow...
    Number_of_riser_sections Heater_channels Cooler_channels T_max_gas

%Load the table of gas properties
if Fluid_type == 1
    co2_data_tables;
elseif Fluid_type == 2
    helium_data_tables;
else
    error('Fluid_type variable is not correctly defined')
end

%set maximum temperatures
T_max_gas=TEMPERATURE_RANGE(2);


%Create output variables
Heater_nodalization=Heater_input(2);
Data_heater=zeros(Heater_nodalization,12,2);

Cooler_nodalization=Cooler_input(2);
Data_cooler=zeros(Cooler_nodalization,12);

Number_of_riser_sections=size(Riser_geometry,1);
Number_of_loop_sections=size(Loop_geometry,1);
Number_of_sections=Number_of_riser_sections+Number_of_loop_sections;
Data_sections=zeros(Number_of_sections,12);

%Initialize variables
Heater_index=Heater_input(1);
Cooler_index=Cooler_input(1);

T_cooler_wall=Cooler_input(3)+273.15;    %defines the temperature in
Kelvin

%Define inital flow as Re=10000
```

```
%calculates properties in heater inlet
Rho_inlet=density_gas_pt(Press,T_cooler_wall);
Viscosity_inlet=viscosity_gas_pt(Press,T_cooler_wall)*1e-6; %using all
SI units
V_inlet=10000*Viscosity_inlet/(Rho_inlet*Riser_geometry(Heater_index,1))
;



Q_average=Heater_input(3);              %average heat flux (kW/m2)
Heater_channels=Heater_input(4);
Cooler_channels=Cooler_input(4);
heater_surface_total=4*Riser_geometry(Heater_index,2)/Riser_geometry(Hea
ter_index,1)*Riser_geometry(Heater_index,3)*Heater_channels;
Q_average_total=heater_surface_total*Q_average; %kW
Cp_inlet=cp_gas_pt(Press,T_cooler_wall);

T_heater_outlet=min(T_cooler_wall+Q_average_total/...

(Cp_inlet*Rho_inlet*V_inlet*Heater_channels*Riser_geometry(Heater_index,
2)),T_max_gas);  %Rising temperature
if T_heater_outlet > T_max_gas
    T_heater_outlet = T_max_gas;
end

Rho_outlet=density_gas_pt(Press,T_heater_outlet);

for j=1:Number_of_sections
    if j <= Number_of_riser_sections
        for k=1:6
            Data_sections(j,k)=Riser_geometry(j,k);
        end
    else
        for k=1:6
            Data_sections(j,k)=Loop_geometry(j-
Number_of_riser_sections,k);
        end
    end

    if j < Heater_index | j > (Cooler_index+Number_of_riser_sections)
        Data_sections(j,7)=T_cooler_wall;
        Data_sections(j,8)=Rho_inlet;
    elseif j == Heater_index | j ==
(Cooler_index+Number_of_riser_sections)
        Data_sections(j,7)=mean([T_cooler_wall,T_heater_outlet]);
        Data_sections(j,8)=mean([Rho_inlet,Rho_outlet]);
    else
        Data_sections(j,7)=T_heater_outlet;
        Data_sections(j,8)=Rho_outlet;
    end
    if j >= Heater_index-1 & j <= Heater_index+1        %also the
reflector has the channels
        Data_sections(j,9)=V_inlet;
    elseif j == (Cooler_index+Number_of_riser_sections)

Data_sections(j,9)=V_inlet*(Rho_inlet*Heater_channels*Riser_geometry(Hea
ter_index,2))/...
            (Data_sections(j,8)*Data_sections(j,2)*Cooler_channels);
    else
```

```
Data_sections(j,9)=V_inlet*(Rho_inlet*Heater_channels*Riser_geometry(Hea
ter_index,2))/...
            (Data_sections(j,8)*Data_sections(j,2));
    end
end
Data_sections(:,10)=Press;
Data_heater(:,6,:)=Press;
Data_cooler(:,6)=Press;


heater_heigth=Riser_geometry(Heater_index,4);
cooler_heigth=Loop_geometry(Cooler_index,4);

Data_heater(:,1,1)=[heater_heigth/Heater_nodalization:heater_heigth/Heat
er_nodalization:heater_heigth]';
Data_heater(:,1,2)=[heater_heigth/Heater_nodalization:heater_heigth/Heat
er_nodalization:heater_heigth]';
Data_cooler(:,1)=[cooler_heigth/Cooler_nodalization:cooler_heigth/Cooler
_nodalization:cooler_heigth]';

F_axial=Peaking_factor(1);
F_radial=Peaking_factor(2);

%Solve for extrapolation length using relative coordinate [Hermansky]
extr=0.02;
extrn=0;

Delta_z = 1/Heater_nodalization;
Norm_z=[Delta_z/2:Delta_z:1-Delta_z/2];

if F_axial ~= 1
    while abs(extr-extrn) > 1e-4
        extrn=extr;
        extr=(pi/2/F_axial/cos(pi*extrn/(1+2*extrn))-1)/2;
    end

Data_heater(:,2,1)=F_radial*Q_average*F_axial*sin(pi*(Norm_z+extr)/(1+2*
extr)); %define the cosine shape in the hot rod

Data_heater(:,2,2)=Q_average*F_axial*sin(pi*(Norm_z+extr)/(1+2*extr));
%define the cosine shape in the average rod

else
    Data_heater(:,2,1)=F_radial*Q_average; %define the cosine shape in
the hot rod
    Data_heater(:,2,2)=Q_average; %define the cosine shape in the
average rod
end



%defines linear initial profile for temperature
%it is necessary to define an initial profile to calculate the
%correlations for Nu number
Delta_T=T_heater_outlet-T_cooler_wall;
Delta_T_heater=Delta_T/Heater_nodalization;
Delta_T_cooler=Delta_T/Cooler_nodalization;
Data_heater(:,3,1)=[T_cooler_wall+Delta_T_heater/2:Delta_T_heater:T_heat
er_outlet-Delta_T_heater/2]';
```

```
Data_heater(:,3,2)=[T_cooler_wall+Delta_T_heater/2:Delta_T_heater:T_heat
er_outlet-Delta_T_heater/2]';
Data_cooler(:,3)=[T_heater_outlet-Delta_T_cooler/2:-
Delta_T_cooler:T_cooler_wall+Delta_T_cooler/2]';

Data_heater(:,4,1)=Data_heater(:,3,1)+100;      %add 100 degrees to the
bulk temperature
Data_heater(:,4,2)=Data_heater(:,3,2)+100;      %add 100 degrees to the
bulk temperature
Data_heater(1,4,1)=Data_heater(1,3,1)+50;      %to avoid a division by
zero in the mean log temperature
Data_heater(1,4,2)=Data_heater(1,3,2)+50;      %to avoid a division by
zero in the mean log temperature


Data_cooler(:,4)=T_cooler_wall;


%check for geometry consistency
if sum(Data_sections(:,4)) >= 1e-5 | sum(Data_sections(:,4)) <= -1e-5
    error('The geometry is not consistent.  Please check that the z
raise in the riser is equal to the z descent in the loop part.')
end


%Set inital condition

Rho=density_gas_pt(Press,T_cooler_wall);
Mass_flow=Rho*V_inlet*Data_sections(Heater_index,2)*Heater_channels;

Hot_flow_fraction=1/Heater_channels;      %flow in the hot rod;

T_inlet_old=T_cooler_wall;

[T_inlet_new,Data_heater,Data_cooler,Data_sections]=Iterate_temperature(
T_inlet_old,Data_heater,Data_cooler,Data_sections,...

Cooler_input,Heater_input,Press,Nu_error_forced,Nu_error_mixed,Nu_error_
free);
Temp_eq=T_inlet_new-T_inlet_old;

[dP_eq,Data_heater,Data_cooler,Data_sections]=Calculates_dP(Mass_flow,Da
ta_heater,Data_cooler,Data_sections,...
    Cooler_input,Press,f_error_forced,f_error_mixed,f_error_free);

Count=1;
while abs(dP_eq) > 1  | abs(Temp_eq) > 1e-1

    Hot_flow_fraction;


    T_count=1;  %this counter is necessary because the temperature
iteration does not always converge
    while abs(Temp_eq) > 1e-1

        %iterate on the temperature
        T_inlet_old=T_inlet_new;

[T_inlet_new,Data_heater,Data_cooler,Data_sections]=Iterate_temperature(
T_inlet_old,Data_heater,Data_cooler,Data_sections,...
```

```
Cooler_input,Heater_input,Press,Nu_error_forced,Nu_error_mixed,Nu_error_
free);
        T_count=T_count+1;
        if T_count==10
            Temp_eq=0;
        else
            Temp_eq=T_inlet_new-T_inlet_old;
        end
        Temp_eq;  %%%%%%%%%%%%%%%%%%%%%%%%%%%%%%%%5
    end

[dP_eq,Data_heater,Data_cooler,Data_sections]=Calculates_dP(Mass_flow,Da
ta_heater,Data_cooler,Data_sections,...
        Cooler_input,Press,f_error_forced,f_error_mixed,f_error_free);

    while abs(dP_eq) > 1
        Mass_flow_old=Mass_flow;
        dP_old=dP_eq;
        if dP_old > 0       %means too much losses
            Mass_flow=0.9*Mass_flow_old;
        else
            Mass_flow=1.1*Mass_flow_old;
        end

[dP_eq,Data_heater,Data_cooler,Data_sections]=Calculates_dP(Mass_flow,Da
ta_heater,Data_cooler,Data_sections,...

Cooler_input,Press,f_error_forced,f_error_mixed,f_error_free);
        dP_slope=(Mass_flow-Mass_flow_old)/(dP_eq-dP_old);
        Mass_flow=Mass_flow_old-dP_slope*dP_old;            %Approach
the balance through linear approximations

[dP_eq,Data_heater,Data_cooler,Data_sections]=Calculates_dP(Mass_flow,Da
ta_heater,Data_cooler,Data_sections,...

Cooler_input,Press,f_error_forced,f_error_mixed,f_error_free);
    end
    T_inlet_old=T_inlet_new;

[T_inlet_new,Data_heater,Data_cooler,Data_sections]=Iterate_temperature(
T_inlet_old,Data_heater,Data_cooler,Data_sections,...

Cooler_input,Heater_input,Press,Nu_error_forced,Nu_error_mixed,Nu_error_
free);
    Temp_eq=T_inlet_new-T_inlet_old;

[dP_eq,Data_heater,Data_cooler,Data_sections]=Calculates_dP(Mass_flow,Da
ta_heater,Data_cooler,Data_sections,...
        Cooler_input,Press,f_error_forced,f_error_mixed,f_error_free);
    Count=Count+1;
    if Count==10
        Temp_eq=0;
        dP_eq=0;
    end
    Temp_eq; %%%%%%%%%%%%%%%%%%%55
end

%transform the temperatures in Celsius
Data_sections(:,7)=Data_sections(:,7)-273.15;
Data_heater(:,3,:)=Data_heater(:,3,:)-273.15;
```

```
Data_heater(:,4,:)=Data_heater(:,4,:)-273.15;
Data_cooler(:,3)=Data_cooler(:,3)-273.15;
Data_cooler(:,4)=Data_cooler(:,4)-273.15;


%%%%%%%%%%%%%%%%%%%%%%%%%%%%%%%%%%%%%%%%%%%%%%%%%%%%%%%%%%%%%%%%%%%%%%%%%%%
%%%%%%%%%%%%%%%%%%%%%%%%%%%%%%%%%%%%%%%%%%%%%%%%%%%%%%%%%%%%%%%%%%%%%%%%%%%



%%%%%%%%%%%%%%%%%%%%%%%%%%%%%%%%%%%%%%%%%%%%%%%%%%%%%%%%%%%%%%%%%%%%%%%%%%%%
%%%%%%%%%%%%%%%%%%%%%%%%%%%%%%%%%%%%%%%%%%%%%%%%%%%%%%%%%%%%%%%%%%%%%%%%%%%%


function
[dP,Data_heater,Data_cooler,Data_sections]=Calculates_dP(Mass_flow,Data_
heater,Data_cooler,Data_sections,...
    Cooler_input,Press,f_error_forced,f_error_mixed,f_error_free)

%we do not consider acceleration losses because they cancel over the
loop

global Heater_index Cooler_index Number_of_sections Heater_nodalization
Cooler_nodalization Hot_flow_fraction ...
    Number_of_riser_sections Heater_channels Cooler_channels

dP=0;       %start from zero at section 1
for j=1:Number_of_sections
    if j == Heater_index
        %we approximate the pressure losses in the core as the pressure
losses
        %of the average channel and we keep the average channel mass
flow
        %equal to the total mass flow divided by the number of channels
        %this approximation holds because of the large number of
channels
        Delta=Data_sections(j,6)/Data_sections(j,1);



%%%%%%%%%%%%%%%%%%%%%%%%%%%%%%%%%%%%%%%%%%%%%%%%%%%%%%%%%%%%%%%%%%%%%%%%%%%%
%%%%%%%%5
        %%%%%%%%%%%%%%%%%%%%%%%%%%%%%%%%%%%%%5

        Rho=density_gas_pt(Press,Data_sections(j-1,7));
        V=Mass_flow/(Rho*Data_sections(j-1,2)*Heater_channels);
        Visc=viscosity_gas_pt(Press,Data_sections(j-1,7))*1e-6;
        Re=Rho*V*Data_sections(j-1,1)/Visc;
        Delta=Data_sections(j-1,6)/Data_sections(j-1,1);
        f=friction_factor(Re,Delta);    %no error on f in normal
sections
        dP_dist=f*(Data_sections(j-1,3)/Data_sections(j-
1,1))*0.5*Rho*V^2;

        %%%%%%%%%%%%%%%%% Form losses
        dP_form=Data_sections(j-1,5)*0.5*Rho*V^2;

        %%%%%%%%%%%%%%%%% Gravity losses
        dP_gravity=9.81*Rho*Data_sections(j-1,4);

        dP_reflector_bottom=dP_gravity+dP_form+dP_dist;
```

```
        Rho=density_gas_pt(Press,Data_sections(j+1,7));
        V=Mass_flow/(Rho*Data_sections(j+1,2)*Heater_channels);
        Visc=viscosity_gas_pt(Press,Data_sections(j+1,7))*1e-6;
        Re=Rho*V*Data_sections(j+1,1)/Visc;
        Delta=Data_sections(j+1,6)/Data_sections(j+1,1);
        f=friction_factor(Re,Delta);    %no error on f in normal
sections

dP_dist=f*(Data_sections(j+1,3)/Data_sections(j+1,1))*0.5*Rho*V^2;

        %%%%%%%%%%%%%%%% Form losses
        dP_form=Data_sections(j+1,5)*0.5*Rho*V^2;

        %%%%%%%%%%%%%%%% Gravity losses
        dP_gravity=9.81*Rho*Data_sections(j+1,4);

        dP_reflector_upper=dP_gravity+dP_form+dP_dist;

%%%%%%%%%%%%%%%%%%%%%%%%5
%%%%%%%%%%%%%%%%%%%%%%%%%%%%%%%%%%%%%%%%%%%%%%%%%%%%%%%%%%%%%%%%%%%%%%%%%%%
%%%%%%%%%%%%5

        dP_complete_average=dP_reflector_upper+dP_reflector_bottom;
        for h=1:Heater_nodalization
            %%%%%%%%%%%%%%%%%% Distributed losses
            Rho=density_gas_pt(Press,Data_heater(h,3,2));
            Data_heater(h,7,2)=Rho;      %store the value of Rho in
Data_heater
            V=Mass_flow/(Rho*Data_sections(j,2)*Heater_channels);
            if h==1
                dP_Acc_in=0.5*Rho*V^2;
            elseif h==Heater_nodalization
                dP_Acc_out=0.5*Rho*V^2;
            end
            Data_heater(h,9,2)=V;          %store the value of V in
Data_heater
            Visc=viscosity_gas_pt(Press,Data_heater(h,3,2))*1e-6;
            Re=Rho*V*Data_sections(j,1)/Visc;
            Data_heater(h,8,2)=Re;

            if Data_heater(h,11,2)==10
                f_error=f_error_forced;
            elseif Data_heater(h,11,2)==20
                f_error=f_error_mixed;
            else
                f_error=f_error_free;
            end


            [f,regime]=friction_factor(Re,Delta);
            f=f*f_error;
            Data_heater(h,12,2)=regime;

dP_dist=f*(Data_sections(j,3)/Heater_nodalization/Data_sections(j,1))*0.
5*Rho*V^2;

            if h==1
                %%%%%%%%%%%%%%%% Form losses
                dP_form=Data_sections(j,5)*0.5*Rho*V^2; %form losses are
concentrated in the first node
```

```
            else
                dP_form=0;
            end

            %%%%%%%%%%%%%%%% Gravity losses
            dP_gravity=9.81*Rho*Data_sections(j,4)/Heater_nodalization;

            dP=dP+dP_gravity+dP_form+dP_dist;       %increase dP of the
amount calculated

dP_complete_average=dP_complete_average+dP_gravity+dP_form+dP_dist;
            Data_heater(h,10,2)=dP_form+dP_dist;%+dP_gravity;
        end
        Data_sections(j,8)=mean(Data_heater(:,7,2));    %Rho
        Data_sections(j,9)=mean(Data_heater(:,9,2));    %V
        Data_sections(j,12)=mean(Data_heater(:,8,2));   %Re
        Data_sections(j,11)=sum(Data_heater(:,10,2));   %dP


        % now we have to calculate the split of flow between the hot
channel and the average channel
        % It is necessary to take into accoutn also the acceleration
losses for this calculation

        dP_complete_average=dP_complete_average+(dP_Acc_out-dP_Acc_in);

        %%%%%%%%%%%%%%%%%%%%%%%% Now the pressure losses in the hot
channel
        dP_complete_hot=0;




        Step_size=min(0.1,Hot_flow_fraction/2);
        direction=1;


        while(abs(dP_complete_hot-dP_complete_average)) > 1


            Step_size=min(Step_size,Hot_flow_fraction/2);

            if dP_complete_hot-dP_complete_average > 0
                if direction == 1
                    Step_size=Step_size/2;
                    direction = -1;
                end
            else
                if direction == -1
                    Step_size=Step_size/2;
                    direction = 1;
                end
            end

            if direction ==1
                Hot_flow_fraction=Hot_flow_fraction+Step_size;
            elseif direction == -1
                Hot_flow_fraction=Hot_flow_fraction-Step_size;
            end
```

```
            Delta=Data_sections(j,6)/Data_sections(j,1);


%%%%%%%%%%%%%%%%%%%%%%%%%%%%%%%%%%%%%%%%%%%%%%%%%%%%%%%%%%%%%%%%%%%%%%%%%%%%%%%%
%%%%%%%%%5
            %%%%%%%%%%%%%%%%%%%%%%%%%%%%%%%%%%%%%5

            Rho=density_gas_pt(Press,Data_sections(j-1,7));
            V=Mass_flow*Hot_flow_fraction/(Rho*Data_sections(j-1,2));
            Visc=viscosity_gas_pt(Press,Data_sections(j-1,7))*1e-6;
            Re=Rho*V*Data_sections(j-1,1)/Visc;
            Delta=Data_sections(j-1,6)/Data_sections(j-1,1);
            f=friction_factor(Re,Delta);    %no error on f in normal
sections
            dP_dist=f*(Data_sections(j-1,3)/Data_sections(j-
1,1))*0.5*Rho*V^2;

            %%%%%%%%%%%%%%%%% Form losses
            dP_form=Data_sections(j-1,5)*0.5*Rho*V^2;

            %%%%%%%%%%%%%%%%% Gravity losses
            dP_gravity=9.81*Rho*Data_sections(j-1,4);

            dP_reflector_bottom=dP_gravity+dP_form+dP_dist;


Rho=density_gas_pt(Press,Data_heater(Heater_nodalization,3,1));
            V=Mass_flow*Hot_flow_fraction/(Rho*Data_sections(j+1,2));

Visc=viscosity_gas_pt(Press,Data_heater(Heater_nodalization,3,1))*1e-6;
            Re=Rho*V*Data_sections(j+1,1)/Visc;
            Delta=Data_sections(j+1,6)/Data_sections(j+1,1);
            f=friction_factor(Re,Delta);    %no error on f in normal
sections

dP_dist=f*(Data_sections(j+1,3)/Data_sections(j+1,1))*0.5*Rho*V^2;

            %%%%%%%%%%%%%%%%% Form losses
            dP_form=Data_sections(j+1,5)*0.5*Rho*V^2;

            %%%%%%%%%%%%%%%%% Gravity losses
            dP_gravity=9.81*Rho*Data_sections(j+1,4);

            dP_reflector_upper=dP_gravity+dP_form+dP_dist;

            %%%%%%%%%%%%%%%%%%%%%%%%5

%%%%%%%%%%%%%%%%%%%%%%%%%%%%%%%%%%%%%%%%%%%%%%%%%%%%%%%%%%%%%%%%%%%%%%%%%%%%%%%%
%%%%%%%%%%%%5

            dP_complete_hot=dP_reflector_upper+dP_reflector_bottom;
            for h=1:Heater_nodalization
                %%%%%%%%%%%%%%%%%% Distributed losses
                Rho=density_gas_pt(Press,Data_heater(h,3,1));
                Data_heater(h,7,1)=Rho;      %store the value of Rho in
Data_heater
                V=Mass_flow*Hot_flow_fraction/(Rho*Data_sections(j,2));
```

```
                if h==1
                    dP_Acc_in=0.5*Rho*V^2;
                elseif h==Heater_nodalization
                    dP_Acc_out=0.5*Rho*V^2;
                end
                Data_heater(h,9,1)=V;          %store the value of V in
Data_heater
                Visc=viscosity_gas_pt(Press,Data_heater(h,3,1))*1e-6;
                Re=Rho*V*Data_sections(j,1)/Visc;
                Data_heater(h,8,1)=Re;

                if Data_heater(h,11,1)==10
                    f_error=f_error_forced;
                elseif Data_heater(h,11,1)==20
                    f_error=f_error_mixed;
                else
                    f_error=f_error_free;
                end



                [f,regime]=friction_factor(Re,Delta);
                f=f*f_error;
                Data_heater(h,12,1)=regime;

dP_dist=f*(Data_sections(j,3)/Heater_nodalization/Data_sections(j,1))*0.
5*Rho*V^2;

                if h==1
                    %%%%%%%%%%%%%%%%% Form losses
                    dP_form=Data_sections(j,5)*0.5*Rho*V^2; %form losses
are concentrated in the first node

                else
                    dP_form=0;
                end

                %%%%%%%%%%%%%%%%% Gravity losses

dP_gravity=9.81*Rho*Data_sections(j,4)/Heater_nodalization;


dP_complete_hot=dP_complete_hot+dP_gravity+dP_form+dP_dist;

            end
            dP_complete_hot=dP_complete_hot+(dP_Acc_out-dP_Acc_in);


        end
        %%%%%%%%%%%%%%%%%%%

    elseif j == Cooler_index + Number_of_riser_sections
        Delta=Data_sections(j,6)/Data_sections(j,1);
        Mass_flow=Mass_flow/Cooler_input(5); %divides by the number of
loops
        for h=1:Cooler_nodalization
            %%%%%%%%%%%%%%%%%% Distributed losses
            Rho=density_gas_pt(Press,Data_cooler(h,3));
            Data_cooler(h,7)=Rho;      %store the value of Rho in
Data_cooler
            V=Mass_flow/(Rho*Data_sections(j,2)*Cooler_channels);
```

```
            Data_cooler(h,9)=V;          %store the value of V in
Data_cooler
            Visc=viscosity_gas_pt(Press,Data_cooler(h,3))*1e-6;
            Re=Rho*V*Data_sections(j,1)/Visc;
            Data_cooler(h,8)=Re;

            if Data_cooler(h,11)==10
                f_error=f_error_forced;
            elseif Data_cooler(h,11)==20
                f_error=f_error_mixed;
            else
                f_error=f_error_free;
            end



            [f,regime]=friction_factor(Re,Delta);
            f=f*f_error;
            Data_cooler(h,12)=regime;

dP_dist=f*(Data_sections(j,3)/Cooler_nodalization/Data_sections(j,1))*0.
5*Rho*V^2;
            if h==1
                %%%%%%%%%%%%%%%% Form losses
                dP_form=Data_sections(j,5)*0.5*Rho*V^2; %form losses are
concentrated in the first node

            else
                dP_form=0;
            end

            %%%%%%%%%%%%%%%% Gravity losses
            dP_gravity=9.81*Rho*Data_sections(j,4)/Cooler_nodalization;

            dP=dP+dP_gravity+dP_form+dP_dist;       %increase dP of the
amount calculated
            Data_cooler(h,10)=dP_form+dP_dist;%+dP_gravity;
        end
        Mass_flow=Mass_flow*Cooler_input(5); %multiplies by the number
of loops
        Data_sections(j,8)=mean(Data_cooler(:,7));   %Rho
        Data_sections(j,9)=mean(Data_cooler(:,9));   %V
        Data_sections(j,12)=mean(Data_cooler(:,8));  %Re
        Data_sections(j,11)=sum(Data_cooler(:,10));  %dP

    else
        %here we are in normal sections
        %%%%%%%%%%%%%%%% Distributed losses
        Rho=density_gas_pt(Press,Data_sections(j,7));
        Data_sections(j,8)=Rho;      %store the value of Rho in
Data_sections

        if j < Heater_index-1 | j > Heater_index+1  %the bottom and
upper reflector have the same number of channels as the core
            if j > Number_of_riser_sections
                V=Mass_flow/(Rho*Data_sections(j,2)*Cooler_input(5));
            else
                V=Mass_flow/(Rho*Data_sections(j,2));
            end
        else
            V=Mass_flow/(Rho*Data_sections(j,2)*Heater_channels);
```

```
        end
        Data_sections(j,9)=V;          %store the value of V in
Data_sections
        Visc=viscosity_gas_pt(Press,Data_sections(j,7))*1e-6;
        Re=Rho*V*Data_sections(j,1)/Visc;
        Data_sections(j,12)=Re;        %store the value of Re in
Data_sections
        Delta=Data_sections(j,6)/Data_sections(j,1);
        [f,regime]=friction_factor(Re,Delta);    %no error on f in
normal sections
        dP_dist=f*(Data_sections(j,3)/Data_sections(j,1))*0.5*Rho*V^2;

        %%%%%%%%%%%%%%%%% Form losses
        dP_form=Data_sections(j,5)*0.5*Rho*V^2;

        %%%%%%%%%%%%%%%%% Gravity losses
        dP_gravity=9.81*Rho*Data_sections(j,4);

        dP=dP+dP_gravity+dP_form+dP_dist;       %increase dP of the
amount calculated
        Data_sections(j,11)=dP_form+dP_dist;  %+dP_gravity; %store the
value of dP in Data_sections

        %%%%%%%%%%%%%%%%%%%%%%%%%%%%%%%%%%%%%%%%%%%%%%%%%%%%%%%%%%%%
%         %this line has been added to check the blower with LOCA COLA
%         if j==1
%             dP=dP-3150;
%             Data_sections(j,11)=Data_sections(j,11)-3150;
%         end
%         %
    end
end

%%%%%%%%%%%%%%%%%%%%%%%%%%%%%%%%%%%%%%%%%%%%%%%%%%%%%%%%%%%%%%%%%%%
%%%%%%%%%%%%%%%%%%%%%%%%%%%%%%%%%%%%%%%%%%%%%%%%%%%%%%%%%%%%%%%%%%%
%%%%%%%%%%%%%%%%%%%%%%%%%%%%%%%%%%%%%%%%%%%%%%%%%%%%%%%%%%%%%%%%%%%



function [f,regime] = friction_factor(Re,delta)

%function f = friction_factor(Re,delta)
%takes as an argument the Reynolds number and
%the ratio of the roughness and the hydraulic diameter (delta)
%returns the friction factor.
%The result is valid for all regimes
%
%Written by L. Pagani - Nov 2003


%First define transition points for different regimes

%Re0 is the limit between from laminar flow to transition region
%Re1 is the limit between transition region to increasing friction
factor
%Re2 is the limit between increasing friction factor and turbulent
depending on Re
%Re3 is the limit between turbulent depending on Re and fully developed
turbulent independent on Re

if delta < 0.007
```

```
    Re0=2000;
    Re1=2000;
else
    Re0=754*exp(0.0065/delta);
    Re1=1160/(delta^0.11);
end

Re2=2090/(delta^0.0635);
Re3=441.19/(delta^1.1772);

%Depending on the type of flow calculates the friction factor
if Re <= Re0
    f=64/Re;                                        %Laminar flow
    regime=1;
elseif Re <= Re1
    if delta < 0.007
        f1=0.032;
        f2=0.03979;
        f=f1+(f2-f1)/2000*(Re-2000);                %Transition flow -
interpolation between Hagen-Poiseuille and Blasius laws
    else
        f=4.4*Re^(-0.595)*exp(-0.00275/delta);   %Transition flow
%%%%%%%%%%%%ERROR FOUND
    end
    regime=2;
elseif Re <= Re2
    %Calculate iteratively the value of friction factor from Colebrook-
White formula
    f2=0.11*(delta+68/Re2)^0.25;                    %Starting point
    fn=0;
    while abs(fn-f2) > 0.001   %Defines the error on the result
        fn=f2;
        f2=1/(2*log10(2.51/Re2/sqrt(fn)+delta/3.7))^2;  %Colebrook-White
formula
    end
    if delta < 0.007
        f1=0.032;
    else
        f1=0.0758-0.0109/(delta^0.286);
    end
    f=(f2-f1)*exp(-(0.0017*(Re2-Re))^2)+f1;     %Increasing friction
factor
    regime=3;
elseif Re <=Re3
    %Calculate iteratively the value of friction factor from Colebrook-
White formula
    f=0.11*(delta+68/Re)^0.25;                  %Starting point
    fn=0;
    while abs(fn-f) > 0.001   %Defines the error on the result
        fn=f;
        f=1/(2*log10(2.51/Re/sqrt(fn)+delta/3.7))^2;  %Colebrook-White
formula - Turbulent flow depending on Re
    end
    regime=4;
else
    %Calculate iteratively the value of friction factor from Colebrook-
White formula
    f=0.11*(delta+68/Re3)^0.25;                 %Starting point
    fn=0;
    while abs(fn-f) > 0.001   %Defines the error on the result
        fn=f;
```

```
        f=1/(2*log10(2.51/Re3/sqrt(fn)+delta/3.7))^2;  %Colebrook-White
formula - Turbulent flow independent on Re
    end
    regime=5;
end


%%%%%%%%%%%%%%%%%%%%%%%%%%%%%%%%%%%%%%%%%%%%%%%%%%%%%%%%%%%%%%%%%%%%
%%%%%%%%%%%%%%%%%%%%%%%%%%%%%%%%%%%%%%%%%%%%%%%%%%%%%%%%%%%%%%%%%%%%
%%%%%%%%%%%%%%%%%%%%%%%%%%%%%%%%%%%%%%%%%%%%%%%%%%%%%%%%%%%%%%%%%%%%


function
[T_inlet_new,Data_heater,Data_cooler,Data_sections]=Iterate_temperature(
T_inlet_old,Data_heater,Data_cooler,Data_sections,...

Cooler_input,Heater_input,Press,Nu_error_forced,Nu_error_mixed,Nu_error_
free)

global Heater_index Number_of_sections Heater_nodalization Cooler_index
Hot_flow_fraction Mass_flow...
    Number_of_riser_sections Heater_channels Cooler_nodalization
T_max_gas

T_previous=T_inlet_old;
if T_inlet_old > T_max_gas
    T_previous=T_max_gas;
elseif T_inlet_old < 303.15
    T_previous=303.15;
end

for j=1:Number_of_sections

    if j == Heater_index
        D=Data_sections(Heater_index,1);
        Ltot=Data_sections(Heater_index,3);
        L=Data_sections(Heater_index,3)./Heater_nodalization;
%%%%%%%%%%%%%%%%%%%%%%%%%%%%%%%%%%%
        for k=1:2                %does the average and hot rod
            if k==1
                Mass_flow_core=Mass_flow*Hot_flow_fraction;
            else
                Mass_flow_core=Mass_flow*(1-
Hot_flow_fraction)/(Heater_channels-1);         %this is approximate
because of the large number of channels
            end
            %define parameters for heat transfer coefficient calculation
            T_wall_average=mean(Data_heater(:,4,k));
            T_in_bulk=Data_heater(1,3,k);
            T_out_bulk=Data_heater(Heater_nodalization,3,k);
            T_in_wall=Data_heater(1,4,k);
            T_out_wall=Data_heater(Heater_nodalization,4,k);
            Type=1;     %heat flux imposed
            T_bulk_average=mean(Data_heater(:,3,k));

            T_wall_average=min(T_wall_average,T_max_gas);
            T_bulk_average=min(T_bulk_average,T_max_gas);

            for h=1:Heater_nodalization
```

```
T_successive=T_previous+Data_heater(h,2,k)*(Heater_input(5)*Data_section
s(Heater_index,3)...

/Heater_nodalization)/(Mass_flow_core*cp_gas_pt(Press,T_previous));
                T_successive=min(T_successive,T_max_gas);
                Data_heater(h,3,k)=T_successive;
                T_previous=Data_heater(h,3,k);

                %calculates the heat transfer coefficient and the wall
temperature


                Rho=density_gas_pt(Press,T_previous);
                V=Mass_flow_core/(Rho*Data_sections(Heater_index,2));

                [Alpha,regime] =
Heat_transfer_coefficient(D,Ltot,L,V,Press,T_previous,T_wall_average,T_b
ulk_average,...

T_in_bulk,T_out_bulk,T_in_wall,T_out_wall,Type,Nu_error_forced,Nu_error_
mixed,Nu_error_free);
                Data_heater(h,11,k)=regime;
                Data_heater(h,5,k)=Alpha;

Data_heater(h,4,k)=Data_heater(h,3,k)+Data_heater(h,2,k)/Alpha;
            end
            T_previous=Data_sections(j-1,7);        %Set the variables
again to calculate the average rod now
        end
        %Theoretically should calculate the mix of the
        %temperatures but because of the large number of channels
        %the final temperature is supposed to be the average temperature
        T_previous=Data_heater(Heater_nodalization,3,2);
        Data_sections(j,7)=mean(Data_heater(:,3,2));

    elseif j == Cooler_index + Number_of_riser_sections
        %define parameters for heat transfer coefficient calculation
        D=Data_sections(Cooler_index+Number_of_riser_sections,1);
        Ltot=Data_sections(Cooler_index+Number_of_riser_sections,3);

L=Data_sections(Cooler_index+Number_of_riser_sections,3)./Cooler_nodaliz
ation;  %%%%%%%%%%%%%%%%%%
        T_wall_average=mean(Data_cooler(:,4));
        T_in_bulk=Data_cooler(1,3);
        T_out_bulk=Data_cooler(Cooler_nodalization,3);
        T_in_wall=Data_cooler(1,4);
        T_out_wall=Data_cooler(Cooler_nodalization,4);
        Type=-1;     %wall temperature imposed
        T_bulk_average=mean(Data_cooler(:,3));

        T_bulk_average=min(T_bulk_average,T_max_gas);
        T_bulk_average=max(T_bulk_average,T_wall_average);

        for h=1:Cooler_nodalization

            T_previous;
            Rho=density_gas_pt(Press,T_previous);

V=Mass_flow/(Rho*Data_sections(Cooler_index+Number_of_riser_sections,2)*
Cooler_input(4)*Cooler_input(5));
```

```
            [Alpha,regime] =
Heat_transfer_coefficient(D,Ltot,L,V,Press,T_previous,T_wall_average,T_b
ulk_average,...

T_in_bulk,T_out_bulk,T_in_wall,T_out_wall,Type,Nu_error_forced,Nu_error_
mixed,Nu_error_free);
            Data_cooler(h,5)=Alpha;
            Data_cooler(h,11)=regime;
            Q_out=Alpha*(T_previous-Data_cooler(h,4));      %kW/m2K -
heat out of fluid to wall
            Data_cooler(h,2)=Q_out;
            T_successive=T_previous-Q_out*(Cooler_input(6)...

*Data_sections(Cooler_index+Number_of_riser_sections,3)/Cooler_nodalizat
ion)/(Mass_flow/Cooler_input(4)/Cooler_input(5)*...
                cp_gas_pt(Press,T_previous));
            T_successive=max(T_successive,T_wall_average);
            Data_cooler(h,3)=T_successive;
            T_previous=Data_cooler(h,3);
        end
        Data_sections(j,7)=mean(Data_cooler(:,3));
    else
        Data_sections(j,7)=T_previous;
    end
end

T_inlet_new=Data_sections(Number_of_sections,7);

%%%%%%%%%%%%%%%%%%%%%%%%%%%%%%%%%%%%%%%%%%%%%%%%%%%%%%%%
%%%%%%%%%%%%%%%%%%%%%%%%%%%%%%%%%%%%%%%%%%%%%%%%%%%%%%%%
%%%%%%%%%%%%%%%%%%%%%%%%%%%%%%%%%%%%%%%%%%%%%%%%%%%%%%%%



function [Alpha,regime] =
Heat_transfer_coefficient(D,Ltot,L,V,Press,Temp,T_wall_average,T_bulk_av
erage,...

T_in_bulk,T_out_bulk,T_in_wall,T_out_wall,Type,Nu_error_forced,Nu_error_
mixed,Nu_error_free)

%function Alpha =
Heat_transfer_coefficient(D,L,V,Press,Temp,T_wall_average,T_bulk_average
,...
%T_in_bulk,T_out_bulk,T_in_wall,T_out_wall,Type,Nu_forced_error,Nu_mixed
_error,Nu_free_error)
%
%Calculates the heat transfer coefficient (kW/m2-K)
%D id the diameter (m)
%L is the length (m) of the heater/cooler
%V is the velocity of the fluid
%Press is the operating pressure
%Temp is the bulk temperature of the fluid
%T_wall_average is the average wall temperature in heater/cooler
%T_bulk_average is the average temperature in heater/cooler
%T_in_bulk is the inlet bulk temperature
%T_out_bulk is the outlet bulk temperature
%T_in_wall is the inlet wall temperature
%T_out_wall is the outlet wall temeprature
%Type is the type of correlation to be used
```

```
%if positive it means that the heat flux is imposed
%otherwise it means that the temperature is imposed
%Nu_error is the error coefficient of the correlations
%
%Written by L. Pagani - Nov 2003

%get Prandtl number and Reynolds number
%for mixed and free convection the film properties have to be used
%for forced convection the bulk properties are used

%film properties

Temp_film=0.5*(T_wall_average+T_bulk_average);
Rho_film=density_gas_pt(Press,Temp_film);
Visc_film=viscosity_gas_pt(Press,Temp_film)*1e-6;
Cp_film=cp_gas_pt(Press,Temp_film)*1000;    %J/kg-K
Cond_film=cond_gas_pt(Press,Temp_film);

%calculates Pr
Pr_film=Visc_film*Cp_film/Cond_film;

%bulk properties
Rho=density_gas_pt(Press,Temp);
Visc=viscosity_gas_pt(Press,Temp)*1e-6;
Cp=cp_gas_pt(Press,Temp)*1000;  %J/kg-K
Cond=cond_gas_pt(Press,Temp);

%calculates Re and Pr
Re=Rho*V*D/Visc;
Pr=Visc*Cp/Cond;


%calculates Rayleigh number and modified Rayleigh number
Delta_temp_log=(abs(T_out_wall-T_out_bulk)-abs(T_in_wall-T_in_bulk))/...
    log(abs(T_out_wall-T_out_bulk)/abs(T_in_wall-T_in_bulk));  %channel
log mean temperature difference

if isnan(Delta_temp_log)
    Delta_temp_log=1;
end

Ra=9.81/T_bulk_average*Delta_temp_log*Pr_film*D^3/(Visc_film/Rho_film)^2
;

Temp_gradient=abs(T_out_bulk-T_in_bulk)/Ltot;

Ram=Ra*Temp_gradient*D/Delta_temp_log;


%calculates the transition point between different regimes
Re1=(Ra^(1/3)/(0.05*Pr_film^0.4))^(1/0.8);      %Aicher line
Re2=sqrt(Ra/Pr_film);                           %Burmeister line


%calculates Nusselt number
% if Re > Re1                   %forced convection regime
%     Nu_forced=Nusselt_forced(Re,Pr,Type)*Nu_error_forced;
%     regime_forced=10;
%
% elseif Re > Re2               %mixed convection regime
%     Nu_mixed=Nusselt_mixed(Re,Pr,Ra,Ram,D,Ltot,Type)*Nu_error_mixed;
```

```
%     regime_mixed=20;
% else                          %free convection regime
%     Nu_free=Nusselt_free(Pr,Ra,Ram,D,Ltot,Type)*Nu_error_free;
%     regime_free=30;
% end


%%%%%%%%%%%%%%%%%%%%%%%%%%%%%%%%%%%%%%%%%%%%
% define distance from decision Re points
%%%%%%%%%%%%%%%%%%%%%%%%%%%%%%%%%%%%%%%%%%%%
Nu_forced=Nusselt_forced(Re,Pr,Type)*Nu_error_forced;
regime_forced=10;
Nu_mixed=Nusselt_mixed(Re,Pr,Ra,Ram,D,Ltot,Type)*Nu_error_mixed;
regime_mixed=20;
Nu_free=Nusselt_free(Pr,Ra,Ram,D,Ltot,Type)*Nu_error_free;
regime_free=30;

coef_1=(Re-Re1)/Re1/0.1;
coef_2=(Re-Re2)/Re2/0.1;

coef_forced=min(max(coef_1/0.1+1,0),1);
coef_free=min(max(-coef_2/0.1+1,0),1);
if coef_1>0
    coef_mixed=min(max(-coef_1/0.1+1,0),1);
elseif coef_2<0
    coef_mixed=min(max(coef_2/0.1+1,0),1);
else
    coef_mixed=1;
end


Nu=(coef_forced*Nu_forced+coef_mixed*Nu_mixed+coef_free*Nu_free)/(coef_f
orced+coef_mixed+coef_free);
regime=(coef_forced*regime_forced+coef_mixed*regime_mixed+coef_free*regi
me_free)/(coef_forced+coef_mixed+coef_free);

%calculates the heat transfer coefficient
Alpha=Nu*Cond/D/1e3;    %return kW/m2-K

%%%%%%%%%%%%%%%%%%%%%%%%%%%%%%%%%%%%%%%%%%%%%%%%%%%%%%%%%%%%
%%%%%%%%%%%%%%%%%%%%%%%%%%%%%%%%%%%%%%%%%%%%%%%%%%%%%%%%%%%%
%%%%%%%%%%%%%%%%%%%%%%%%%%%%%%%%%%%%%%%%%%%%%%%%%%%%%%%%%%%%



function Nu = Nusselt_free(Pr,Ra,Ram,D,L,Type)

%function Nu = Nusselt_free(Pr,Ra,Ram,D,L,Type)
%
%Calculates the Nusselt number for free convetion regime
%Pr is the Prandlt number
%Ra is the Rayleigh number
%Ram is the modified Rayleigh number
%D id the diameter (m)
%L is the length (m)
%Type is the type of correlation to be used
%if positive it means that the heat flux is imposed
%otherwise it means that the temperature is imposed
%
%Written by L. Pagani - Nov 2003
```

```
if Type > 0     %heat flux imposed
    NuT=0.15*Ra^(1/3)/((1+(0.492/Pr)^(9/16))^(16/27));
%%%%%%%%%%%%%%change in 0.122 the 0.15
    NuL=0.846*Ram^0.25;

    Nu=max(NuT,NuL);

else            %wall temperature imposed
    NuT=0.15*Ra^(1/3)/((1+(0.492/Pr)^(9/16))^(16/27));
%%%%%%%%%%%%%%change in 0.122 the 0.15
    NuL=0.75*(Ra*D/L)^0.25/((1+(0.492/Pr)^(9/16))^(4/9));

    Nu=max(NuT,NuL);
End


%%%%%%%%%%%%%%%%%%%%%%%%%%%%%%%%%%%%%%%%%%%%%%%%%%%%
%%%%%%%%%%%%%%%%%%%%%%%%%%%%%%%%%%%%%%%%%%%%%%%%%%%%
%%%%%%%%%%%%%%%%%%%%%%%%%%%%%%%%%%%%%%%%%%%%%%%%%%%%



function Nu = Nusselt_mixed(Re,Pr,Ra,Ram,D,L,Type)

%function Nu = Nusselt_mixed(Re,Pr,Ra,Ram,D,L,Type)
%
%Calculates the Nusselt number for mixed convetion regime
%Re is the Reynolds number
%Pr is the Prandlt number
%Ra is the Rayleigh number
%Ram is the modified Rayleigh number
%D id the diameter (m)
%L is the length (m)
%Type is the type of correlation to be used
%if positive it means that the heat flux is imposed
%otherwise it means that the temperature is imposed
%
%Written by L. Pagani - Nov 2003


%we use the Churchill formulae - 1998
if Type > 0   %heat flux imposed
    NuML=(4.364^6+(0.846*Ram^0.25)^6)^(1/6);

else          %wall temperature imposed

NuML=(3.657^3+((0.75*(Ra*D/L)^0.25)/((1+(0.492/Pr)^(9/16))^(4/9)))^3)^(1
/3);
end

Argument = Nusselt_forced(Re,Pr,Type)^3-
(0.122*Ra^(1/3)/(1+(0.492/Pr)^(9/16))^(16/27))^3;
%%%%%%%%%%%%%%change in 0.122 the 0.15

if Argument >=0
    NuMT=max((Nusselt_forced(Re,Pr,Type)^3-
(0.122*Ra^(1/3)/(1+(0.492/Pr)^(9/16))^(16/27))^3)^(1/3),...
%%%%%%%%%%%%%%change in 0.122 the 0.15
    0.5*0.122*Ra^(1/3)/(1+(0.492/Pr)^(9/16))^(16/27));     %The NuMT is
limited to 50% NuNT                %%%%%%%%%%%%%%change in 0.122 the
0.15
```

```
else
    NuMT = 0.5*0.122*Ra^(1/3)/(1+(0.492/Pr)^(9/16))^(16/27);
%%%%%%%%%%%%%change in 0.122 the 0.15
end

Nu=max(NuMT,NuML);


%%%%%%%%%%%%%%%%%%%%%%%%%%%%%%%%%%%%%%%%%%%%%%%%%%%%
%%%%%%%%%%%%%%%%%%%%%%%%%%%%%%%%%%%%%%%%%%%%%%%%%%%%
%%%%%%%%%%%%%%%%%%%%%%%%%%%%%%%%%%%%%%%%%%%%%%%%%%%%



function Nu = Nusselt_forced(Re,Pr,Type)

%function Nu = Nusselt_forced(Re,Pr,Type)
%
%Calculates the Nusselt number for forced convetion regime
%Re is the Reynolds number
%Pr is the Prandlt number
%Type is the type of correlation to be used
%if positive it means that the heat flux is imposed
%otherwise it means that the temperature is imposed
%
%Written by L. Pagani - Nov 2003

if Re <= 2300   %laminar forced regime
    if Type >0  %heat flux imposed
        Nu=4.364;
    else
        Nu=3.657;
    end

elseif Re > 5000      %turbulent regime, use the Gnielinski correlation,
1976
    if Pr > 2000 | Pr < 0.5
        error('Prandlt number is out of range for Gnieliski correlation
to be used')
    end
    if Re >5000000
        error('Reynolds number is out of range for Gnielinski
correlation to be used')
    end
    f=(1.8*log10(Re)-1.5)^(-2);
    Nu=f/8*(Re-1000)*Pr/(1+12.7*sqrt(f/8)*(Pr^(2/3)-1));   %Gnielisnki
correlation

else                %transitional regime
    gamma=(Re-2300)/(5000-2300);
    f=(1.8*log10(5000)-1.5)^(-2);
    NuG=f/8*(5000-1000)*Pr/(1+12.7*sqrt(f/8)*(Pr^(2/3)-1));
%Gnielisnki correlation at Re=5000
    if Type >0  %heat flux imposed
        NuL=4.364;
    else
        NuL=3.657;
    end
    Nu=(1-gamma)*NuL+gamma*NuG;
end
```

APPENDIX E: MATLAB CODE FOR THE MONTE CARLO ALGORITHM

```
function [y,x]=exp_mc9D_min(N,initial,nominal)

%function [y,x]=exp_mc9D_min(N,initial,nominal)
%
%Inputs:
%N: number of simulations
%initial: lower bound for the initial failure probability
%nominal: nominal values of the operating parameters
%
%Outputs:
%y: estimate of failure probability
%x: 95% confidence errors


%set the initial points
mu_in=norminv((1-initial)^(1/9),0,1);
for j=1:9
      mu(j)=mu_in;
end


if ~Failure_function(mu,nominal)
      error('The probability of failure is less than initial… input
      value')
end

B=mu;
C=-mu.^2./2;

y=zeros(1,N);
x=zeros(1,N);

for j=1:N
      extraction=randn(1,9)+mu;
     if Failure_function(extraction,nominal)
            result(j)=1/((exp(B(1)*extraction(1)+C(1)))*…
            (exp(B(2)*extraction(2)+C(2)))*(exp(B(3)*…
            extraction(3)+C(3)))*(exp(B(4)*extraction(4)+…
            C(4)))*(exp(B(5)*extraction(5)+C(5)))*(exp(B(6)*…
            extraction(6)+C(6)))*(exp(B(7)*extraction(7)+…
            C(7)))*(exp(B(8)*extraction(8)+C(8)))*(exp(B(9)*…
            extraction(9)+C(9))));
            if norm(extraction) < norm(mu)
            mu=extraction;
            B=mu;
                  C=-mu.^2./2;
            end
      else
      result(j)=0;
     end
      y(j)=mean(result(1:j));
      x(j)=1.96*std(result(1:j))/sqrt(j);
end
```

APPENDIX F: FRAPCON AND FRAPTRAN INPUT FILES

F.1 Frapcon

```
*************************************************************************
******
*         frapcon3, steady-state fuel rod analysis code, version 1
*
*-----------------------------------------------------------------------
*
*
*
*          CASE DESCRIPTION: Test Case Oconee Rod 15309 as base case
*
*
*
*UNIT      FILE DESCRIPTION
*
*----      ------------------------------------------------Output:
*
*          Output :
*
*     6         STANDARD PRINTER OUTPUT
*
*
*
*          Scratch:
*
*     5         SCRATCH INPUT FILE FROM ECH01
*
*
*
*   Input:    FRAPCON2 INPUT FILE (UNIT 55)
*
*
*
*************************************************************************
******
* GOESINS:
FILE05='nullfile', STATUS='scratch', FORM='FORMATTED',
          CARRIAGE CONTROL='LIST'
*
* GOESOUTS:
FILE06='out.n',     STATUS='UNKNOWN', CARRIAGE CONTROL='LIST'
FILE66='plot.out',     STATUS='UNKNOWN', CARRIAGE CONTROL='LIST'
FILE22='restart', STATUS='UNKNOWN', CARRIAGE CONTROL='LIST'
/*********************************************************************
******
          Oconee rod 15309 modified
 $frpcn
```

```
 im=21, na=12,
 ngasr = 15, nr=17,
 $end
 $frpcon
 ntape=1,
 cpl = 8.4, crdt = 0.2, crdtr = 0.0, thkcld = 0.0265,
 dco = 0.430, pitch = 0.56,
 den = 95., thkgap=0.0035, dishsd = 0.050,dspg = 0.348,
 dspgw = 0.06, enrch = 3.5, fa= 1.0, fgpav = 300,
 hplt = 0.402, hdish = 0.014, icm = 4,
 icor = 0, idxgas = 1, iplant =-2, iq = 0, jdlpr = 0,
 totl = 11.5, jn = 13, jst = 21*1,
 rc = 0.0, roughc = 4.49e-5, nplot = 1,
 roughf = 8.3e-5, vs = 25.0,
 nunits = 1, rsntr = 150.,

qf(1)=0.25,0.958,1.094,1.112,1.104,1.09,1.09,1.088,1.102,1.082,1.006,0.
786,0.29,
 x(1)=0,1,2,3,4,5,6,7,8,9,10,11,11.5
 flux = 13*0.25e17, p2(1) = 2200.0, tw(1) = 555.0, go(1) = 2.6e6,
 ProblemTime=  1.00,100.00,200.00,300.00,400.00,500.00,600.00,
700.00,800.00,900.00,1000.00,1100.00,1200.00,1300.00,1400.00,
1500.00,1600.00,1700.00,1800.00,1800.50,1810.00,
 qmpy = 8.000, 7.900, 7.800, 7.700, 7.600, 7.500, 7.400,
 7.300, 7.200, 7.100, 7.000, 6.900, 6.800, 6.700, 6.600,
 6.500, 6.400, 6.300, 6.201, 0.124, 0.124,
 slim = .05,
 $end
```

F.2 Fraptran

```
* Prob-1A-RIA.in
*
**********************************************************************
*
* FRAPTRAN, Transient fuel rod analysis code
*
*
*  CASE DESCRIPTION: Standard Problem 1A:  RIA,
*                    assumes a 10msec RIA for a PWR rod from hot
standby
*                    FRAPCON-3 initialization for burnup conditions
*                    English input/SI output
*
*
FILE05='nullfile', STATUS='scratch', FORM='FORMATTED',
*
        CARRIAGE CONTROL='LIST'
*
FILE15='sth2xt',  STATUS='old', FORM='UNFORMATTED'
*
*
*
FILE06='Prob-1A-RIA.out',   STATUS='UNKNOWN', CARRIAGE CONTROL='LIST' *
FILE66='stripf.Prob-1A-RIA', STATUS='UNKNOWN', FORM='FORMATTED',    *
        CARRIAGE CONTROL='LIST'
*
FILE22='restart', STATUS='OLD', FORM='FORMATTED'
/**********************************************************************
*
Standard Problem 1A:  PWR RIA (FRAPTRAN 1.1.1, May 2003),
 $begin
   ProblemStartTime=0.0,
   ProblemEndTime=5.0,
 $end
start
 $iodata
  unitin=0, unitout=1, dtpoa(1)=0.01,
  dtplt=0.0025, inp=1, trest=4.86e+007,
 $end
 $solution
   dtmaxa(1)=0.0005,0., 0.00005,0.03, 0.0005,1.2, 0.005,2.2,
   dtss=1.0, prsacc=0.001, tmpac1=0.001, maxit=100, noiter=100,
   epsht1=1.0,
   naxn=12, nfmesh=15, ncmesh=5,
 $end
 $design
   RodLength=11.5, RodDiameter=0.0358, rshd=0.003302, dishd=0.0125,
   pelh=0.0335, dishv0=1.1788e-8, FuelPelDiam=0.0308, roughf=2.12,
   frden=0.95, fotmtl=2.0, tsntrk=1773.0, fgrns=10.0, gadoln=0.0,
   ncs=25, gapthk=2.917e-4, coldw=0.5, roughc=1.14, cldwdc=0.04,
```

```
  spl=0.7, scd=0.029, swd=0.005, vplen=6.e-4, gfrac=1.0,6*0.,
  gappr0=300., tgas0=300.0, cfluxa=7.5e17, tflux=4.86e+007,
$end
$power
  RodAvePower =
            0.000, 0.481,
       0.000, 0.482,
       0.000, 0.484,
      0.000, 0.486,
      0.001, 0.488,
     0.149, 0.490,
    13.369, 0.492,
    442.716, 0.494,
    5393.383, 0.496,
    24171.467, 0.498,
    39852.011, 0.500,
    24171.467, 0.502,
     5393.383, 0.504,
     442.716, 0.506,
      13.369, 0.508,
       0.149, 0.510,
       0.001, 0.512,
       0.000, 0.514,
       0.000, 0.516,
       0.000, 0.518,
       0.000, 0.519,
         AxPowProfile =
       0.5963,0.0000, 0.6959,0.2490, 0.8473,0.7480, 0.9320,1.2470,
       0.9446,1.8930, 0.9418,2.6870, 0.9532,3.4810, 0.9807,4.2750,
       1.0101,5.0690, 1.0316,5.8580, 1.0482,6.6470, 1.0655,7.4410,
       1.0877,8.2350, 1.1165,9.0290, 1.1514,9.8230, 1.1570,10.4700,
       0.9780,10.968, 0.7694,11.5,
$end
$model
  internal='on', nthermex=1,
  metal='on', cathca=1,
  deformation='on', noball=0,
  itransient=1,
$end
$boundary
  heat='on',
  press=2, pbh2=2250.,0., 2250.,6.,
  zone=1, htclev=11.6,
  htco=2, htca=20000.,0., 20000.,6.,
  tem=2, tblka=532.,0., 532.,6.,
$end
$tuning
$end
```

APPENDIX G: CODE FOR HIGH BURNUP VIRTUAL EXPERIMENTS

G.1 File List

The algorithm used to generate the virtual experiments is composed by the following files

File Name	Language	Description
esegui.m	Matlab	This is the main program, that performs the random extraction for the uncertainties and calls the other subroutines to generate the final results
scrivinputfrapcon.m	Matlab	Writes the input files for Frapcon
scrivinputfraptran.m	Matlab	Wirtes the input file for Fraptran
bu_time.m	Matlab	Calculates the burnup as a function of time
modificarestartfrapcon	FORTRAN	Modifies the restart file from frapcon to correct for the oxide layer thickness and the hydrogen content
burnup	FORTRAN	Reads the relationship between burnup and time from the frapcon output
leggifraptran	FORTRAN	Reads the results from the Fraptran output file

G.2 Matlab Code

```
%calcola il burnup come funzione del tempo e plottalo
!burnup

load -ascii tempo;
load -ascii burnup;

figure

%subplot(2,2,1)
%plot(tempo/(24*3600),mean(burnup')./1e5)
%xlabel('tempo [gg]')
%ylabel('burnup [GWd/MTU]')

clear resultsdata;
resultsdata=zeros(Nstorie,7);

rand('state',sum(100*clock))

for i=1:Nstorie

      time=0;
    %      power=0.8;
%           oxidation=1;
%           hydrogen=1;
%           CSEDerror=1;
    %      spallation=ones(12,1);
    %     %
    while (time<4.8e7 | time>5.2e7)
        %estrai sei numeri casuali
        extraction=rand(17,1);
        oxidation=extraction(1)*0.7+0.65;
        hydrogen=extraction(2)*0.6+0.7;
        time=extraction(3)*1800*24*3600;
        power=extraction(4)*6;
        CSEDerror=extraction(5)+0.5;
        spallation=extraction(6:17);
    end

    %chiama frapcon per calcolare lo steady state
    scrivinputfrapcon(time);
    !frapcon3_2
    !copy restart restart.ori

    %modifica il file restart includendo le incertezze su ossido e
idrogeno
    fid=fopen('incertezze','w');
    fprintf(fid,'%6.5f\n',oxidation);
    fprintf(fid,'%6.5f\n',hydrogen);
    status=fclose(fid);
    !modificarestartfrapcon
```

```
    %crea il file di input per fraptran
    scrivinputfraptran(time+24*3600,power);

    %lancia fraptran
    !fraptran1_2

    %crea i file di dati necessari
    !leggifraptran
    load -ascii Enthalpy.txt;
    load -ascii Oxide.txt;
    load -ascii SEDEPRI.txt;
    load -ascii SEDPNNL.txt;
    load -ascii Tempo.txt;
    load -ascii Temperature.txt;
    load -ascii IDoxigen.txt;

    %  subplot(2,2,2);
    %hold on;
    % plot(time./(24*3600),mean(Oxide(1,:).*1e3),'o');
    %ylabel('ossidazione [microns]');
    %xlabel('tempo [gg]');
    %subplot(2,2,3);
    %hold on
    %plot(time./(24*3600),max(Oxide(1,:).*1e3),'o');
    %ylabel('ossidazione massima [microns]');
    %xlabel('tempo [gg]');



    %verifica se si e' rotta
    failure=0;
    failureburst=0;
    failureCSED=0;
    rodspallation=zeros(1,12);
    failurespallation=0;
    tempostep=max(size(Tempo));
    maxenthalpy=max(max(Enthalpy));
    failureenthalpy=ones(1,12).*1e3;
    Rox=Oxide(1,:)./(0.0265*2.54*10);     %ratio with cladding
thickness
    resultsdata(i,7)=max(Rox);
    CSED=41.5*exp(-6.6*Rox);
    for k=1:12
        if Rox(k)>0.1
            if spallation(k)>0.8
                CSED(k)=0.371*Rox(k).^(-1.24);
                rodspallation(k)=1;
            end
        end
    end
    CSED=CSED*CSEDerror;
    if tempostep==2001
        for j=1:tempostep
```

```
            for k=1:12       %nodi assiali
                %if IDoxigen(j,k)>0     %rottura per burst
                if Temperature(j,k)>1073    %rottura per temperatura
                    failureenthalpy(k)=Enthalpy(j,k);
                    failure=1;
                    failureburst=1;
                end
                if SEDPNNL(j,k)>CSED(k) %rottura per CSED
                    failureenthalpy(k)=Enthalpy(j,k);
                    failure=1;
                    failureCSED=1;
                end
            end
            if failure==1
                break;
            end
        end
        %    subplot(2,2,4);
        figure(1)
        hold on;
        figure(2)
        hold on;

        if failure==0
            resultsdata(i,1)=time;
            resultsdata(i,2)=maxenthalpy;
            resultsdata(i,3)=0;
            resultsdata(i,4)=failureburst;
            resultsdata(i,5)=failureCSED;
            resultsdata(i,6)=sum(rodspallation);
            xlabel('burnup [GWd/MTU]');
            ylabel('entalpia [cal/gm]');
            if sum(rodspallation)>0
                figure(1)
                plot(bu_time(time),maxenthalpy,'v');
                figure(2)
                plot(resultsdata(i,7),maxenthalpy,'v');
            else
                figure(1)
                plot(bu_time(time),maxenthalpy,'o');
                figure(2)
                plot(resultsdata(i,7),maxenthalpy,'o');
            end
        else
            resultsdata(i,1)=time;
            %%%%%%%%%%%%%%%%%%%%%%%%%%%%%%%%%%%%%%%%%%%%%%%%%%%% for the max
enthalpy instead of failure enthalpy
            resultsdata(i,2)=min(failureenthalpy);
            %resultsdata(i,2)=maxenthalpy;
            resultsdata(i,3)=1;
            resultsdata(i,4)=failureburst;
            resultsdata(i,5)=failureCSED;
            resultsdata(i,6)=sum(rodspallation);
```

```
            xlabel('burnup [GWd/MTU]');
            ylabel('entalpia [cal/gm]');
            if failureburst==1
                figure(1)
                plot(bu_time(time),resultsdata(i,2),'or');
                figure(2)
                plot(resultsdata(i,7),resultsdata(i,2),'or');
            elseif sum(rodspallation)>0
                figure(1)
                plot(bu_time(time),resultsdata(i,2),'vr');
                figure(2)
                plot(resultsdata(i,7),resultsdata(i,2),'vr');
            else
                figure(1)
                plot(bu_time(time),resultsdata(i,2),'sr');
                figure(2)
                plot(resultsdata(i,7),resultsdata(i,2),'sr');
            end
        end
    end
end
```

```
function scrivinputfraptran(BU,h);

%1) sostituisco a ProblemEndTime e tflux il valore del tempo (BU) che
passo
%alla funzione. Lo passo come stringa
%2) il vattore entalpia e' il picco e lo moltiplico per la costante h
che gli
%passo
%3) FWHM e' la larghezza in ms del picco e viene determinata
automaticamente

entalpia=zeros(1,21);
%tempo=num2str(BU);
FWHM=8.9729/(h)^0.4857;
sigma=FWHM/sqrt(2*log(2))/2000;
x=[0.5-10*sigma:sigma:0.5+10*sigma];
entalpia=normpdf(x,0.5,sigma);
entalpia=entalpia*10000/max(entalpia);
%entalpia=[0.0,0.0,2.053,43.644,470.39,2102.2,4322.7,6417.1,8409,9726.5
,10000,9726.5,8409.,6417.,4322.7,2102.2,470.39,43.644,2.053,0.,0.];
entalpia=entalpia*h;

%inizio a scrivere
fid=fopen('fraptran.inp','w');

fprintf(fid,'* Prob-1A-RIA.in\n');
fprintf(fid,'*\n');
fprintf(fid,'**********************************************************
**************\n');
fprintf(fid,'* FRAPTRAN, Transient fuel rod analysis code  \n');
fprintf(fid,'*\n');
fprintf(fid,'*\n');
fprintf(fid,'*  CASE DESCRIPTION: Standard Problem 1A:  RIA,\n');
fprintf(fid,'*                    assumes a 10msec RIA for a PWR rod
from hot standby\n');
fprintf(fid,'*                    FRAPCON-3 initialization for burnup
conditions\n');
fprintf(fid,'*                    English input/SI output\n');
fprintf(fid,'*
*\n');
fprintf(fid,'FILE05=''nullfile'', STATUS=''scratch'',
FORM=''FORMATTED'',                  *\n');
fprintf(fid,'        CARRIAGE CONTROL=''LIST''
*\n');
fprintf(fid,'FILE15=''sth2xt'',  STATUS=''old'', FORM=''UNFORMATTED''
*\n');
fprintf(fid,'*
*\n');
fprintf(fid,'FILE06=''Prob-1A-RIA.out'',   STATUS=''UNKNOWN'', CARRIAGE
CONTROL=''LIST'' *\n');
fprintf(fid,'FILE66=''stripf.Prob-1A-RIA'', STATUS=''UNKNOWN'',
FORM=''FORMATTED'',    *\n');
fprintf(fid,'        CARRIAGE CONTROL=''LIST''
*\n');
```

```
fprintf(fid,'FILE22=''restart'', STATUS=''OLD'',
FORM=''FORMATTED''\n');
fprintf(fid,'/************************************************************
**************\n');
fprintf(fid,'Standard Problem 1A:  PWR RIA (FRAPTRAN 1.1.1, May
2003),\n');
fprintf(fid,' $begin\n');
fprintf(fid,'   ProblemStartTime=0.0,\n');
fprintf(fid,'   ProblemEndTime=5.0,\n');
fprintf(fid,' $end\n');
fprintf(fid,'start\n');
fprintf(fid,' $iodata\n');
fprintf(fid,'  unitin=0, unitout=1, dtpoa(1)=0.01,\n');
fprintf(fid,'  dtplt=0.0025, inp=1, trest=%1.2e,\n',BU);
fprintf(fid,' $end\n');
fprintf(fid,' $solution\n');
fprintf(fid,'   dtmaxa(1)=0.0005,0., 0.00005,0.03, 0.0005,1.2,
0.005,2.2,\n');
fprintf(fid,'   dtss=1.0, prsacc=0.001, tmpac1=0.001, maxit=100,
noiter=100,\n');
fprintf(fid,'   epsht1=1.0,\n');
fprintf(fid,'   naxn=12, nfmesh=15, ncmesh=5,\n');
fprintf(fid,' $end\n');
fprintf(fid,' $design\n');
fprintf(fid,'   RodLength=11.5, RodDiameter=0.0358, rshd=0.003302,
dishd=0.0125,\n');
fprintf(fid,'   pelh=0.0335, dishv0=1.1788e-8, FuelPelDiam=0.0308,
roughf=2.12,\n');
fprintf(fid,'   frden=0.95, fotmtl=2.0, tsntrk=1773.0, fgrns=10.0,
gadoln=0.0,\n');
fprintf(fid,'   ncs=25, gapthk=2.917e-4, coldw=0.5, roughc=1.14,
cldwdc=0.04,\n');
fprintf(fid,'   spl=0.7, scd=0.029, swd=0.005, vplen=6.e-4,
gfrac=1.0,6*0.,\n');
fprintf(fid,'   gappr0=300., tgas0=300.0, cfluxa=7.5e17,
tflux=%1.2e,\n',BU);
fprintf(fid,' $end\n');
fprintf(fid,' $power\n');
fprintf(fid,'   RodAvePower =\n');
fprintf(fid,'      %0.0000,0.0000,\n');
fprintf(fid,'      %6.3f,%6.3f,\n',entalpia(1,1),x(1,1));
fprintf(fid,'      %6.3f,%6.3f,\n',entalpia(1,2),x(1,2));
fprintf(fid,'      %6.3f,%6.3f,\n',entalpia(1,3),x(1,3));
fprintf(fid,'     %6.3f,%6.3f,\n',entalpia(1,4),x(1,4));
fprintf(fid,'     %6.3f,%6.3f,\n',entalpia(1,5),x(1,5));
fprintf(fid,'    %6.3f,%6.3f,\n',entalpia(1,6),x(1,6));
fprintf(fid,'    %6.3f,%6.3f,\n',entalpia(1,7),x(1,7));
fprintf(fid,'    %6.3f,%6.3f,\n',entalpia(1,8),x(1,8));
fprintf(fid,'    %6.3f,%6.3f,\n',entalpia(1,9),x(1,9));
fprintf(fid,'    %6.3f,%6.3f,\n',entalpia(1,10),x(1,10));
fprintf(fid,'    %6.3f,%6.3f,\n',entalpia(1,11),x(1,11));
fprintf(fid,'    %6.3f,%6.3f,\n',entalpia(1,12),x(1,12));
fprintf(fid,'     %6.3f,%6.3f,\n',entalpia(1,13),x(1,13));
fprintf(fid,'     %6.3f,%6.3f,\n',entalpia(1,14),x(1,14));
```

```
fprintf(fid,'      %6.3f,%6.3f,\n',entalpia(1,15),x(1,15));
fprintf(fid,'      %6.3f,%6.3f,\n',entalpia(1,16),x(1,16));
fprintf(fid,'      %6.3f,%6.3f,\n',entalpia(1,17),x(1,17));
fprintf(fid,'      %6.3f,%6.3f,\n',entalpia(1,18),x(1,18));
fprintf(fid,'      %6.3f,%6.3f,\n',entalpia(1,19),x(1,19));
fprintf(fid,'      %6.3f,%6.3f,\n',entalpia(1,20),x(1,20));
fprintf(fid,'      %6.3f,%6.3f,\n',entalpia(1,21),x(1,21));
fprintf(fid,'      %0.0000,0.0000,\n');
fprintf(fid,'   AxPowProfile =\n');
fprintf(fid,'       0.5963,0.0000, 0.6959,0.2490, 0.8473,0.7480,
0.9320,1.2470,\n');
fprintf(fid,'       0.9446,1.8930, 0.9418,2.6870, 0.9532,3.4810,
0.9807,4.2750,\n');
fprintf(fid,'       1.0101,5.0690, 1.0316,5.8580, 1.0482,6.6470,
1.0655,7.4410,\n');
fprintf(fid,'       1.0877,8.2350, 1.1165,9.0290, 1.1514,9.8230,
1.1570,10.4700,\n');
fprintf(fid,'       0.9780,10.968, 0.7694,11.5,\n');
fprintf(fid,' $end\n');
fprintf(fid,' $model\n');
fprintf(fid,'   internal=''on'', nthermex=1,\n');
fprintf(fid,'   metal=''on'', cathca=1,\n');
fprintf(fid,'   deformation=''on'', noball=0,\n');
fprintf(fid,'   itransient=1,\n');
fprintf(fid,' $end\n');
fprintf(fid,' $boundary\n');


fprintf(fid,'   heat=''on'',\n');
fprintf(fid,'   press=2, pbh2=2250.,0., 2250.,6.,\n');
fprintf(fid,'   zone=1, htclev=11.6,\n');
fprintf(fid,'   htco=2, htca=20000.,0., 20000.,6.,\n');
fprintf(fid,'   tem=2, tblka=532.,0., 532.,6.,\n');
%fprintf(fid,'   chf=1,\n');
fprintf(fid,' $end\n');
fprintf(fid,' $tuning\n');
fprintf(fid,' $end\n');

status = fclose(fid);
```

```
function scrivinputfrapcon(t);

%trasformo il tempo da secondi in giorni
t=t/(24*3600);

%matrice tempo-potenza

N=19;

tp=zeros(N,2);

%tempi

 tp(1,1)=1;
 tp(2,1)=100;
 tp(3,1)=200;
 tp(4,1)=300;
 tp(5,1)=400;
 tp(6,1)=500;
 tp(7,1)=600;
 tp(8,1)=700;
 tp(9,1)=800;
 tp(10,1)=900;
 tp(11,1)=1000;
 tp(12,1)=1100;
 tp(13,1)=1200;
 tp(14,1)=1300;
 tp(15,1)=1400;
 tp(16,1)=1500;
 tp(17,1)=1600;
 tp(18,1)=1700;
 tp(19,1)=1801;
 %potenze
 tp(1,2)=8.0;
 tp(2,2)=7.9;
 tp(3,2)=7.8;
 tp(4,2)=7.7;
 tp(5,2)=7.6;
 tp(6,2)=7.5;
 tp(7,2)=7.4;
 tp(8,2)=7.3;
 tp(9,2)=7.2;
 tp(10,2)=7.1;
 tp(11,2)=7.0;
 tp(12,2)=6.9;
 tp(13,2)=6.8;
 tp(14,2)=6.7;
 tp(15,2)=6.6;
 tp(16,2)=6.5;
 tp(17,2)=6.4;
 tp(18,2)=6.3;
 tp(19,2)=6.2;

 %Fisso il BU al momento giusto
```

```
i=0;
index=N;
for i=1:N
    if (tp(i,1)>t)
        index=i-1;
        break
    end
end

if (index==0)
    'hai dato un tempo inferiore al minimo, idiota!'
    return
end

%t=0->index=0 = BU=0; t>tmax da' index=N cioe' BU max

%definisco la nuova matrice

Pprint=zeros(21,1);
Tprint=zeros(21,1);

for i=1:index
    Tprint(i,1)=tp(i,1);
    Pprint(i,1)=tp(i,2);
end

Tprint(index+1,1)=t;

%interpola linearmente

Pint=0;
Pint=(((tp(index+1,2)-tp(index,2))/(tp(index+1,1)-tp(index,1)))*(t-
tp(index,1)))+tp(index,2);

%

Pprint(index+1,1)=Pint;
Tprint(index+2,1)=t+0.5;  %la potenza scende in mezza giornata
Tprint(index+3:21,1)=t+10;
Pprint(index+2:21,1)=0.02*Pint;  %e scende al 2%


%inizio a scrivere
fid=fopen('frapcon.inp','w');

fprintf(fid,'**********************************************************
******************\n');
fprintf(fid,'*        frapcon3, steady-state fuel rod analysis code,
version 1           *\n');
fprintf(fid,'*-------------------------------------------------------
-------------     *\n');
fprintf(fid,'*
*\n');
```

```
fprintf(fid,'*         CASE DESCRIPTION: Test Case Oconee Rod 15309 as
base case         *\n');
fprintf(fid,'*
*\n');
fprintf(fid,'*UNIT     FILE DESCRIPTION
*\n');
fprintf(fid,'*----     -----------------------------------------------
Output:            *\n');
fprintf(fid,'*         Output :
*\n');
fprintf(fid,'*    6         STANDARD PRINTER OUTPUT
*\n');
fprintf(fid,'*
*\n');
fprintf(fid,'*         Scratch:
*\n');
fprintf(fid,'*    5         SCRATCH INPUT FILE FROM ECH01
*\n');
fprintf(fid,'*
*\n');
fprintf(fid,'*  Input:   FRAPCON2 INPUT FILE (UNIT 55)
*\n');
fprintf(fid,'*
*\n');
fprintf(fid,'************************************************************
******************\n');
fprintf(fid,'* GOESINS:\n');
fprintf(fid,'FILE05=''nullfile'', STATUS=''scratch'',
FORM=''FORMATTED'',\n');
fprintf(fid,'         CARRIAGE CONTROL=''LIST''\n');
fprintf(fid,'*\n');
fprintf(fid,'* GOESOUTS:\n');
fprintf(fid,'FILE06=''out.n'',    STATUS=''UNKNOWN'', CARRIAGE
CONTROL=''LIST''\n');
fprintf(fid,'FILE66=''plot.out'',    STATUS=''UNKNOWN'', CARRIAGE
CONTROL=''LIST''\n');
fprintf(fid,'FILE22=''restart'',    STATUS=''UNKNOWN'', CARRIAGE
CONTROL=''LIST''\n');
fprintf(fid,'/************************************************************
******************\n');
fprintf(fid,'         Oconee rod 15309 modified\n');
fprintf(fid,' $frpcn\n');
fprintf(fid,' im=%d, na=12,\n',21);
fprintf(fid,' ngasr = 15, nr=17,\n');
fprintf(fid,' $end\n');
fprintf(fid,' $frpcon\n');
fprintf(fid,' ntape=1,\n');
fprintf(fid,' cpl = 8.4, crdt = 0.2, crdtr = 0.0, thkcld = 0.0265,\n');
fprintf(fid,' dco = 0.430, pitch = 0.56, \n');
fprintf(fid,' den = 95., thkgap=0.0035, dishsd = 0.050,dspg =
0.348,\n');
fprintf(fid,' dspgw = 0.06, enrch = 3.5, fa= 1.0, fgpav = 300,\n');
fprintf(fid,' hplt = 0.402, hdish = 0.014, icm = 4,\n');
fprintf(fid,' icor = 0, idxgas = 1, iplant =-2, iq = 0, jdlpr = 0,\n');
```

```
fprintf(fid,' totl = 11.5, jn = 13, jst = %d*1,\n',21);
fprintf(fid,' rc = 0.0, roughc = 4.49e-5, nplot = 1,\n');
fprintf(fid,' roughf = 8.3e-5, vs = 25.0,\n');
fprintf(fid,' nunits = 1, rsntr = 150.,\n');
fprintf(fid,'
qf(1)=0.25,0.958,1.094,1.112,1.104,1.09,1.09,1.088,1.102,1.082,1.006,0.
786,0.29,\n');
fprintf(fid,' x(1)=0,1,2,3,4,5,6,7,8,9,10,11,11.5\n');
fprintf(fid,' flux = 13*0.25e17, p2(1) = 2200.0, tw(1) = 555.0, go(1) =
2.6e6,\n');
fprintf(fid,' ProblemTime=');
fprintf(fid,'%6.2f,',Tprint(1:7)');
fprintf(fid,' \n');
fprintf(fid,'%6.2f,',Tprint(8:15)');
fprintf(fid,' \n');
fprintf(fid,'%6.2f,',Tprint(16:21)');
fprintf(fid,' \n');
fprintf(fid,' qmpy =');
fprintf(fid,'%6.3f,',Pprint(1:7)');
fprintf(fid,' \n');
fprintf(fid,'%6.3f,',Pprint(8:15)');
fprintf(fid,' \n');
fprintf(fid,'%6.3f,',Pprint(16:21)');
fprintf(fid,' \n');
fprintf(fid,' slim = .05,\n');
fprintf(fid,' $end\n');

status = fclose(fid);
```

```
function bu=bu_time(time)

%burnup is in GWd/MTU while time is in seconds

mediabu =[0.0
4.148728527
8.24901851
12.29678772
16.29198928
20.23462317
24.12468941
27.96218798
31.74711889
35.47948214
39.15927773
42.78650566
46.36116594
49.88325854
53.35278349
56.76974078
60.13413041
63.44595238
66.70573177
66.71006361];

tempo =[86400
     8640000
    17280000
    25920000
    34560000
    43200000
    51840000
    60480000
    69120000
    77760000
    86400000
    95040000
   103680000
   112320000
   120960000
   129600000
   138240000
   146880000
   155520000
   155606400];


index=min(find(tempo>time));
if isempty(index)
    bu=mediabu(max(size(mediabu)));
elseif index >1
    lowertime=tempo(index-1);
    uppertime=tempo(index);
    gamma=(time-lowertime)/(uppertime-lowertime);
```

```
    bu=gamma*(mediabu(index)-mediabu(index-1))+mediabu(index-1);
elseif index ==1
    lowertime=0;
    uppertime=tempo(index);
    gamma=(time-lowertime)/(uppertime-lowertime);
    bu=gamma*(mediabu(index));
end
```

G.3 FORTRAN Code

```
      program burnup

      dimension VariableE12(12), VariableI3(3), VariableE19(19)
      dimension VariableE7(7)



      open(unit=22, file = 'restart.ori', status = 'unknown')
      open(unit=23, file = 'burnup', status = 'unknown')
      open(unit=24, file = 'tempo', status = 'unknown')

      do 100 k=0,19
            read(22,10,end=110) VariableE
            write(24,10) VariableE
            read(22,20,end=110) VariableI
            do 200 l=1,4
                  read(22,10,end=110) (VariableE12(i),i=1,12)
200         continue
            read(22,10,end=110) (VariableE12(i),i=1,12)
            write(23,10) (VariableE12(i),i=1,12)
            read(22,20,end=110) (VariableI3(i),i=1,3)
            read(22,10,end=110) VariableE
            read(22,10,end=110) (VariableE7(i),i=1,7)
            read(22,10,end=110) (VariableE19(i),i=1,19)
            do 400 l=1,48
                  read(22,10,end=110) VariableE
400         continue
            do 500 l=1,12
                  read(22,10,end=110) (VariableE19(i),i=1,19)
500         continue
            do 600 l=1,3
                  read(22,10,end=110) (VariableE12(i),i=1,12)
600         continue
            do 700 l=1,409
                  read(22,10,end=110) VariableE
700         continue


100   continue

110   stop


10    format(2x,30(e10.4,2x))
20    format(2x,30(i5,2x))

      end
```

```
program modificarestartfrapcon

      dimension VariableE12(12), VariableI3(3), VariableE19(19)
      dimension VariableE7(7)



      open(unit=22, file = 'restart.ori', status = 'old')
      open(unit=23, file = 'restart', status = 'unknown')
      open(unit=24, file = 'incertezze', status = 'old')

      read(24,'(f7.5)') oxide
      read(24,'(f7.5)') hydrogen


      do 100 k=0,21
            read(22,10,end=110) VariableE
            write(23,10) VariableE
            read(22,20,end=110) VariableI
            write(23,20) VariableI
            read(22,10,end=110) (VariableE12(i),i=1,12)
            do 1000 i=1,12
                  VariableE12(i)=VariableE12(i)*oxide
1000        continue
            write(23,10) (VariableE12(i),i=1,12)
            read(22,10,end=110) (VariableE12(i),i=1,12)
            do 2000 i=1,12
                  VariableE12(i)=VariableE12(i)*oxide*hydrogen
2000        continue
            write(23,10) (VariableE12(i),i=1,12)

            do 200 l=1,3
                  read(22,10,end=110) (VariableE12(i),i=1,12)
                  write(23,10) (VariableE12(i),i=1,12)
200         continue
            read(22,20,end=110) (VariableI3(i),i=1,3)
            write(23,20) (VariableI3(i),i=1,3)
            read(22,10,end=110) VariableE
            write(23,10) VariableE
            read(22,10,end=110) (VariableE7(i),i=1,7)
            write(23,10) (VariableE7(i),i=1,7)

            read(22,10,end=110) (VariableE19(i),i=1,19)
            write(23,10) (VariableE19(i),i=1,19)
            do 400 l=1,48
                  read(22,10,end=110) VariableE
                  write(23,10) VariableE
400         continue
            do 500 l=1,12
                  read(22,10,end=110) (VariableE19(i),i=1,19)
                  write(23,10) (VariableE19(i),i=1,19)
500         continue
            do 600 l=1,3
                  read(22,10,end=110) (VariableE12(i),i=1,12)
```

```
                write(23,10) (VariableE12(i),i=1,12)
600         continue
            do 700 l=1,409
                read(22,10,end=110) VariableE
                write(23,10) VariableE
700         continue


100   continue

110   stop




10    format(2x,30(e10.4,2x))
20    format(2x,30(i5,2x))

      end
```

```
PROGRAM TEXT1

c     legge il file plot di fraptran e scrive in file separati i dati
necessari all'analisi
c     i file possono poi essere letti da matlab con il comando load -
ascii
c
c     i file sono i seguenti
c     - Tempo.txt
c     - SEDPNNL.txt
c     - SEDERI.txt
c     - Oxide.txt
c     - Temperature.txt
c     - Enthalpy.txt
c
c     importante: i nodi assiali devono essere 12

      character sr*3
      REAL(8) Time
      dimension SEDPNNL(12), SEDEPRI(12), Oxide(12), Temp(12), Enth(12)
      dimension IDoxigen(12)

      OPEN (UNIT = 9, FILE = 'stripf.prob-1a-ria', STATUS = 'unknown')
      OPEN (UNIT=666,FILE='Tempo.txt')
      open (unit=667,file='SEDPNNL.txt')
      open (unit=668,file='SEDEPRI.txt')
      open (unit=669,file='Oxide.txt')
      open (unit=670,file='Temperature.txt')
      open (unit=671,file='Enthalpy.txt')
      open (unit=672,file='IDoxigen.txt')

200   sr='+++'

      DO 10 WHILE (sr .NE. '===')
            READ   (9, *,END=100) sr
10    END DO

      READ(9,'("1 ",D)') Time
      WRITE(666,*) Time


      DO 20 WHILE (sr .NE. '122')
            READ   (9, *,END=100) sr
20    END DO

      Backspace 9
      read(9,'("122 ",100(e13.5))') (SEDPNNL(k),k=1,12)
      write(667,'(100(e13.5))') (SEDPNNL(k),k=1,12)
      read(9,'("121 ",100(e13.5))') (SEDEPRI(k),k=1,12)
      write(668,'(100(e13.5))') (SEDEPRI(k),k=1,12)

      DO 30 WHILE (sr .NE. '127')
            READ   (9, *,END=100) sr
30    END DO
```

```
      Backspace 9
      read(9,'("127 ",100(e13.5))') (Oxide(k),k=1,12)
      write(669,'(100(e13.5))') (Oxide(k),k=1,12)

      DO 35 WHILE (sr .NE. '132')
            READ   (9, *,END=100) sr
35    END DO

      Backspace 9
      read(9,'("132 ",100(e13.5))') (IDoxigen(k),k=1,12)
      write(672,'(100(e13.5))') (IDoxigen(k),k=1,12)


      DO 40 WHILE (sr .NE. '142')
            READ   (9, *,END=100) sr
40    END DO

      Backspace 9
      read(9,'("142 ",100(e13.5))') (Temp(k),k=1,12)
      write(670,'(100(e13.5))') (Temp(k),k=1,12)


      DO 50 WHILE (sr .NE. '162')
            READ   (9, *,END=100) sr
50    END DO

      Backspace 9
      read(9,'("162 ",100(e13.5))') (Enth(k),k=1,12)
      write(671,'(100(e13.5))') (Enth(k),k=1,12)


      GOTO 200

100   STOP
      END
```

APPENDIX H: MATLAB CODE FOR THE HIGH BURNUP FAILURE LIMIT

```
function y=bulimit(bu,enth)

if bu<35       %only non-spallated
    y=logncdf(enth,5.6315-0.0184*bu,0.0471+0.0035*bu);
else               %spallated and non-spallated
    spalla=(bu-35)/(65-35)*0.8;
        y=(1-spalla)*logncdf(enth,5.6315-
0.0184*bu,0.0471+0.0035*bu)+spalla*logncdf(enth,4.9684-0.0195*bu,-
0.0880+0.0047*bu);
end
```